Matias Vikse

A Nonsmooth Approach to Modeling and Optimization

– Applications to Liquefied Natural Gas Processes and Work and Heat Exchange Networks

Doctoral thesis
for the degree of Philosophiae Doctor

Trondheim, December 2019

Norwegian University of Science and Technology
Faculty of Engineering
Department of Energy and Process Engineering

NTNU

Norwegian University of Science and Technology

Doctoral thesis
for the degree of Philosophiae Doctor

Faculty of Engineering
Department of Energy and Process Engineering

ISBN (printed version)
ISBN (electronic version)
ISSN 1503-8181

Doctoral theses at NTNU,

Printed by NTNU-trykk

Preface

This thesis is submitted as part of a Ph.D. project undertaken at the Norwegian University of Science and Technology (NTNU). The work was carried out at the Department of Energy and Process Engineering, with Prof. Truls Gundersen as main supervisor. Dr. Chao Fu at SINTEF Energy and Prof. Paul I. Barton at MIT were the candidate's co-supervisors. This research was conducted as part of the FME project HighEFF – Centre for an Energy Efficient and Competitive Industry for the Future, with additional funding from NORAM to cover part of a 1-year research stay at MIT.

Abstract

Despite their implicit presence in many process systems engineering applications, nonsmooth functions have repeatedly been shunned due to the existence of nondifferentiable points that cause issues for numerical solvers and gradient based optimization methods. Instead, alternative methods have been widely explored, such as providing smooth approximations around nonsmooth points, or by reformulating the function altogether using disjunctions. However, recent advances in nonsmooth analysis have provided a numerically tractable approach for computing sensitivity information for certain classes of nonsmooth functions, thus paving the way for a new paradigm in process modeling. Rather than circumventing the use of nonsmooth functions by exploring alternative options, they can instead be employed actively for implementing certain decisions into the model. Furthermore, nonsmooth formulations have the potential of reducing the overall model size wherever the previous models relied on disjunctive reformulations.

Along with the new developments in nonsmooth analysis came a promising application of the framework for modeling multistream heat exchangers. Multistream heat exchangers are an integral part of natural gas liquefaction processes that, due to cooling at cryogenic temperatures, call for self-refrigeration. Nevertheless, existing process simulation software suffer from several disadvantages with regards to the modeling of multistream heat exchangers, in particular when it comes to enforcing feasible heat transfer at interior points. As a result of this, alternative modeling approaches have been explored where mixed integer programs and embedded pinch location methods are used. However, these formulations come at the expense of additional binary variables that can only be handled in an optimization environment, as well as adverse scalability to large-scale processes. The nonsmooth multistream heat exchanger, on the other hand, profits from its hybrid modeling strategy that capitalizes on assets from both an equation-oriented

and a sequential-modular approach. The result is a model that could simulate the single-mixed refrigerant PRICO process with a cubic equation of state by solving a nonlinear nonsmooth equation system. Nevertheless, the PRICO process is among the most basic natural gas liquefaction processes available on the market, and has already been studied extensively. Therefore, in order to demonstrate the true capabilities of the nonsmooth framework, more complex and commercially interesting liquefaction processes must be modeled. In this thesis, simulation models for complex single mixed refrigerant and dual mixed refrigerant processes are developed. Cases are constructed, where results are compared with existing software for validation. In addition, a dual mixed refrigerant process is subjected to an optimization study using IPOPT. Although significantly larger than the PRICO flowsheet, the nonsmooth framework retains a moderate model size also for the most complex dual mixed refrigerant process, and is thus capable of simulating all cases presented here within respectable CPU times. Furthermore, it adds versatility to the designer, which makes it possible to locate feasible operating points where the current state-of-the-art process simulators cannot.

Lastly, the advantages of the nonsmooth framework is expanded to the more general topic of work and heat exchange networks. Existing literature resort to mixed integer nonlinear models for dealing with unclassified process streams and locating pinch points. Although these methods are effective at handling small-scale problems, they suffer from an exponential scaling, which can become troublesome when additional variable pressure streams are considered. Here, an alternative approach using nonsmooth operators for assigning the true identity is presented. The extension achieves favorable scaling compared to existing formulations, and can be solved using a similar strategy as with the liquefied natural gas models. To test the new extension, different case studies related to exergy targeting of work and heat exchange networks are discussed.

Acknowledgements

My research career started on a warm summer's day in early August of 2015 as I checked into an AirBnB® with a Murphy bed and a window overlooking the buzzling Broadway Street in Cambridge, MA. A Fulbright scholarship combined with my enthusiastic supervisor Truls Gundersen from NTNU had presented me with the opportunity to venture across the vast Atlantic Ocean to take part in a research stay at the process systems engineering laboratory (PSEL) at MIT. There, I would get to work with a PhD candidate, who would later become one of my best friends, and scientific mentor all-through my studies. Our brief encounter on a wintry day in Trondheim earlier that same summer was, for a while, the only connection I had with the city that would be my home the coming year. Although his expectations were probably minuscule of this rookie master student (if you read his acknowledgement section, you will see that this was indeed the case) with some prior knowledge about natural gas, but very little knowledge on anything else that would be required for achieving his tasks, Harry (the PhD student mentioned earlier), however, always offered a helping hand and useful tips that helped me understand the problem at hand. For instance, he helped me develop the required knowledge for detecting memory leaks in a poorly written C++ code, and for understanding the underlying mathematical theory. More importantly, however, he made sure to introduce me to all his friends, and in doing so, made a Norwegian feel at home in this surprisingly large (yes, I know all my Bostonian friends will call me crazy for saying that) city.

Never could I have been better received in this new research environment than I was at PSEL. My co-supervisor professor Paul Barton always offered valuable insight in modeling aspects as well as thermodynamic behavior, necessary to interpret weird behavior when probing for coding errors. Professor Peter Stechlinski (then Post Doc. Stechlinski) became one of my best friends in Boston ever since

I set my first foot in the office and we later ended up testing the quality of all the gin and tonics found within a mile radius of Faneuil Hall (ending the only way possible, with me sleeping on his couch together with a Golden Doodle named Winston). Together with the other PSEL members, notably José Gonmez, Garrett Dowdy, and Rohit Kannan) we had many-a scientific discussions, and even more (I feel I can take some of the credit for this) non-scientific ones.

As summer approached and the oil price plummeted (and with it, any remaining hope of securing a vacant engineering position), my supervisor Truls Gundersen went beyond the call of duty to help me obtain a PhD position. I was to take part in an exciting new project of improving the energy efficiency in industry. In doing so, I would get to continue my work from MIT, but also move towards work and heat exchange networks, the brain-child of my co-supervisor Chao Fu. His insight, and eagerness to help despite a very tight schedule from his job in SINTEF, was invaluable.

It cannot be swept under the carpet, however, that my PhD years at NTNU presented quite a tumultuous time in my life. I contemplated throwing in the towel at multiple occasions (probably more than most PhD candidates even), and doubted my existence here from early on. Needless to say, it is a very strange feeling to sit here writing the acknowledgement section at 4.15 AM on a November night, a point at which I for the longest time doubted I would ever reach. Although a cliche, it is in no way less true that I would never have made it here if it wasn't for my dad Arne and my sister Svanhild, who always (I should probably have written sometimes here, but "always" seemed so much better) managed to get my mind off work and towards less useful things like snow quality at Vågsli, or on the various highly scientifically flawed studies on how older brothers are likely to be anything from worse drivers to less successful than their younger siblings. However, my mother Åse Margrethe deserves a special thanks in this acknowlegement for the way she repeatedly chose to listen to a hysterical PhD candidate (despite having a demanding job of her own with lots of responsibility) on all his woes and supposed ailments. It truly helped (although it is probably hard for you to see now), and may very well have been the deciding factor that made me finish what I started.

I know that this acknowledgement starts to drag on to the point that it reminds you of one of those Academy Award speeches that went on 5 minutes too long. Nevertheless, I have to thank my colleagues at NTNU for commemorative lunches and intriguing discussions. A special thanks goes to my friends Karl Oskar and Christoph for inviting me along to their weekly work-out sessions, and thus helping me get in shape after a year of excessive fun (read: eating, drinking and absolutely no working out) in the US. I would also like to thank Kathrin for helping me see an end to my PhD, and offering advice on how to turn a difficult situation into

something good by seizing every opportunity you get (although I am still a bit unsure on whether this also applies to doing modeling work). Donghoi, my very good friend and office companion, who is probably surprised to see his name even mentioned here as I merely promised him a footnote (I was just joking Donghoi, like always), I would like to thank you for all our memorable office moments and room shares at various conferences. An extended thanks is also directed to the rest of my research group from NTNU (no one mentioned, no one forgotten).

The day before leaving to the US for a second stay at the PSEL laboratory, I had a serious talk with my family on whether I should continue this PhD, or simply drop out and look for something else. I decided after much deliberation, to move on, and return to the US. Little did I know then that such a small decision could have such a great impact on my life as a whole. Not only did I get to rekindle my friendships in Boston (as well as making new ones: Suzane and Caroline, I have not forgotten the two of you), but it led me to find my soulmate, and love-of-my-life, Rouan. With her at my side, my year in Boston truly became the best I have ever had (until now), to the point that I dreaded from early on my eventual return to Norway. You can imagine my delight, therefore, when she decided follow me to Norway and "ta opp den gamle skikk" as an NTNU student. As I was sitting at home earlier today, I contemplated on my three and half years of PhD studies, and on whether I would do it again knowing where I would wound up in the end. I know I said contemplated here, but actually the answer was a resounding yes! PhD is but a journey, an arduous one at times, yet as with all journeys, it is the people you meet along the way that truly help shaping it (please forgive me for ending it on a bit of a hippie note here).

And thus I concluded that my PhD years were absolutely worth it!

Trondheim, November 2019

Matias Vikse

Nomenclature

Abbreviations

AD	automatic differentiation
C3MR	propane precooled mixed refrigerant
CMR	cold mixed refrigerant
DAE	differential-algebraic equations
DMR	dual mixed refrigerant
FLNG	floating liquefied natural gas
FPSO	floating production, storage and offloading
GCC	grand composite curves
GA	generic algorithm
HEN	heat exchanger network
HP	high pressure
HPR	high pressure refrigerant
L	lexicographic
LCO_2	liquefied CO_2
LD	lexicographic directional
LIN	liquefied nitrogen
LNG	liquefied natural gas
LP	linear program
LP	low pressure
LPG	liquefied petroleum gas
LPR	low pressure refrigerant
MER	maximized energy recovery
MHEX	multistream heat exchanger
MINLP	mixed integer nonlinear program
MR	mixed refrigerant
NGL	natural gas liquids

NLP	nonlinear program
NM	nonsmooth model
PA	pinch analysis
PSE	process systems engineering
PSO	particle swarm optimization
SMR	single mixed refrigerant
SQP	sequential quadratic program
SSTC	single shaft turbine compressor
TAC	total annualized cost
SRQPD	sequential reduced quadratic programming
SWHX	spiral wound heat exchanger
WEN	work exchange network
WHEN	work and heat exchange network
WMR	warm mixed refrigerant

Roman letters

$\mathcal{C}^1$	class of continuous differentiable functions
EBP	enthalpies of the extended composite curves [W]
f_x	molar flowrate of component x [kmol/s]
f	total heat capacity flowrate of cold stream [kW/K]
f_i	heat capacity flowrate of stream branch i [kW/K]
F	total heat capacity flowrate of hot stream [kW/K]
F	feed flowrate [kmol/s]
$f'(\mathbf{x};\mathbf{M})$	LD-derivative of a function f at $\mathbf{x}$ taken in directions $\mathbf{M}$
$\mathbf{f}^k_{\mathbf{x},\mathbf{M}}$	the kth directional derivative of a function $\mathbf{f}$ at point $\mathbf{x}$
$\mathcal{F}_{\mathbf{f}}(\mathbf{x})$	the set of collection functions for a function $\mathbf{f}$ at point $\mathbf{x}$
$\mathbf{G}$	element of the generalized derivative
h	specific enthalpy [kJ/kmol]
$\mathbf{J}_{\mathrm{L}}$	Jacobian matrix
K_i	equilibrium constant for component i
L	flowrate of the liquid product [kmol/s]
L	Lipschitz constant
$\mathbf{M}$	directions matrix
n_{c}	total number of components
P	absolute pressure [Pa]
$\mathcal{PC}^1$	class of piecewise differentiable functions
Q	heat duty [W]

Q	quality of a source term
$Q_{\text{C,min}}$	heat deficit at MER design
$Q_{\text{co},x}$	heat from compression at temperature x
$Q_{\text{H,min}}$	heat surplus at MER design
$Q_{\text{ex},x}$	cooling from expansion at temperature x
q	quality of a sink term
r_{SK}	waste resource
R_{SR}	fresh resource supply
RBP	resource balance term
S	state of a source term
s	state of a sink term
t	temperature of cold stream [K]
T	temperature [K]
T_0	amabient temperature [K]
UA	heat exchanger conductance [W/K]
V	flowrate of the vapor product [kmol/s]
$\mathbf{y}$	equation residuals
x_i	liquid component i [mol%]
y_i	vapor component i [mol%]
Y	boolean variable used in the disjunctive formulation
z_i	feed component i [mol%]
W	work [kW]
W_{net}	net work output [kW]

Greek letters

α	vapor fraction
β	user defined smoothing parameter
ΔT_{LM}	log mean temperature difference [K]
ΔT_{min}	minimum approach temperature [K]
η	isentropic efficiency
γ	variable in the LP-Newton

Subscripts and superscripts

2p	two-phase substream
BP	bubble point
C	cold mixed refrigerant
CU	cold utility
DP	dew point
f	feed stream
HP	high pressure refrigerant

HU	hot utility
in/out	inlet/outlet of a substream
IN/OUT	inlet/outlet of a process stream
l	liquid product
LP	low pressure refrigerant
MR	mixed refrigerant
p	pinch candidate
PI	pinch
s	supply
SK	sink
SR	source
sub	subcooled substream
sup	superheated substream
t	target
v	vapor product
W	warm mixed refrigerant

Contents

List of Tables

List of Figures

Chapter 1

Introduction

1.1 Motivation

The development of a mathematical representation of flowsheet models, where computation and anaylsis are aided by computers, have long since been an integral part of process systems engineering. In the past, system design was performed manually, sometimes on an ad hoc basis, as additional equipment were introduced to the process. Engineering knowledge was a crucial step in the design of such systems, and the layout often featured solutions that had already proved advantageous. Although knowledge is undoubtedly a key in plant design, most chemical processes feature complex operations and interactions between different units that would otherwise be difficult to spot with a manual design approach. An exhaustive mathematical representation, in the form of a model, would help revealing the different driving mechanisms in the process, as well as any possible improvements that can be made. Simulation provides a powerful tool here, as by solving the mathematical model for different operating points, one can investigate how the design responds to perturbations in operating conditions. Moreover, it opens up for sensitivity studies of current operating points to examine potential savings with relatively few amendments to the system. Nevertheless, the main advantage of rigorous simulation models is their central role in optimization. Since computers first entered the field of process engineering, focus has been directed towards how systems could be evaluated and improved by the means of mathematical optimization. Mathematical models provide invaluable sensitivity information, underlining the interactions between different part of the flowsheet, which can be exploited in an optimization algorithm. As such, the designer no longer has to rely on engineering knowledge alone to improve the design, but instead use a mathematical approach to obtain solutions that would elseways be non-intuitive.

Different techniques may be required to describe the model satisfactory. Simple unit operations or small processes for instance, can sometimes be represented fully using continuously differentiable models. Analytical derivatives can be obtained accordingly, and are readily implemented in an optimization procedure. Additional design decisions are often required, however, which involve discrete choices for which there exist no available derivative information. As such, more exhaustive optimization methods may be necessary, relying either on heuristic methods (e.g. stochastic search methods), problem relaxation, or by searching over differentiable subdomains in a branch and bound algorithm. The computational complexity naturally depends on the formulation used for representing the model, leaving a trade-off between accurate description and solvability. Recent developments in nonsmooth analysis bridge the gap between these two modeling approaches by providing a tractable method to obtain gradient information for certain classes of nondifferentiable functions. Nonsmooth functions have traditionally been avoided in modeling due to their nondifferentiability at certain points, which can cause failures of derivative based optimization methods and numerical equation solvers. Alternative formulations have instead been favored that either approximate the nonsmooth function around nondifferentiable points or reformulate it using binary variables. However, this results in an inflation in the number of variables and constraints in the problem, and hence, additional computational complexity. The new framework for computing sensitivity information of nonsmooth functions, therefore offers a great potential in improving existing process models.

Liquefied natural gas (LNG) has been receiving increased attention in recent years. Natural gas is considered a clean alternative to oil and coal for electricity production, with lower CO_2 emissions, sulfur emissions and no particulate matter. However, the mobility over long distances and flexibility in demand make traditional pipeline transport of natural gas challenging. Instead, the growing demand for natural gas must be covered by new transportation methods, where LNG has been seen as a viable alternative, primarily due to the increased density in liquid form. In addition, the boil-off gas during transport can be utilized for propulsion, hence replacing traditional diesel fuel, offering environmental benefits of shipping. However, the liquefaction process is very energy intensive, accounting for a considerable portion of the overall costs of the LNG product, which necessitates the need for developing energy efficient designs. Simulation and optimization of LNG processes is a notoriously challenging task, though, featuring either single or multiple refrigerant mixtures, to maintain a close approximation of the natural gas cooling curve over large temperature spans. Commercial simulation tools exhibit limited capability of analyzing such processes, due to a simplified implementation of multistream heat exchangers that only takes into account the overall energy balance, without any rigorous checks for temperature crossovers in the heat ex-

changers. With this in mind, a multistream heat exchanger model that applies the recent breakthrough in nonsmooth analysis to the concept of pinch analysis and composite curves was developed. The model provides a suitable reformulation of traditional pinch location models to the application of multistream heat exchangers, for which a feasible temperature difference between the hot and cold composite curves are sustained through a single nonsmooth equation. As a result, no embedded optimization models must be solved upon enforcing a minimum temperature difference, which is advantageous to flowsheet simulation. Moreover, as large portions of the flowsheet are embedded in subroutines, the model achieves advantageous scaling compared to existing models in the literature. Model scalability is ofttimes an obstacle in these models, leading them to be applied to relative simple single mixed refrigerant processes only, whereas commercial simulation tools are still relied on for designing larger and more commercially interesting processes.

Liquefied natural gas processes are a subset of the class of problems retained to work and heat exchange networks (WHENs). Stricter environmental laws and increased competition calls for process intensification to uphold a profitable business. Pinch analysis has proved to be instrumental in this transition, offering a clear cut approach to improving energy efficiecy through enhanced heat integration. The method has been so successful, actually, that the concept has since then been extended to other fields such as waste water treatment and scheduling. However, focusing merely on heat integration curbs the potential for improvements in processes that involve pressure manipulation through equipment such as compressors, expanders and valves, etc. Pressure change affects the temperature as well, and will impact the possible heat integration accordingly. Attempts at accommodating these fundamental limitations gave rise to the new paradigm of simultaneous work and heat integration. Different superstructures have been developed for this purpose with attention directed towards minimizing exergy consumption or the total annualized cost of the process. However, the ensuing mathematical models are more involved, and require extensions of the original algorithms to handle instances of correct integration of pressure-changing equipment and a priori unclassified process streams. Different methods have already been suggested in the literature, but these rely on either iterative procedures or large mixed integer models that are laborious to solve for more complex integration problems.

1.2 Objectives

As a new paradigm for process modeling is developed, it opens up new possibilities of improving current implementations that are suited for this newly acquired methodology. Multistream heat exhanger models, for instance, have been modeled

using large and complex mixed integer nonlinear models, entrusting binary formulations and auxiliary variables to handle issues such as phase transitions and feasible heat transfer. The implementations suffered from limitations due to scaling, however, and was therefore only used to study simple single mixed refrigerant processes. With a new alternative to process modeling, a multistream heat exchanger model that accomplished better scaling was developed, and used as basis for simulating the basic single mixed refrigerant PRICO process. However, its framework has yet to be implemented into larger and more complex flowsheet models, which until now remains firmly within the domain of commercial software tools for process design and analysis. With this in mind, the thesis expands on the work on developing a multistream heat exchanger model for simulating LNG processes, by embedding it in flowsheet models for different single mixed and dual mixed refrigerant processes, and as such to demonstrate the capability of the nonsmooth modeling framework of designing large and complex refrigeration cycles. The goal is to confirm the validity of the models, as well as their versatility and robustness to aid flowsheet calculations, and thus promote the tool as a better alternative for LNG process design.

A secondary objective is to try to expand on the knowledge from modeling LNG processes to other applications, namely to the field of work and heat integration. Existing superstructure models are, in the same way as for multistream heat exchanger models, in the realm governed by a more traditional approach to modeling, which relies on solving large mixed integer nonlinear models. Problems related to pinch location and other integration challenges, i.e. the handling of unclassified process streams, currently swear to binary formulations. However, as attested by this new modeling paradigm, not all decisions require the use of binary variables, and can simply be rewritten using alternative nonsmooth formulations. Scalability can in turn be improved, thus opening up for either more detailed calculations or larger problem sets.

1.3 Scope

The scope of this thesis is limited to the preliminary design of natural gas liquefaction processes and work and heat exchange networks. An emphasis is placed on the former, however, with different flowsheet models for both small-scale and large-scale production of LNG. Primary focus is on the liquefaction cycle and its refrigerant mixtures to minimize the temperature driving forces in the multistream heat exchangers and, in turn, the irreversibilities in the process. Less attention, therefore, was put on the specific compressor setup, which could be improved significantly with either multistage compression, or in the case of dual mixed refrigerant processes, a combination of pumps and compressors. However, as the

liquefaction part is preeminent, accounting for the bulk of the losses, as well as, operational variables in the process, it was deemed necessary to focus on this part of the process to investigate the new framework's capabilities in handling larger systems.

No detailed modeling and geometric considerations are considered in this thesis. Instead, the models developed are intended strictly for preliminary analysis of process systems under steady state behavior. As a result, the models developed can be compared to that of Aspen HYSYS and Aspen Plus, in that rigorous thermodynamic models are included for mapping of the thermodynamic behaviour of a system at different operating points. The intention is that the tool is used during the initial phase of process design, followed up with more detailed calculations of both heat exchanger behaviour and economic analysis at a later stage. As steady state is assumed throughout, no considerations regarding controllability or otherwise the design of control systems for these processes are taken into account here. Furthermore, the operation during start-up and shut-down remains out of scope of current work.

As for work and heat exchange networks, the primary focus was on exergy targeting and thermodynamic operation. No total annualized cost analysis was conducted for the different cases, nor were the heat exchanger networks synthesized. That being said, a superstructure featuring a detailed integration scheme for the pressure changing equipment was embedded in the models, and thus, synthesis can easily be achieved for the process using existing models. These models feature discrete decisions, however, that require the use of disjunctive constraints that can only be resolved outside of a nonsmooth framework. Thereby, the nonsmooth models developed here are intended as an effective approach to obtaining a network of minimum exergy consumption, which can be used in an initial step followed by actual network synthesis. In the same fashion, coupling of pressure changing equipment was also not considered in these models, and must instead be considered in subsequent calculations. Its intended use is therefore, much like the LNG models, to offer an effective calculation tool for preliminary analysis, i.e. the task of finding the best obtainable thermodynamic solution, and apply this information for subsequent detailed analysis that also take into account economic parameters.

1.4 Contributions

The main contributions made by this PhD program can be summarized as follows:

1. Developed code in Julia for the computation of LD-derivatives analytically for implicit functions by using a nonsmooth analog of the implicit function theorem. This code was embedded in the modular flash calculations, making

it possible to nest them in the flowsheet models and thus improve the overall scalability of the flowsheet models.

2. Embedded the nonsmooth multistream heat exchanger model in simulation models for complex single mixed refrigerant processes, thus showing how a hybrid framework with nested subroutines for the flash calculations is capable of going beyond simulating the PRICO process. Also demonstrated the importance of versatile simulation models, where several variables can be solved for simultaneously, to obtain solutions elseways unobtainable with commercial software. The same flowsheet models were later used as the foundation for an optimization study on single mixed refrigerant processes.

3. Demonstrated the importance of not only using the same equation of state, but also the same thermodynamic property package when gauging the performance of different models. Although Aspen HYSYS and Aspen Plus both applied the Peng-Robinson equation of state in their simulations, the two models diverged at colder temperatures, something that was accredited to different methods for calculating ideal enthalpy in the models.

4. Extended the flowsheet models to that of dual mixed refrigerant processes, and in doing so, presented a first attempt at simulating large-scale liquefaction processes using tailor-made multistream heat exchanger models. In successfully simulating different models for both large-scale and small-scale LNG production, it also demonstrated the new tool's ability to not only compete with, but also outperform existing software.

5. Optimized a dual mixed refrigerant process and compared results with the current state-of-the-art, to find that improvements could be made throughout by supplying the solver with sensitivities obtained from the nonsmooth models. Current state-of-the-art rely on commercial software, with stochastic search methods for optimization. However, by using the alternative modeling framework together with a deterministic solver, both improvements in the objective value, as well as in the overall computation time can be achieved.

6. Presented an overview on mathematical programming as a tool for simultaneous work and heat integration. The priority was on existing superstructures for targeting and synthesis of work and heat exchangers, and how their formulations can impact the thermodynamic performance, i.e. the total exergy consumption in the network. A suitable superstructure was selected based on this information together with suggested improvements from a modeling perspective.

7. Extended the simultaneous optimization and heat integration algorithm by Duran and Grossmann to instances with unclassified process streams. The extension is compact with only two additional nonsmooth equations used for assigning the correct stream identity. The result is a model that attain auspicious scalability compared to what has already been achieved in the literature, and thus making it a suitable alternative for exergy targeting of larger problems.

1.5 Thesis structure

This thesis is divided into nine chapters, where Chapters 3-6 are allocated to LNG and more specifically on simulation and optimization of different liquefaction processes. Chapters 7 and 8, on the other hand, are about different superstructures for work and heat exchange networks and the optimization of these.

- **Chapter 1** is an introductory chapter featuring motivation, objectives, scope of work, and contributions of this thesis.
- **Chapter 2** presents a brief overview of the mathematical background needed for solving the models in this thesis.
- **Chapter 3** provides background on LNG processes and different optimization studies conducted on the liquefaction in particular.
- **Chapter 4** contains the simulation models for single mixed refrigerant processes. Three processes are modeled, and results are compared with simulations by the commercial process simulators Aspen HYSYS and Aspen Plus.
- **Chapter 5** is a continuation of the previous chapter, but where the same modeling framework is extended to that of dual mixed processes.
- **Chapter 6** concludes the LNG part of the thesis with an optimization study on one of the DMR processes in the preceeding chapter. IPOPT is used for the optimization, using both the total heat exchanger conductance and minimum approach temperature as specifications in the model. Results are compared to the current state-of-the-art, which is to run the simulations in Aspen HYSYS with an external stochastic search algorithm.
- **Chapter 7** transitions the thesis from the relatively specific topic of liquefaction of natural gas processes to the more general concept of work and heat exchange networks. General background on the topic is given, followed by

a discussion on the available superstructures for optimization, targeting and synthesis of work and heat exchange networks.

- **Chapter 8** proposes a nonsmooth extension to the simultaneous optimization and heat integration algorithm by Duran and Grossmann for the handling of unclassified process streams. The extended model is used, together with one of the superstructures from Chapter 7, for exergy targeting of different work and heat exchange networks.

- **Chapter 9** concludes the studies presented in this thesis, before highlighting promising avenues for future work.

1.6 Publications

Full text publications:

1. M. Vikse, H. A. J. Watson, D. Kim, P. I. Barton, and T. Gundersen. Optimization of a dual mixed refrigerant process using a nonsmooth approach. *In review*.

2. H. Yu, C. Fu, M. Vikse, and T. Gundersen. Work and heat integration–A new field in process synthesis and process systems engineering. *AIChE Journal*, 65(7): e16477, 2019.

3. M. Vikse, H. A. J. Watson, P. I. Barton, and T. Gundersen. Nonsmooth formulation for handling unclassified process streams in the optimization of work and heat exchange networks. *Industrial & Engineering Chemistry Research*, 58(22): 9526-9539, 2019.

4. H. Yu, C. Fu, M. Vikse, C. He, and T. Gundersen. Identifying optimal thermodynamic paths in work and heat exchange network synthesis. *AIChE Journal*, 65(2): 549-561, 2019.

5. H. Yu, M. Vikse, R. Anantharaman, and T. Gundersen. Model reformulations for work and heat exchange network (WHEN) synthesis problems. *Computers and Chemical Engineering*, 125: 89-97, 2019.

6. M. Vikse, H. A. J. Watson, T. Gundersen, and P. I. Barton. Simulation of dual mixed refrigerant natural gas liquefaction processes using a nonsmooth framework. *Processes*, 6(10): 193, 2018.

7. C. Fu, M. Vikse, and T. Gundersen. Work and heat integration: An emerging research area. *Energy*, 158: 796-806, 2018.

8. H. A. J. Watson, M. Vikse, T. Gundersen, and P. I. Barton. Optimization of single mixed-refrigerant natural gas liquefaction processes described by nondifferentiable models. *Energy*, 150: 860-876, 2018.

9. M. Vikse, H. A. J. Watson, T. Gundersen, and P. I. Barton. Versatile simulation method for complex single mixed refrigerant natural gas liquefaction processes. *Industrial & Engineering Chemistry Research*, 57(17): 5881-5894, 2018.

10. H. A. J. Watson, M. Vikse, T. Gundersen, and P. I. Barton. Reliable Flash Calculations: Part 2. Process flowsheeting with nonsmooth models and generalized derivatives. *Industrial & Engineering Chemistry Research*, 56(50): 14848-14864, 2017.

11. H. A. J. Watson, M. Vikse, T. Gundersen, and P. I. Barton. Reliable flash calculations: Part 1. Nonsmooth inside-out algorithms. *Industrial & Engineering Chemistry Research*, 56(4):960-973, 2017.

Conference publications:

1. P. I. Barton, T. Gundersen, C. J. Nielsen, and M. Vikse. Nonsmooth analysis in process modeling, design and optimization. *Computer Aided Chemical Engineering*, 47: 7-16, 2019.

2. M. Vikse, H. A. J. Watson, P. I. Barton, and T. Gundersen. Simulation of a Dual Mixed Refrigerant LNG Process using a Nonsmooth Framework. *Computer Aided Chemical Engineering*, 44: 391-396, 2018.

3. H. Yu, M. Vikse, and T. Gundersen. Comparison of reformulations of the Duran-Grossmann model for work and heat exchange network (WHEN) synthesis.*Computer Aided Chemical Engineering*, 43: 489-494, 2018.

4. H. A. J. Watson, M. Vikse, T. Gundersen, and P. I. Barton. Robust flash calculations through Nonsmooth inside-out algorithms. *Computer Aided Chemical Engineering*, 40: 235-240, 2017.

5. M. Vikse, C. Fu, P. I. Barton, and T. Gundersen. Towards the use of mathematical optimization for work and heat exchange networks. *Chemical Engineering Transactions*, 61: 1351-1356, 2017.

6. C. Fu, M. Vikse, and T. Gundersen. Challenges in work and heat integration. *Chemical Engineering Transactions*, 61: 601-606, 2017.

Presentations:

1. M. Vikse, H. A. J. Watson, P. I. Barton, and T. Gundersen. A nonsmooth formulation for handling unclassified process streams in the optimization of work and heat exchange networks. AIChE Annual Meeting. 10-15 November 2019, Orlando, USA. Poster presentation.

2. M. Vikse, H. A. J. Watson, P. I. Barton, and T. Gundersen. Simulation of a Dual Mixed Refrigerant LNG Process using a Nonsmooth Framework. Process Systems Engineering (PSE) conference. 1-5 July 2018, San Diego, USA. Poster presentation

3. M. Vikse, C. Fu, P. I. Barton, and T. Gundersen. Development of a superstructure for work and heat exchange networks (WHENs). AIChE Annual Meeting, 29 October - 3 November 2017, Minneapolis, USA. Oral presentation.

4. M. Vikse, C. Fu, P. I. Barton, and T. Gundersen. Towards the use of mathematical optimization for work and heat exchange networks. 20th Conference on Process Integration for Energy Saving and Pollution Reduction (PRES 2017), 21-24 August 2017, Tianjin, China. Oral presentation.

5. M. Vikse, H. A. J. Watson, T. Gundersen, and P. I. Barton. Implementing robust vapor-liquid equilibrium calculations in nonsmooth multi-stream heat exchanger models. AIChE Annual Meeting, 13-18 November 2016, San Fransisco, USA. Oral presentation

Chapter 2

Nonsmooth analysis

Abstract

This chapter is divided into two parts. First, an introduction to the use of nonsmooth models in applications relevant to Process Systems Engineering is given; where it is advantageous and how it can be used to improve scalability of the models. Different examples of nonsmooth behavior occurring naturally in modeling problems are also discussed. Then, alternative formulations of the nonsmooth models, either through smooth approximations or disjunctive reformulations are provided. The second part presents a methodology for calculating generalized derivative elements needed to solve or optimize nonsmooth models. In particular, the procedure involves calculating the lexicographic (L-)derivative, using an automatic differentiation framework for computing the lexicographic directional (LD-)derivatives. Lastly, nonsmooth equation solving using semismooth or linear program (LP) Newton methods is discussed.

2.1 Nonsmooth modeling in Process Systems Engineering

The development of mathematical models and solving them with the aid of computers, have long since been a standard procedure in Process Systems Engineering (PSE). In the past, design was performed using engineering charts and knowledge based designs. Optimal designs were rather sought using engineering knowledge and trial-and-error approaches than rigorous mathematical models. However, significant improvements in computational power, developments of rigorous optimization algorithms, and a globally competitive market, spawned a need for robust and accurate models of the system. Long since are the days where only a feasible solution to the process problem is sought. Instead, in order to maintain a competitive advantage, designers are often concerned with obtaining the best feasible design to a process, rendering engineering knowledge insufficient. The optimal solution is frequently non-intuitive, obtainable only through the use of mathematical programming to a process model. The size and complexity of the model in question depends on the individual design problem. Normally, the system in question is composed of a series of elemental operations such as stream mixing, separation, heating or cooling, and expansion or compression, compiled to form the overall process model. As a consequence, obtaining a solution to the process model often entails solving a system of equations, sometimes analytically, though more frequently, through the use of numerical methods.

Describing the process model often requires navigating the trade-off between accuracy and computational complexity. Accurate description of the system is important to the validity of the model, and for its use in aiding the design and decision making process. Yet approximations are sometimes required to reduce unnecessary computational complexity. Despite the vast improvements in hardware over the last decade, and a myriad of efficient numerical solvers and optimization algorithms; too much detail or a bad model formulation can leave the model unsolvable with currently available tools. Emphasis must be put on the choice of modeling approach, and specifically how it affects the solution of the problem. Different model types exist in the literature. The easiest are continuously differentiable (smooth) models. Smooth models have well-defined derivatives everywhere, and can therefore be solved effectively using numerical solvers. They suffer from limited applicability, however, and can only be used to model a small subset of the problems encountered in the process industries. More frequently, the model involves taking discrete decisions (e.g. investing in a particular type of equipment), or other discrete changes (e.g. phase changes) that introduce nondifferentiabilities to the problem. Discrete models are significantly more complex to solve than their smooth counterparts, though they receive a lot of attention in PSE due to their versatile nature.

A modeling approach that have until recently received only very little attention in the PSE community, however, are nonsmooth models. Nonsmooth models can best be described as providing a link between smooth and discrete models. Although not as general as the latter, it expands some of the numerical tractability of smooth formulations to certain types of nondifferentiable models, in particular, related to decisions that can be reformulated with the help of nonsmooth operators (i.e. min, max and mid, where mid is a function mapping to the median of its arguments). The relatively low interest in nonsmooth models until recently, is a result of these problems being traditionally difficult to solve. Instead, modelers used smooth approximations [1] or discrete reformulations to remove the nonsmooth terms. However, with the development of a mathematical framework for constructing useful gradient information of certain classes of nonsmooth functions (see Section 2.2), nonsmooth formulations have received renewed interest.

2.1.1 Modeling of countercurrent heat exchangers

Heat exchangers are essential components in process design. Although detailed models exist for the accurate characterization of heat transfer, accounting for geometrical, material and heat transfer properties, a simple model of countercurrent heat exchangers can be developed by applying the first and second Law of thermodynamics. Specifically, a cold stream of heat capacity flowrate f should be heated from an inlet temperature t^{in} to a specified outlet temperature t^{out} by an external source term Q_{H}. In countercurrent heat exchangers, this external source is a hot stream of heat capacity flowrate F, which is cooled from an inlet temperature T^{in} to a temperature T^{out}. The first law of thermodynamics then dictates that energy must be conserved, and that the heat added to the cold stream must come from the hot stream if no other sources are present. Hence, the following energy balance must hold:

$$F\left(T^{\text{in}} - T^{\text{out}}\right) - f\left(t^{\text{out}} - t^{\text{in}}\right) = 0. \tag{2.1}$$

However, the first law alone does not guarantee that feasible heat transfer occurs in the heat exchanger. Specifically, the temperature of the source $T_{\text{SR}}(x)$ at point x in the heat exchanger must always be above that of the sink $T_{\text{SI}}(x)$. There exists an inverse relation between the minimum approach temperature ΔT_{min} in the heat exchanger and total heat transfer area needed, where the approach temperature must be nonnegative for feasible heat transfer. The second law in its general form can be formulated using the following nonsmooth formulation:

$$\Delta T_{\text{min}} \coloneqq \min(T_{\text{SR}}(x) - T_{\text{SI}}(x)) \geq 0, \quad \forall x \in [0, L], \tag{2.2}$$

where L is the length of the countercurrent heat exchanger. In the simple case of constant heat capacity flowrates, the minimum temperature difference will occur at either of the two endpoints unless there is phase change involved. Hence, the following nonsmooth formulation can be used instead:

$$\Delta T_{\text{min}} = \min \left\{ T^{\text{in}} - t^{\text{out}}, T^{\text{out}} - t^{\text{in}} \right\}. \tag{2.3}$$

Although a simple example, the countercurrent heat exchanger example demonstrates the natural occurrence of nonsmooth properties in physical systems. Furthermore, there exist several applications that expand on this simple relation to more advanced process problems, such as process integration and multistream heat exchanger models.

2.1.2 A nonsmooth flash formulation

Phase changes are an integral part of process design. For instance, streams may be heated or cooled across phase boundaries, undergo pressure changes that invoke phase changes, or mixed to form a new multiphase mixture. Phase changes, and in particular the relative volatility of different compounds, are also frequently exploited to obtain the given product specifications in equipment such as separators and distillation columns. Nevertheless, phase changes often represent a modeling challenge in process design. The phase boundaries define discrete regimes for which mixtures behave differently and are guided by different model equations. Single-phase vapor and liquid and two-phase liquid-vapor regimes are most commonly encountered, where a model equation that is valid in a specific phase regime, may not be valid in another. As a consequence, the transition between the different regimes is inherently nonsmooth, for which a discrete change in the governing equations is necessary. In the two-phase regime the following vapor-liquid equilibrium equations are active:

$$L + V = F, \tag{2.4}$$

$$x_i L + y_i V = z_i F, \quad \forall i = 1, \ldots, n_{\text{C}}, \tag{2.5}$$

$$y_i = K_i x_i, \quad \forall i = 1, \ldots, n_{\text{C}}, \tag{2.6}$$

$$h_{\text{l}} L + h_{\text{v}} V = h_{\text{f}} F + Q, \tag{2.7}$$

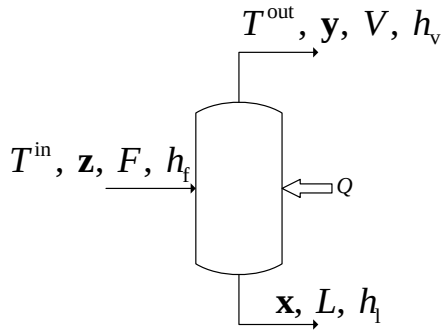

Figure 2.1 A pressure-enthalpy flash problem.

$$\sum_i y_i = 1, \ \sum_i x_i = 1, \tag{2.8}$$

or equivalently [2]

$$\sum_i y_i - \sum_i x_i = 0. \tag{2.9}$$

Equations (2.4)-(2.5) represent the overall and component molar balances; F, V and L are the respective molar flowrates of the feed, vapor and liquid streams, and z_i, y_i and x_i are the corresponding molar fractions of component i. Phase equilibrium is enforced by Equation (2.6), where K_i is the equilibrium constant of component i. The overall energy balance is described by Equation (2.7), where $h_{\text{f/v/l}}$ are the molar enthalpies of the feed, vapor and liquid streams, respectively, and Q is the external heat flow to the system. Furthermore, the individual molar fractions for the vapor and liquid products should each sum to one at equilibrium, which is enforced by the Constitutive equation in (2.9). Equations (2.4)-(2.9) completely describe the pressure-enthalpy flash problem depicted in Figure 2.1.

The vapor-liquid equilibrium problem requires solving a $2n_{\text{C}} + 3$ equation system, where n_{C} are the number of components in the mixture. Rachford and Rice [2] provided an alternative formulation:

$$\sum_i^{n_{\text{C}}} \frac{z_i(K_i - 1)}{1 + \alpha(K_i - 1)} = 0 \tag{2.10}$$

that is monotonically decreasing with respect to the vapor fraction α:

$$\alpha \coloneqq \frac{V}{F}. \tag{2.11}$$

This can be shown by the derivative of Equation (2.10) that is negative for all values of α.

Equation (2.10) is derived from the component and overall material balances, phase equilibrium equation and the constitutive equation. As the function is monotonically decreasing, it contains no false α-roots, i.e. nonphysical roots, and thus no false solutions to the Newton method. Furthermore, the problem is reduced from $2n_{\mathrm{C}} + 3$ equations to only one equation, making it advantageous to numerical solvers.

A solution to the vapor-liquid equilibrium equations can only be obtained for the two-phase region. As the mixture enters a single-phase regime, the equilibrium concept, as determined by Equation (2.6), loses meaning and is no longer valid. The same is true for Equation (2.9), as the non-existing phase will be assigned a nonphysical composition that does not necessarily sum to one. Hence, outside the two-phase region, only the molar balances and the overall energy balance still hold, and there exists a discrete change in modeling equations between the single-phase and two-phase regimes. This represents a modeling issue in processes where the phase states are not necessarily known a priori. Instead, a versatile model that can handle instances of both single-phase and multiphase conditions should be encouraged. A disjuctive formulation can be employed where binary variables are assigned to the different phase states. However, such a formulation would require additional variables and constraints [3, 4], something that should be avoided, particularly when dealing with large systems. Alternative methods involving complementarity constraints have also been suggested [5]. Nevertheless, either solution strategy requires solving a nonconvex optimization problem to global optimality.

A nonsmooth formulation for phase detection was proposed by Watson and Barton [6] by exploiting the fact that no new equations must be added for correctly characterizing single-phase behavior. Instead, in the single-phase regime, Equation (2.9), and hence Equation (2.10), are no longer valid, and should be disregarded in the model. This can be achieved by the nonsmooth formulation:

$$\mathrm{mid}\left\{\alpha, \alpha - 1, -\sum_{i}^{n_{\mathrm{C}}} \frac{z_i(K_i - 1)}{1 + \alpha(K_i - 1)}\right\} = 0, \tag{2.12}$$

where the third argument is the negated Rachford and Rice term.

The nonsmooth formulation works as follows. For an all vapor outlet, $\alpha = 1$, Equation (2.10) will be positive rather than zero since equilibrium no longer exists [7]. It follows that the third argument is negative, and with a positive vapor flowrate, the median of the three arguments (the liquid flowrate) is evaluated to

zero. Then, from the mass balance in (2.4) the vapor flowrate V must equal the feed flowrate F. The argument for an all liquid outlet is analogous. Likewise, in the two phase region, the Rachford-Rice term will be zero, and the vapor fraction will be evaluated to $0 \leq \alpha \leq 1$.

Solving the vapor-liquid equilibrium equations robustly and efficiently represents an important issue in process modeling. The Rachford and Rice reformulation reduced the problem to that of a single, monotonically decreasing function. Although easier to solve than the $2n_{\mathrm{C}} + 3$ equation system directly, it still proves challenging to converge for problems with rigorous thermodynamic models. In particular, employing cubic equations of state, e.g. Peng-Robinson, leads to convergence issues of Equation (2.10), and hence Equation (2.12). Boston and Britt [8] therefore came up with an alternative, though more abstract, formulation where the vapor-liquid equilibrium equations are represented by surrogate variables in convoluted inner and outer problems. The formulation is commonly referred to as the inside-out algorithm, and has proven to be efficient in handling flash problems with nonideal thermodynamics. The algorithm has worked up a significant pedigree in process modeling, where it has served as a workhorse in commercial process simulators such as Aspen Plus [9] and Aspen HYSYS [10].

The idea behind the inside-out algorithm is to isolate the numerically difficult part of the flash problem, i.e. the equilibrium equation in (2.6), and solve it separately using simplified surrogate models. As a result, instead of solving an equation system for the equilibrium vapor and liquid compositions y_i and x_i, the problem is reduced to a single equation (an energy balance) by including a surrogate variable R that incorporates information about the equilibrium constants as well as the individual compositions [8]. Other surrogate variables $\boldsymbol{\Phi}, A, B, C, D, E, F$ are then included to approximate the enthalpy-temperature dependence as affine functions near the solution [11]. These are then updated in an outer loop, and convergence is achieved when both the outer and inner problems are converged. The inner problem is resolved by converging the following energy balance

$$\Psi := h_{\mathrm{f}} F + Q - L(h_{\mathrm{l}} - h_{\mathrm{v}}) - F h_{\mathrm{v}} = 0, \tag{2.13}$$

where R is implicitly defined through the variables h_{v}, h_{l} and V, as well as the outer loop surrogate variables. Enthalpies are calculated using ideal thermodynamics together with departure functions that are assumed affinely dependent on the flash temperature near the solution.

The algorithm then works as follows. First, initial values for the surrogate variables $\boldsymbol{\Phi}, A, B, C, D, E, F$ are obtained, either by using ideal models or heuristics. Next, an initial guess is provided for R, and from this, liquid and vapor compositions, molar flowrates, as well as the reference equilibrium constant can be computed.

Furthermore, the flash temperature is held fixed in the inner loop iterations, and hence, all the enthalpies can now be expressed in terms of R, and the energy balance is resolved. Then in the outer loop, the surrogate variables are updated using rigorous thermodynamic models, and the algorithm repeats itself until both loops converge (see [8] or [12] for full details). As the inside-out algorithm decomposes the problem, different solution strategies can be employed for solving the two loops. Watson *et al.* [12] propose Anderson acceleration [13, 14] for handling the outer loop, and a Newton solve for the inner loop.

Despite the apparent success of the inside-out algorithm in handling vapor-liquid equilibrium calculations with nonideal thermodynamics, it still suffers from the same issue of single-phase solutions. In particular, the inner loop variable R is an analog to the vapor fraction α and is therefore limited to values $0 \leq R \leq 1$, where $R = 1$ is the vapor dewpoint and $R = 0$ is the corresponding bubble point. As a result, the algorithm in its original implementation can only operate in the two-phase region, and will fail to detect solutions with superheated vapor or subcooled liquid. Instead, some post-processing methods have been suggested [11].

The documented [11] Aspen Plus [9] approach when accounting possible single-phase solutions, is to start from the nonconverged all-liquid $R = 0$ or all-vapor $R = 1$ result from the pressure-enthalpy (PQ)-flash calculation, and vary the temperature to satisfy the unconverged energy balance. Then a pressure-temperature (PT)-flash is performed, and based on the result of this calculation, the single-phase candidate solution is either discarded or accepted. If it is discarded, then the PQ-flash is restarted using the PT-flash results as an initial point. Parekh and Mathias [11] suggested an alternative approach very similar to this, but where the procedure was initiated on any iteration where single-phase solutions were detected.

Watson *et al.* [12] came up with a nonsmooth equivalent for the inner problem.

$$\text{mid}(R, \sum_{i=1}^{n_\text{C}} r_i - K_\text{r} \sum_{i=1}^{n_\text{C}} \text{e}^{\phi_i} r_i, R - 1) = 0. \tag{2.14}$$

In (2.14), the surrogate variable R is used as a proxy for the vapor fraction α. The second argument is equivalent to the Rachford and Rice term in (2.12), but expressed in terms of the surrogate variables. Similar to (2.12), the function has three solutions; single-phase vapor ($R = 1$), single-phase liquid ($R = 0$), or a two-phase solution. To differentiate between different single-phase solutions, the nonsmooth formulation also includes a second inner loop variable (K_r) for the temperature calculations in the energy balance. The nonsmooth formulation is capable of handling instances of single-phase flow robustly and efficiently without

employing heuristic post-processing methods. The proposed algorithm also proved better at handling instances near the critical point than the original inside-out algorithm [12]. A nonsmooth extension for locating the correct root for the density extrapolations in super critical behavior was also presented [15].

2.1.3 A nonsmooth formulation of the simultaneous optimization and process integration problem

Process integration is an important tool for improving design. The problem involves arranging complementary sources and sinks to minimize the use of external utilities. Pinch analysis (PA) is a central concept in process integration, which will be explained in detail in Chapter 7. Specifically, it involves locating the point (i.e. temperature) where the process is most constrained, in the sense that the driving forces are at a minimum. This limiting situation is known as the pinch point and provides a measure for the degree of integration possible in the process. Maximum degree of integration of the resource in question imparts a decomposition at the pinch; with a resource deficit above and a resource abundance below. Any additional utility sinks (or sources) below (above) the pinch lead to cross pinch resource transfer and suboptimal integration.

Location of the pinch point, in the aspect of heat integration, can be seen as an extension of the countercurrent heat exchanger problem, where the individual stream contributions are bundled together in the hot and cold composite curves (see Figure 2.2). Graphically, the pinch point will then be the temperature where the two composite curves approach, and at the optimum there will exist no net heat transfer across this point. Furthermore, the minimum required utilites can be identified as the part of the composite curves that are not overlapping. Although a graphical representation can aid process integration, locating potential matches can be challenging from the composite curves alone especially for large processes. Different manual procedures have been developed for this purpose, including tabular or cascade representation that identify residual heat that can be utilized in lower quality sinks. Nevertheless, these procedures suffer from inherent limitations such as the inability to consider processes with unknown states or qualities. With these obstacles in mind, a new paradigm emerged for which mathematical programming is used to formulate the process integration problem, and subsequently solve for a set of unknown process variables to yield a network of optimal resource utilization.

The first and perhaps best known simultaneous optimization and heat integration formulation was developed by Duran and Grossmann [16]. Their mathematical formulation is based on the concept of the process pinch, and in particular the decomposition that exists at this point, where there is a net heat deficit above, and a heat surplus below the pinch point. The resulting optimization problem is

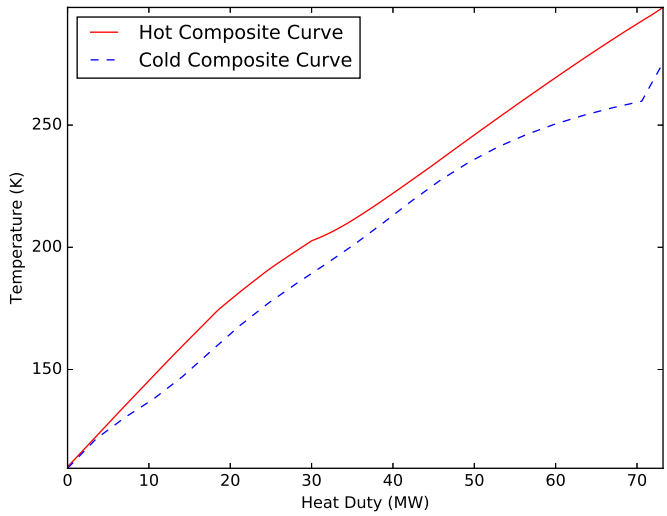

Figure 2.2 Hot and cold composite curves for a natural gas liquefaction process.

presented in Program (2.15).

$$\begin{aligned} \min_{\mathbf{x}} \quad & c_{\text{CU}} Q_{\text{CU}} + c_{\text{HU}} Q_{\text{HU}} \\ \text{s.t.} \quad & \sum_{i \in H} F_i (T_i^{\text{s}} - T_i^{\text{t}}) - \sum_{j \in C} f_j (t_j^{\text{t}} - t_j^{\text{s}}) + Q_{\text{HU}} - Q_{\text{CU}} = 0, \\ & z^p - Q_{\text{HU}} \leq 0, \quad \forall p \in H \cup C, \\ & Q_{\text{HU}} \geq 0, Q_{\text{CU}} \geq 0, \end{aligned} \tag{2.15}$$

where $\mathbf{x}$ are the decision variables and z^p is defined by the following expression

$$\begin{aligned} z^p \coloneqq & \sum_{j \in C} f_j [\max\{0, t_j^{\text{t}} - (T^p - \Delta T_{\min})\} - \max\{0, t_j^{\text{s}} - (T^p - \Delta T_{\min})\}] \\ & - \sum_{i \in H} F_i [\max\{0, T_i^{\text{s}} - T^p\} - \max\{0, T_i^{\text{t}} - T^p\}], \end{aligned} \tag{2.16}$$

and the pinch candidate temperatures T^p are provided by Equations (2.17) and (2.18) for hot and cold streams, respectively.

$$T^p = T_i^s, \quad \forall p = i \in H, \tag{2.17}$$

$$T^p = t_j^s + \Delta T_{\min}, \quad \forall p = j \in C. \tag{2.18}$$

The Duran and Grossmann formulation looks at all candidate pinch points T^p in the process and calculates the net heat deficit above each candidate. Commonly, the individual streams are approximated as having constant heat capacity flowrates F, defined as the product of flowrate and specific heat capacity. This limits the set of pinch candidates to that of the inlet temperatures of the hot and cold streams (Equations (2.17)-(2.18)). Cases with non-constant heat capacity flowrates or phase-changing streams are dealt with by dividing streams into segments, where each segment is approximated to having a constant heat capacity flowrate. Overall energy balance of the system is enforced in the equality constraint in Program (2.15). The individual stream contributions above a pinch point p is given as a sum of nonsmooth terms (see Equation (2.16)). The nonsmooth operators ensure that only streams that are partially, or fully above a given pinch temperature are taken into consideration. Contributions from streams fully below the pinch candidate temperature are in turn evaluated to zero by the max terms. Any remaining heat deficit above pinch are covered by hot utilities in the inequality constraint in Program (2.15), which will be active at the pinch only.

The Duran and Grossmann formulation considered heat integration only. A generalized nonsmooth operator for process integration was later formulated by Nielsen and Barton [17] that expresses the pinch problem in terms of nonsmooth equations. The formulation is applicable to all types of resource recovery problems, where the resource in question has a quality parameter that provides driving forces for resource transfer. Rather than solving a nonlinear program (NLP) or mixed integer nonlinear program (MINLP) for the minimum resource consumption targets, the formulation only requires a nonsmooth equation solve. A resource is transferred from a set of sources SR to a set of sinks SK, where each source $i \in SR$ has a state S_i and undergoes a change in quality from Q_i^{s} to Q_i^{t}. Similarly, each sink $j \in SK$ has a state s_j and undergoes a change in quality from q_j^{s} to q_j^{t}. The following nonsmooth equation system then minimizes the fresh resource supply R_{SR} and waste resource r_{SK}:

$$\begin{aligned} 0 &= \sum_{i \in SR} S_i(Q_i^{\mathrm{s}} - Q_i^{\mathrm{t}}) - \sum_{j \in SK} s_j(q_j^{\mathrm{t}} - q_j^{\mathrm{s}}) + R_{SR} - r_{SK}, \\ 0 &= \min_{p \in P}\{RBP_{SK}^p - RBP_{SR}^p\} + r_{SK}, \end{aligned} \tag{2.19}$$

where P is the set of pinch candidates and

$$
\begin{aligned}
RBP^p_{SR} \coloneqq & \sum_{i \in SR} S_i[\max\{0, Q^p - Q^{\mathrm{t}}_i\} - \max\{0, Q^p - Q^{\mathrm{s}}_i\} \\
& - \max\{0, Q^{\min} - Q^p\} + \max\{0, Q^p - Q^{\max}\}], \quad \forall p \in P \\
RBP^p_{SK} \coloneqq & \sum_{j \in SK} s_j[\max\{0, (Q^p - \Delta Q_{\min}) - q^{\mathrm{s}}_j\} \\
& - \max\{0, (Q^p - \Delta Q_{\min}) - q^{\mathrm{t}}_j\} + \max\{0, (Q^p - \Delta Q_{\min}) - q^{\max}\} \\
& - \max\{0, q^{\min} - (Q^p - \Delta Q_{\min})\}], \quad \forall p \in P,
\end{aligned}
$$

where $\Delta Q_{\min}$ is the minimum quality difference between a source and a sink, and the candidate pinch qualities are given by Equations (2.20) and (2.21).

$$Q^p = Q^{\mathrm{s}}_i, \quad \forall p = i \in SR, \tag{2.20}$$

$$Q^p = q^{\mathrm{s}}_j + \Delta Q_{\min}, \quad \forall p = j \in SK. \tag{2.21}$$

The formulation in (2.19) is similar to the one by Duran and Grossmann in that nonsmooth equations are used for characterizing whether a source or sink is located completely above, across or completely below a pinch candidate $p \in P$. However, the new formulation only requires solving two nonsmooth equations, and therefore scales better with an increasing number of process streams. Moreover, with a simple extension, the formulation can be used to handle threshold problems where no pinch points exist [17].

2.1.4 Alternative smooth or disjunctive reformulations

Examples in the previous sections highlight the use of nonsmooth formulations for handling certain types of discrete problems in process modeling. Nevertheless, their use in the literature have been somewhat limited, primarily due to the location of nondifferentiable points. Specifically, the nonsmooth functions have kinks on their domain for which the Jacobian is undefined. This is problematic in numerical solvers that require derivative information, i.e. Newton type solvers and derivative based optimization, as the solver may terminate early or take on a nondescending direction upon locating the kink. Different reformulations of nonsmooth operators have therefore been suggested in the literature [1, 18, 19].

Perhaps the most common approach is to approximate the nonsmooth operator around points of nondifferentiability using smooth approximations [20–22]. The

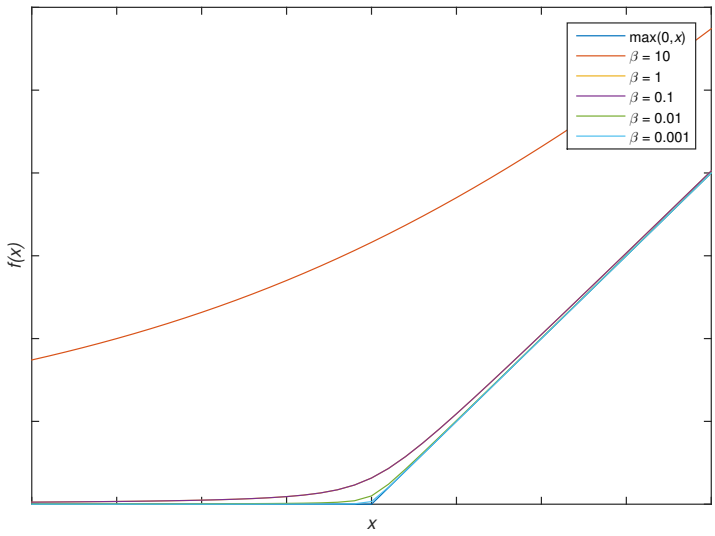

Figure 2.3 Variations of the smoothing parameter β for the function $\max(0, x)$.

following approximation was proposed by Balakrishna and Biegler [1] for the max operator:

$$\max\{0, f(x)\} \approx \frac{\left(\sqrt{f(x)^2 + \beta^2} + f(x)\right)}{2}, \tag{2.22}$$

The approximation relies on the selection of a user defined "smoothing" parameter β. Its selection is nontrivial, however, and both reliability of the approximation and its derivative depend on the chosen value. Figure 2.3 plots the function

$$f : X \to \mathbb{R} : x \to \max(0, x), \quad \forall x \in X \tag{2.23}$$

along with its corresponding smooth approximations, where β is varied from 0.001 to 10. As can be seen in the figure, the quality of the approximation improves as β is lowered. Necessarily, this also implies a simultaneous reduction in the conditioning of the derivative as it approaches the original function [18].

Another strategy is to reformulate the nonsmooth function using disjunctions, and solve the problem using advances in mixed integer (nonlinear) programming [18]. Binary variables are then used for modeling the discrete decisions. Quirante *et al.* [19] proposed the following disjunction for the function $f : X \to \mathbb{R} : x \to$

$\max(0, x)$:

$$\begin{bmatrix} Y \\ x \geq 0 \\ f = x \\ x_{\text{LB}} \leq x \leq x_{\text{UB}} \end{bmatrix} \veebar \begin{bmatrix} \neg Y \\ x \leq 0 \\ f = 0 \\ x_{\text{LB}} \leq x \leq x_{\text{UB}} \end{bmatrix} \tag{2.24}$$
$$Y \in \{True, False\},$$

where Y is a boolean variable used to assign the correct argument to the function f. The disjunctive representation works as follows. If $x \geq 0$, then $Y = True$, and thus f is set equal to x. Otherwise, Y remains $False$, and then f is also set to zero. As a result, f will take on the same values as $f(x) = \max(0, x)$ on $x \in [x_{\text{LB}}, x_{\text{UB}}]$. The corresponding convex hull reformulation [23] of (2.24) is [19]:

$$\begin{aligned} &f = x + s, \\ &y f_{\text{LO}} \leq f \leq y f_{\text{UP}}, \\ &(1 - y) s_{\text{LO}} \leq s \leq (1 - y) s_{\text{UP}}, \\ &s \geq 0, \quad f \geq 0, \end{aligned} \tag{2.25}$$

The reformulation in (2.25) is equivalent to $\max(s, x)$. If $y = 1$ it maps to $f = x$, as s is constrained to zero, and vice versa for $y = 0$. Unlike the smooth approximation, this reformulation is exact, and will result in accurate representation of the nonsmooth functions. However, it introduces nonconvexity in the binary variables and bilinear constraints that are known to be difficult to handle. Additional variables and constraints are required to solve the nonsmooth functions using disjunctions, which can lead to large models whenever several nonsmooth operators must be reformulated. As a consequence, such a reformulation is computationally expensive to solve and requires a mixed integer nonlinear program (MINLP) solver (e.g BARON [24] or ANTIGONE [25]). Alternatively, the nonsmooth functions can be handled analytically using developments in nonsmooth analysis, specifically the concept of generalized derivative evaluations.

2.2 Solving nonsmooth equation systems

Numerical equation solvers and gradient based optimization methods require accurate derivative information. A procedure for calculating gradients is therefore essential for analyzing process models. For continuously differentiable functions, the derivative is defined everywhere and can be estimated using finite differences or calculated analytically using automatic differentiation [26]. Nonsmooth functions, on the other hand, contain kink points, i.e. nondifferentiable points, where the derivative is undefined. Treating such functions using conventional derivative

methods can therefore lead to convergence issues or even failures as a result of inaccurate sensitivity information. Approximations and disjunctive reformulations of the nonsmooth function were discussed in Section 2.1.4. However, they can lead to either an inaccurate or ill-conditioned representation, or large and computationally expensive optimization problems. Alternatively, sensitivity information for the nonsmooth functions can be obtained using an extended definition of the conventional derivative to certain classes of nonsmooth functions.

Definition 2.1. *(From Scholtes [27]). A function* $\mathbf{f} : X \to \mathbb{R}^m$ *for an open set* X *and some* $x \in X$ *is piecewise continuously differentiable (*$\mathcal{PC}^1$*) at* $\mathbf{x}$ *if there exists a neighborhood* $N \subset X$ *of* $\mathbf{x}$ *and a finite collection* $\mathcal{F}_\mathbf{f}(\mathbf{x})$ *of* $\mathcal{C}^1$ *selection functions mapping* N *to* $\mathbb{R}^m$*, where* $\mathbf{f}$ *is continuous and*

$$\mathbf{f}(\mathbf{y}) \in \{\phi(\mathbf{y}) : \phi \in \mathcal{F}_\mathbf{f}(\mathbf{x})\}, \quad y \in N.$$

Piecewise contineously differentiable functions ($\mathcal{PC}^1$) are necessarily nonsmooth at points for which more than one selection function is active. For instance, the nonsmooth operator $\max(0, x)$ is nondifferentiable at $x = 0$, where the two selection functions $\mathcal{F}_\mathbf{f}(0) = \{0, x\}$ are active. $\mathcal{PC}^1$ functions feature several advantageous properties; they are locally Lipschitz continuous and are directionally differentiable everywhere on their domain. Furthermore, the class of $\mathcal{PC}^1$ functions is closed under composition.

Definition 2.2. *A function* $\mathbf{f} : X \subset \mathbb{R}^n \to \mathbb{R}^m$ *is said to be Lipschitz continuous on* X *if there exist a Lipschitz constant* $L \geq 0$ *such that*

$$\|\mathbf{f}(\mathbf{x}) - \mathbf{f}(\hat{\mathbf{x}})\| \leq L \|\mathbf{x} - \hat{\mathbf{x}}\|, \quad \forall \mathbf{x}, \hat{\mathbf{x}} \in X$$

Lipschitz continuity is a strong form of uniform continuity, in that the function is bounded in how much it can change on its domain. Functions with vertical asymptotes or discontinous steps are therefore not Lipschitz continuous from Definition 2.2. A relaxed condition is provided by Definition 2.3.

Definition 2.3. *A function* $\mathbf{f} : X \subset \mathbb{R}^n \to \mathbb{R}^m$ *is locally Lipschitz continuous on* X*, if for each* $\mathbf{x} \in X$*, there exist a neighborhood* N *of* $\mathbf{x}$ *such that* $\mathbf{f}$ *is Lipschitz continuous on* N*.*

It follows from Definition 2.3 that directional derivatives of a locally Lipschitz continuous function are defined on the function's domain. Nonsmooth functions satisfying local Lipschitz continuity thus exhibit useful sensitivity information, i.e. existing subgradients, that can be exploited in numerical solvers. Different extensions of the classical derivative to nonsmooth functions that are locally Lipschitz

continuous exist in literature [28–30]. The Clarke Generalized Jacobian represents one such generalized derivative and is defined as the convex hull of the B-subdifferential [28].

Definition 2.4. *Let* $\mathbf{f} : X \to \mathbb{R}^m$ *be locally Lipschitz continuous on an open set* $X \subset \mathbb{R}^n$*, and* $S \subset X$ *be the set where* $\mathbf{f}$ *is differentiable. Then, the B-subdifferential of* $\mathbf{f}$ *at* $\mathbf{x} \in X$ *is defined as:*

$$\partial_B \coloneqq \left\{ \mathbf{A} \in \mathbb{R}^{m \times n} : A = \lim_{j \to \infty} \mathbf{J}\mathbf{f}(\mathbf{x}_j), \quad \mathbf{x} = \lim_{j \to \infty} \mathbf{x}_j, \quad \mathbf{x}_j \in S, \quad \forall j \in \mathbb{N} \right\}.$$

In other words, the B-subdifferential at a point $\mathbf{x}$ is the set of limiting Jacobians as $\mathbf{x}$ is approached from any direction of differentiability. A challenge with using elements of the Clarke Jacobian, however, is that these elements only follow calculus rules (e.g. the chain rule) as inclusions, and are therefore impractical to calculate for most composite functions. Another generalized derivative is the lexicographic (L-)derivative for functions that satisfy the conditions for lexicographic (L-)smoothness as described by Nesterov [29].

Definition 2.5. *A locally Lipschitz continuous function* $\mathbf{f} : X \subset \mathbb{R}^n \to \mathbb{R}^m$*, where* X *is open, is said to be lexicographically (L-)smooth at* $\mathbf{x} \in X$ *if* $\mathbf{f}$ *is directionally differentiable at* $\mathbf{x}$ *and its higher order directional derivatives are well-defined for any* $\mathbf{M} \in [\mathbf{m}_1 \dots \mathbf{m}_k] \in \mathbb{R}^{n \times k}$ *and* $k \in \mathbb{N}$*:*

$$\begin{aligned}
\mathbf{f}^0_{\mathbf{x},\mathbf{M}} : \mathbb{R}^n \to \mathbb{R}^m \quad &: \mathbf{d} \to \mathbf{f}'(\mathbf{x}; \mathbf{d}) \\
\mathbf{f}^1_{\mathbf{x},\mathbf{M}} : \mathbb{R}^n \to \mathbb{R}^m \quad &: \mathbf{d} \to \left[\mathbf{f}^0_{\mathbf{x},\mathbf{M}}\right]' (\mathbf{m}_1; \mathbf{d}) \\
&\vdots \\
\mathbf{f}^k_{\mathbf{x},\mathbf{M}} : \mathbb{R}^n \to \mathbb{R}^m \quad &: \mathbf{d} \to \left[\mathbf{f}^{k-1}_{\mathbf{x},\mathbf{M}}\right]' (\mathbf{m}_k; \mathbf{d})
\end{aligned}$$

Khan and Barton [31] showed that L-derivatives are elements of the plenary hull [32] of the Clarke Jacobian and are therefore just as useful in nonsmooth equation solvers. Moreover, they follow sharp calculus rules and can be computed for composite functions. The lexicographic directional (LD)-derivative is a generalization of the classic directional derivative that is computed sequentially along the directions provided by the columns of a directions matrix $\mathbf{M}$. As with the lexicographic derivative, the LD-derivative follows sharp calculus rules. Given some $k \in \mathbb{N}$, a directions matrix $\mathbf{M} = [\mathbf{m}_1 \dots \mathbf{m}_k] \in \mathbb{R}^{n \times k}$ and a function $\mathbf{f} : X \to \mathbb{R}^m$ that is L-smooth at $\mathbf{x} \in X \subset \mathbb{R}^n$ where X is open, then the LD-derivative of $\mathbf{f}$ at $\mathbf{x}$ in the directions $\mathbf{M}$ is defined as [30]:

$$\mathbf{f}'(\mathbf{x}; \mathbf{M}) \coloneqq \left[\mathbf{f}^0_{\mathbf{x},\mathbf{M}}(\mathbf{m}_1)\ \mathbf{f}^1_{\mathbf{x},\mathbf{M}}(\mathbf{m}_2)\ \dots\ \mathbf{f}^{k-1}_{\mathbf{x},\mathbf{M}}(\mathbf{m}_k)\right] \tag{2.26}$$

Provided $\mathbf{M}$ is square and nonsingular, the following relationship between the LD-derivative and L-derivative holds:

$$\mathbf{f}'(\mathbf{x}, \mathbf{M}) = \mathbf{J}_{\mathrm{L}}\mathbf{f}(\mathbf{x}; \mathbf{M})\mathbf{M}. \tag{2.27}$$

The sequential calculation of higher-order directional derivatives probes the local sensitivity of the function and is guaranteed to yield useful generalized derivative information given a sufficient number of useful directions [33]. Moreover, a nonsmooth analog of the vector forward mode of automatic differentiation was developed by Khan and Barton [30] for calculating LD-derivatives of composite functions. The procedure is suitable for implementation and also includes commonly used nonsmooth operators such as max, min, mid and the absolute function. The LD-derivative of $\mathcal{PC}^1$ functions taken in the identity matrix directions are guaranteed to be elements of the function's B-subdifferential [30]. B-subdifferential elements are elements of the Clarke Jacobian and exhibit desirable properties in nonsmooth equation solving methods such as local second-order convergence [34]. A detailed review of evaluating LD-derivatives and their applications is provided by Barton *et al.* [33]

Generalized derivative elements provide useful sensitivity information that can be exploited in numerical equation solvers. In the semismooth Newton solver by Qi and Sun [35], a generalized derivative element is used to compute the following Newton step:

$$\mathbf{G}(\mathbf{x}^k)(\mathbf{x}^{k+1} - \mathbf{x}^k) = -\mathbf{f}(\mathbf{x}^k). \tag{2.28}$$

Here, $\mathbf{G}(\mathbf{x}^k)$ is a generalized derivative element of function $\mathbf{f}$ at the point $\mathbf{x}^k$. Equation (2.28) solves for the next iterate $\mathbf{x}^{k+1}$ provided $\mathbf{G}(\mathbf{x}^k)$ is nonsingular. Singular generalized derivative elements may occur in nonsmooth equation systems, e.g. due to equations of type $\min(0, x)$. In such cases, a Newton-type solver that is applicable to singular generalized derivative elements is the linear programming (LP) Newton method by Facchinei *et al.* [36], which solves the following linear program at every iteration:

$$\begin{aligned}
&\min_{\gamma,\mathbf{x}} \ \gamma \\
&\text{s.t.} \ \left\|\mathbf{f}(\mathbf{x}^k) + \mathbf{G}(\mathbf{x}^k)(\mathbf{x} - \mathbf{x}^k)\right\|_\infty \leq \gamma \min\left(\left\|\mathbf{f}(\mathbf{x}^k)\right\|_\infty, \left\|\mathbf{f}(\mathbf{x}^k)\right\|_\infty^2\right), \\
&\quad \left\|(\mathbf{x} - \mathbf{x}^k)\right\|_\infty \leq \gamma \left\|\mathbf{f}(\mathbf{x}^k)\right\|_\infty, \\
&\quad \mathbf{x} \in X,
\end{aligned} \tag{2.29}$$

where X is a polyhedral set of bounds on the problem and γ is a supplementary variable to drive convergence towards the solution. Moreover, the next iterate

$\mathbf{x}^{k+1}$ is given by the $\mathbf{x}$ part of the solution. Fischer *et al.* [37] showed that the LP Newton method can be adapted to ensure global convergence for continuously differentiable and piecewise differentiable functions by including a backtracking line search. Experience working with the LP Newton method taught us that the algorithm may still take poor quality steps when $\mathbf{G}(\mathbf{x})$ is singular. A possible explanation is that an ill-conditioned generalized derivative causes the LP Newton method to take aggressive steps in directions that either diverges the norm of the function residual, or lead to to slow convergence. However, by including the backtracking line search suggested by Fischer *et al.* [37], the step length can be dampened appropriately, avoiding this issue altogether. The steps in the globalized LP Newton method are computationally expensive compared to solving Equation (2.28). Therefore, in order to avoid excessive computing costs, a hybrid method was applied in the simulations, wherein Equation (2.28) is used when $\mathbf{G}(\mathbf{x})$ is nonsingular and well-conditioned, and the global LP Newton is applied otherwise.

Chapter 3

A nonsmooth multistream heat exchanger model

Abstract

This chapter starts off introducing liquefaction processes for natural gas. Both small and large-scale production is considered, and an overview of different liquefaction technologies is provided. Next, different equation oriented multistream heat exchanger models in the literature are presented, and some of their challenges, especially when it comes to modeling complex refrigeration cycles, are discussed. Following the presentation of the existing multistream heat exchanger models, a detailed discussion is provided of the nonsmooth multistream heat exchanger model that constitutes a core component in the flowsheet models developed in this thesis. Finally, different optimization studies of complex liquefaction models are presented.

3.1 Natural gas liquefaction

Natural gas is projected to play a central role in the shift towards green energy sources. According to the BP Energy Outlook from 2017 [38], it is the fastest growing fuel at 1.6% p.a. and is expected to overtake coal in overall demand by 2035. Considered a cleaner alternative to oil and coal due to a low sulfur content, lower CO_2 emissions and no particle emissions, the main challenge with natural gas as a fuel is related to transportation. Today, conventional transport using pipelines is common, though it requires large investments in infrastructure and ties the producer to a set of customers at predetermined locations. Actually, transportation of natural gas via subsea pipelines for distances over 2000 miles have been considered uneconomical, primarily due to high installation and maintenance costs, whereas onshore pipelines are subjected to additional security risks [39]. Accommodating an increasing world natural gas demand must therefore take into account alternative technologies more suitable for long range transport. Owing to this, LNG technology has received significant attention in recent years and is experiencing a growing share of the global natural gas supply to 10.3% in 2017 [40]. A growth rate of 6.4% p.a. in total LNG demand has been observed since the 2000s. Investment in new liquefaction capacity to accommodate the growing demand is thus expected with an increase of 22% in nominal liquefaction capacity by 2024. Moreover, new solutions for floating production, storage and offloading (FPSO) units for natural gas use LNG as the energy carrier for production at remote or low volume offshore gas fields. Nevertheless, liquefaction of natural gas is a very energy intensive process, needing to cool the gas to approximately -162°C. Investments in expensive and proprietary technology such as cryogenic multistream heat exchangers and turbomachinery is necessary, and together with high operating costs, the liquefaction process generally accounts for about 30-40% of the total cost in the LNG chain [41–43].

In general, natural gas liquefaction processes are classified by the types of refrigerant used and the number of refrigeration cycles [42]. Regarding classification based on the type of refrigerant, a distinction is normally made between pure and mixed refrigerant compositions. Pure refrigerant processes use the latent heat of evaporation to cool the natural gas product. However, as the natural gas is cooled over a large temperature span from ambient to cryogenic temperatures, several pure refrigerants and pressure levels must be employed. A refrigerant cascade process was used for the world's first LNG plant with propane, ethylene and methane as refrigerants, and has later been further optimized in both equipment and design [44]. Although relatively efficient, because of the large number of equipment needed in refrigerant cascade processes, they require high capital and maintenance costs. As a consequence, the design is normally only considered for

large-scale production of LNG [42].

Limited liquefaction capacity in small-scale and peak-shaving production mitigating operating costs means that capital costs are of primary concern, thus promoting designs with relatively few pieces of equipment such as single-mixed refrigerant (SMR) processes [45]. Different single-mixed processes exist from the simple PRICO process [46], consisting of a multistream heat exchanger, a cooler, a compressor, and a throttling valve (see Figure 3.1), to the more complex TEALARC process [47] where two refrigerant cycles are used; one for precooling the refrigerant, the second for liquefying the natural gas. Refrigerant mixtures are used to better follow the cooling curve of the feed gas, as they evaporate nonisothermally at isobaric conditions. Another benefit is the additional degrees of freedom provided by the refrigerant composition, which can be optimized to better fit the cooling curve. Along with their compact design and small equipment count make single mixed refrigerant processes an attractive option for peak shaving plants [48], and for small-scale floating LNG (FLNG) systems [45, 49]. Nevertheless, in large-scale and base-load production, the train capacities and production volumes shift the overall cost distribution towards higher operating costs, which should be compensated by the implementation of more energy efficient designs. Additional refrigeration cycles are therefore necessary to limit the temperature driving forces, i.e. heat transfer irreversibilities, in the process.

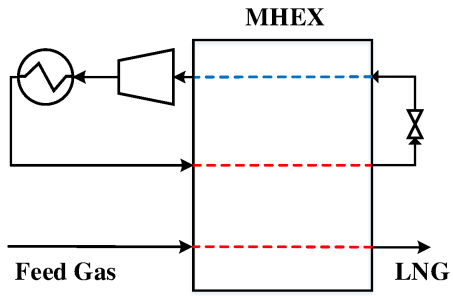

Figure 3.1 The single mixed refrigerant PRICO process.

Typical processes considered for large-scale or base-load production are the more complex propane precooling (C3MR), and dual mixed refrigerant (DMR) liquefaction cycles. The C3MR process [50] is a hybrid option between the pure refrigerant cascade and mixed refrigerant processes. A pure propane cascade process with either three or four pressure levels is employed to cool the natural gas to approximately -40°C, from which a mixed refrigerant is used for condensing the natural gas [42]. Liquefaction and subcooling of the natural gas is achieved in

a multistream heat exchanger using a mixed refrigerant, normally comprised of nitrogen, methane, ethane and propane [42]. The refrigerant mixture limits the temperature differences in the cold part of the process, thus resulting in a more energy efficient design than the pure refrigerant cascade process. The C3MR process is currently the market leader, accounting for approximately 60% of the total market share [40]. Dual mixed refrigerant processes replace the precooling propane cycle with a mixed refrigerant. The result is a lower equipment count compared to C3MR processes [51], as well as smaller temperature differences in the precooler. Economic analysis of the C3MR and DMR processes showed that DMR processes are preferred for medium range plants with capacities between 2 and 4 MTPA [42]. Their compact design compared to other large-scale processes, i.e. refrigerant cascade and C3MR processes, also makes DMR processes suitable for large-scale FLNG units. Efficient and versatile designs are priorities in such large-scale LNG facilities at the expense of higher capital costs (though mitigated by economies of scale) and a larger equipment inventory compared to SMR processes. Projects for which DMR is used for natural gas liquefaction in offshore production are the Shell Prelude and Coral South FLNG. A DMR process is also used for onshore large-scale production at the Sakhalin plant in Russia [40]. Figure 3.2 presents a flowsheet of the AP-DMR process [52], which is currently being considered for the Coral South FLNG project.

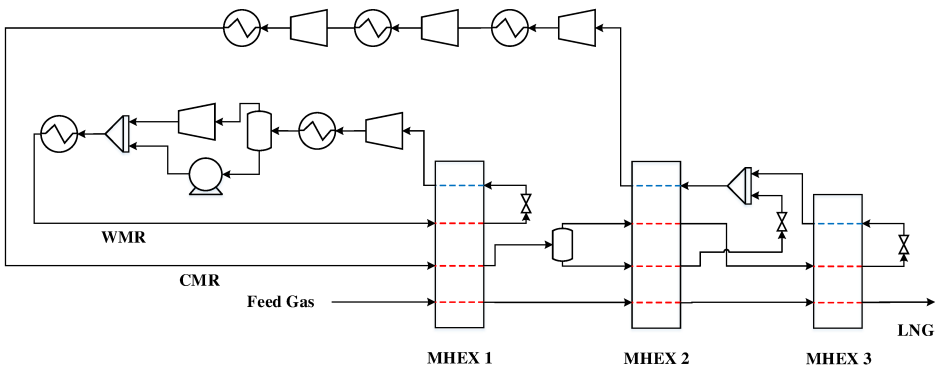

Figure 3.2 Flowsheet of the AP-DMR liquefaction process.

Increased competition between producers along with a growing demand for LNG have spawned research into the design and optimization of LNG processes [53, 54]. Large temperature ranges as well as small temperature differences at cryogenic temperatures make liquefaction processes difficult to analyze. The small driving forces are a consequence of heat exchange at cryogenic temperatures where thermodynamic irreversibilities become significant. Small inaccuracies in the process model, and correspondingly excessive temperature driving forces at such low

temperatures, will necessarily propagate into significant exergy losses in the actual process that must be compensated through additional compression power. An accurate modeling tool is therefore essential for ensuring optimal operation and accurate representation of the real system. However, state-of-the-art process simulators such as Aspen Plus [9] and Aspen HYSYS [10] suffer from significant limitations in the modeling of multistream heat exchangers (MHEXs), which constitute the core of LNG liquefaction cycles. In particular, these process simulators consider the first law of thermodynamics only, by solving an overall energy balance for a single unknown outlet temperature. No rigorous checks are implemented to ensure that the solution also obey the second law of thermodynamics, and that no temperature crossovers exist in the heat exchangers. Instead, by using these tools, suitable parameters had to be determined through a manual iterative trial-and-error approach to MHEX simulation, where process parameters must be changed until feasible operation is obtained.

3.2 Multistream heat exchanger models

Attempts at capturing this lack of functionality in conventional process simulators have resulted in several tailor-made MHEX models. Yee *et al.* [55, 56] and Yee and Grossmann [57] published a series of papers on energy and area targeting, as well as synthesis of heat exchanger networks. A stage-wise superstructure was proposed that potentially matches each hot stream with every cold stream in a predefined number of stages. A nonnegative minimum approach temperature ($\Delta T_{\min}$) is ensured in the superstructure by the use of binary variables. The resulting model is an MINLP that must be solved to global optimality for the heat exchange network synthesis problem. The model was used to perform energy targeting and area calculations for a multistream heat exchanger [55] involving one hot and two cold streams. A two-stage superstructure was used to represent the multistream heat exchanger, where the hot stream was allowed to exchange heat with the two cold streams in both stages. Furthermore, the formulation assumed isothermal mixing and constant heat capacity flowrates for the streams to avoid bilinear terms in the formulation. Wechsung *et al.* [58] developed another superstructure, this time for modeling and optimizing an offshore natural gas liquefaction process utilizing liquefied CO_2 (LCO_2) and liquefied nitrogen (LIN) as cold carriers [59]. The superstructure is described in detail in Chapter 7, and employs a state space approach [60] where pressure manipulations and heat integration are conducted in separate modules. The multistream heat exchanger is here treated as a heat integration problem with constant heat capacity flowrates and solved using a pinch location method. Both the superstructure by Yee *et al.* and by Wechsung *et al.* assume constant heat capacity flowrates for the process streams. However, liquefaction processes for natural gas involve phase changes both for the feed gas and the re-

frigerant mixtures, and with refrigerant mixtures, the two-phase region is highly nonlinear. Process conditions such as temperature, pressure and mixture composition also change during simulation and optimization, resulting in the phase regions varying dynamically. Hence, phase regions traversed in the multistream heat exchanger (and in other auxiliary equipment such as throttling valves) cannot be determined a priori, but must instead be solved for as part of the overall problem. Necessarily, multistream heat exchanger models for LNG liquefaction must take phase changes into account.

Hasan *et al.* [3, 4] developed a model of a spiral wound heat exchanger (SWHX) for LNG liquefaction using a superstructure of two-stream heat exchangers similar to the one by Yee *et al.* The superstructure is organized into separate stages (bundles) where each hot stream is matched with a corresponding cold stream. Each bundle is treated individually as a network of two-stream countercurrent heat exchangers, and then solving a heat exchanger network synthesis problem with no external utilities. Binary variables are used to accommodates for phase changes in the heat exchanger provided the inlet and outlet phase states are known a priori. The result is a mixed integer nonlinear program (MINLP) that is computationally expensive to solve and requires global optimization to guarantee a correct solution. Later, Rao and Karimi [61] proposed a similar superstructure that handles unknown inlet/outlet stream states without introducing boolean variables. Instead, nonlinear constraints are included to ensure that phase boundaries occur at the endpoints of each two-stream heat exchanger such that it operates within a specific phase regime. A process simulator (e.g. Aspen Plus) is used for calculating the stream properties in the model. The final model is a nonconvex NLP that is laborious to solve, particularly due to the repeated property evaluations done by the process simulator that again requires global optimization methods. However, if explicit property correlations are used instead, boolean variables must be added to the model, resulting in an MINLP.

Kamath *et al.* [5] proposed another MHEX model, developed from the concepts of pinch analysis and composite curves. However, rather than solving a network synthesis problem using a superstructure approach, the model performs energy targeting using a simultaneous optimization and heat integration procedure [16], and treating the multistream heat exchanger as a heat integration problem without external utilities. The inlet and outlet phase regimes of the streams need not be known prior to optimization, but these are instead solved for using complementarity constraints. The result is a nonconvex, nonlinear (NLP) optimization problem involving complementarity constraints that violate most conventional constraint qualifications. The model was used to successfully optimize the single mixed refrigerant PRICO process [46].

Pattison and Baldea [62] developed an alternative MHEX model using a pseudo-transient EO approach. The model assumes that the relative sequence of stream temperatures is known (and fixed) prior to simulation in order to construct a series of enthalpy intervals for the composite curves. Each enthalpy interval may be split into additional segments to improve the accuracy of the calculations, especially in the two-phase region where thermal properties of the fluids vary nonlinearly with temperature. The temperatures for each enthalpy interval are then calculated from thermophysical property models by introducing a nonphysical time-dependent temperature variable, and solving the resulting model as a system of differential-algebraic equations (DAEs). The pseudo-transient MHEX model is capable of handling phase changes while avoiding the use of either disjunctive programming or boolean variables. Instead, phase transitions are handled by perturbing the time variable across the nonsmooth phase boundaries whilst keeping the temperature constant. The physical properties are then resolved using the temperature from the previous time step as the initial condition. An extension of the multistream heat exchanger model was proposed by Tsay *et al.* [63] for the detailed design of SWHXs that incorporates industry-accepted pressure-drop and heat tranfer correlations for single-phase and multiphase streams. The model was implemented in gPROMS and used to optimize the PRICO process with an SQP solver.

A multistream heat exchanger model checking for enthalpy feasibility rather than temperature feasibility was introduced by Tak *et al.* [64]. The model partitions the hot composite curve into individual temperature intervals, followed by successive enthalpy calculations at the interior points of the MHEX using an external property model. Phase changes are redirected to the external property package rather than relying on an explicit constraint formulation. To ensure feasible heat transfer and no temperature crossovers in the model, the hot composite curve is shifted by a temperature ΔT_{min}, thus providing a ceiling to the cold composite curve at a given temperature. Enthalpy constraints are then placed on the model that prevent the enthalpy of the cold composite curve at a given internal temperature T from crossing the shifted hot composite curve. As a consequence, expensive temperature calculations from implicit enthalpy functions are avoided. The resulting formulation is a nonconvex NLP that was used to model the PRICO process in gPROMS and solved using an SQP solver.

3.3 A nonsmooth formulation of a multistream heat exchanger model

The literature on MHEX modeling and design for liquefaction processes for natural gas mainly involve flowsheet optimization. The models by Hasan *et al.* [3, 4],

Rao and Karimi [61], Kamath *et al.* [5] and Pattison and Baldea [62] all require solving nonconvex optimization models, sometimes to global optimality, where the minimum approach temperature constraints are enforced as part of the optimization. Even though flowsheet optimization is an essential tool in developing cost and energy efficient process designs, process simulation also provides a powerful assessment tool in the engineering toolbox. In particular, process simulation allows engineers to study existing systems or operating points that are not necessarily optimal. Furthermore, it can be used to probe the behavior and characterize the sensitivity of the system in a neighborhood of the current operating conditions to reveal relatively simple and cost effective improvements at no or little additional investments. Process simulation by solving an equation system is also significantly less computationally expensive than solving a nonconvex optimization problem, and simulation is thus preferred when a feasible rather than an optimal design is sought. Also, a reliable simulation model can be be extremely useful in providing feasible initial guesses to an optimization code, often enhancing the reliability of the optimization [65]. The problem with temperature crossovers in MHEXs observed in Aspen Plus and Aspen HYSYS is more challenging in the context of simulation, primarily due to the absence of a minimum approach temperature constraint. Previously, temperature crossovers were prevented by employing either a superstructure approach for heat exchanger network synthesis or a pinch localization algorithm that solve the heat integration problem for a specified ΔT_{min}. However, these approaches require solving a nonconvex, nonlinear, sometimes mixed integer, optimization problem to global optimality, and they are thus not suited for flowsheet simulation. Moreover, phase states are handled explicitly as part of the optimization problem. Watson *et al.* [66] developed a nonsmooth MHEX model suitable for both flowsheet simulation and optimization by extending the model for a two-stream countercurrent heat exchanger, characterized by Equations (2.1) and (2.3), as well as the equation for total heat exchanger conductance

$$UA = \frac{Q}{\Delta T_{\text{LM}}}, \tag{3.1}$$

where UA is the heat transfer conductance, $Q \equiv F\left(T^{\text{in}} - T^{\text{out}}\right)$ is the total heat exchange duty, and ΔT_{LM} is the log-mean temperature difference.

The energy balance can readily be extended to the case of n_{H} hot and n_{C} cold streams as follows:

$$\sum_{i=1}^{n_{\text{H}}} F_i \left(T_i^{\text{in}} - T_i^{\text{out}}\right) = \sum_{j=1}^{n_{\text{C}}} f_j \left(t_j^{\text{out}} - t_j^{\text{in}}\right). \tag{3.2}$$

Also, the equation for total heat exchanger conductance can be applied to the case of multistream heat exchangers by assuming vertical heat exchange between the

hot and cold composite curves

$$UA = \sum_{k=1}^{K-1} \frac{Q^k}{\Delta T_{\text{LM}}^k}, \tag{3.3}$$

where K is the total number of enthalpy intervals and Q^k is the duty of the interval.

As for the minimum approach temperature constraint in Equation (2.3), however, it cannot readily be extended to that of multistream heat exchangers. Provided the heat capacity flowrates are constant, the minimum temperature difference in two-stream heat exchangers occurs at the one of the endpoints of the heat exchangers. For multistream heat exchangers, on the other hand, the pinch point can occur at any of the stream inlets. In addition, with streams undergoing phase transitions, the pinch point will more times than not occur at interior points rather than at the physical endpoints of the MHEX. As a result, MHEX models use concepts from pinch analysis, in particular a pinch location algorithm for calculating the minimum temperature differenece. Several pinch localization algorithms exist in the literature [16, 18, 19, 67, 68], most of which require solving a disjunctive program to global optimality.

However, in order to avoid solving a separate optimization problem for the minimum temperature calculations, Watson *et al.* [66] developed a reformulation of the Duran and Grossmann model for simultaneous optimization and heat integration [16]. The reformulation solves the pinch location problem through the nonsmooth equation

$$\min_{p \in P} \{EBP_{\text{C}}^p - EBP_{\text{H}}^p\} = 0, \tag{3.4}$$

where P is the (finite) set of candidate pinch points and $EBP_{\text{H/C}}^p$ are the enthalpies of extended hot/cold composite curves below pinch for pinch candidate p as defined in Watson *et al.* [66]. The reformulation represents a specific instance of the generalized nonsmooth operator for process integration (see Section 2.1.3) applicable to heat integration without external utilities. No nonlinear optimization algorithm is therefore required, though requiring a nonsmooth equation solve.

Phase changes in the MHEX present a well-known modeling issue, as phase boundaries and the phases traversed in the heat exchanger are not known a priori. MHEX models in the literature either rely on an external property package with embedded post-processing methods for phase detection, or explicit disjunctive formulations for handling this issue. However, these approaches resulted in large, nonconvex, and computationally expensive models that have to be solved to global optimality and are thus not suitable for implementation in a simulation framework. A

nonsmooth alternative using the nonsmooth operators max, min and mid for correctly identifying the phase state of a process stream was proposed by Watson and Barton [6], which involves partitioning each process stream into superheated (sup), two-phase (2p) and subcooled (sub) substreams whose inlet and outlet temperatures are determined by the following equations:

$$T_{\text{sup}}^{\text{in/out}} = \max\left(T_{\text{DP}}, T^{\text{IN/OUT}}\right), \tag{3.5}$$

$$T_{\text{2p}}^{\text{in/out}} = \text{mid}\left(T_{\text{DP}}, T_{\text{BP}}, T^{\text{IN/OUT}}\right), \tag{3.6}$$

$$T_{\text{sub}}^{\text{in/out}} = \min\left(T_{\text{BP}}, T^{\text{IN/OUT}}\right), \tag{3.7}$$

where $T^{\text{IN/OUT}}$ are the inlet and outlet temperatures of the process stream, $T_{\text{sub/2p/sup}}^{\text{in/out}}$ are the corresponding inlet and outlet temperatures of the substreams, and T_{DP} and T_{BP} are the dew and bubble point temperatures of the process streams. Additional stream segments may be used to improve the accuracy of the calculations, which is particularly important for the two-phase region where enthalpy varies nonlinearly with temperature due to phase change. Watson *et al.* showed, by using the PRICO process as an illustrating example, that 20 segments provided a sufficient accuracy for representing the two-phase region [69].

Stream temperatures in the two-phase region are calculated using successive pressure-enthalpy (PQ-)flash operations for the stream segments. As stream properties and thus phase boundaries change during the simulation, the PQ-flash algorithm must be capable of handling instances of single phase flow. This is also an issue for auxiliary equipment in LNG processes, such as compressors and valves, which may experience instances of single phase flow during the iterations of the nonsmooth solver. For this application, Watson and Barton [12, 15, 69] used the nonsmooth extension of the well-known Boston and Britt [8] flash algorithm from Section 2.1.2. In addition, a methodology for calculating correct sensitivity information from the flash equations was presented, which allows the nonsmooth inside-out algorithm to be integrated in the flowsheet models. Rather than using a fully equation-oriented framework where the MHEX model and flash calculations are solved simultaneously, the flash calculations are nested in the model and solved with a sequential-modular approach. This hybrid modeling framework ensures that the flash calculations are fully converged at each iteration, yet adequate sensitivity information is passed on to the other model equations using the results of a nonsmooth analog of the implicit function theorem [70]. The result is a reduced model size and better scalability with additional streams or additional stream segments.

3.4 Simulation and optimization of complex natural gas liquefaction processes

Natural gas liquefaction processes have been subject to different optimization studies both with regards to minimum cost and minimum total work requirements. Being the simplest of the natural gas liquefaction processes, single mixed refrigerant processes have naturally received a lot of attention [71], specifically the PRICO process. Different multistream heat exchanger models were presented in Section 3.2 where the limitations of the sequential modular modeling framework in commercial process simulators were addressed, especially with regards to adhering to the minimum temperature difference constraint. Alternative equation oriented models were discussed. Nonetheless, most optimization studies still employ commercial simulators for property evaluations and process modeling, and external solvers are used for process optimization. Different solvers are employed, though in broad terms they can be divided into two main solution categories; deterministic optimization and stochastic search algorithms [51].

Early optimization studies of LNG processes normally applied nonlinear programming (NLP) solvers [51]. A PRICO process was optimized with respect to total compressor work input by Wahl *et al.* [72] for different natural gas feed compositions. The simulation model was implemented in Aspen HYSYS, and connected to an external Nonlinear Programming by Quadratic Lagrangrian Programming solver (NLPQLP). Different case studies were considered in the analysis and compared to an earlier study where the PRICO process was optimized using tabu search combined with the Nelder-Mead downhill simplex method [73]. Results showed that the NLPQLP solver obtained better results in all but one case, yet achieving significant savings in total computation time. Effects of the compressor arrangement with regards to the specific work requirements were presented in an optimization study by Tak *et al.* [71] on the PRICO process. Optimization was done for four different compressor configurations, one which includes the use of a pump, as well as three different feed gas compositions. Although different compositions, only small changes in the optimal mixed refrigerant (MR) composition were observed in the study. Moreover, the optimal composition favored heavier components such as n-butane to propane [71]. The optimization study was performed using a model implemented in gPROMS and solved using a successive reduced quadratic programming (SRQPD) method.

Another approach is to use a stochastic search algorithm for optimizing the liquefaction process. Lee *et al.* [74] proposed a new optimization strategy for maximizing the net present value (NPV) of the PRICO process over the life time of a natural gas field. Optimization was performed using a black box methodology with mod-

els developed in Aspen HYSYS and solved using a genetic algorithm (GA) implemented MATLAB. Optimal equipment size and MR composition were determined by maximizing the overall profit for three different design loads. Moreover, scenarios considering a single-train and parallel train operations were considered. The results showed that when considering load variation, the heat exchange area was reduced at the expense of a higher MR flowrate and thus larger compressor capacities. In the case of a single-train operation, the reduction in area was less than the increase in compressor capacity, resulting in an increase in overall cost compared to steady-state design. However, the increase in compressor cost was smaller than the decrease in heat exchanger cost for the parallel train case. Shirazi and Mowla [48] optimized a two-stage compression PRICO process with regards to optimal compression power using GA. Following the optimization study, an exergy analysis was performed to account for the lost work in the process. The multistream heat exchanger was responsible for approximately 27% of the total lost work. Other significant losses were accredited to the LP compressor and the water cooler downstream of the HP compressor. Nogal *et al.* [75] developed a nonlinear optimization model for the optimization of SMR and DMR processes. The process model was developed using WORK, which constitutes a part of the process design software from the Centre for Process Integration at the University of Manchester, with an in-built thermodynamic property model. Optimization was conducted using GA with the objective of minimizing compression work, with capital costs incorporated in the objective function. The optimization study managed to find improvements in the design of two previously published case studies. Khan and Lee [76] optimized the PRICO process using particle swarm optimization (PSO). The model was implemented in the commerical simulator UniSim, with an external optimization solver coded in MATLAB. An energy saving of 10% and improved exergy efficiency of 5% were achieved compared to the base case. Moreover, better solutions were obtained than using gradient based solvers, although at higher computational costs.

The complexity of DMR processes, which includes additional refrigerant streams, MHEXs, and splitting or mixing of streams, make them significantly more difficult to optimize than SMR processes. A large temperature span and phase changes in the MHEXs also result in a highly nonlinear variation in the enthalpy as a function of temperature. To account for this nonlinearity, the process streams are frequently partitioned into smaller stream segments with constant heat capacity flowrate. Therefore, additional variables must be added for each MHEX making the optimization problem large and challenging to solve. As a result, most optimization studies on DMR processes use conventional process modeling tools such as Aspen HYSYS [10] or Aspen Plus [9] for simulation and optimization, or together with an external solver for optimization [53]. Wang *et al.* [77] optimized onshore

DMR and C3MR processes for mid-scale production. The total annualized cost, combined cost of compressors and MHEX, and total shaft work were considered in the study with flowsheet models developed in Aspen HYSYS. The results show that a shaft work analysis without limitation on the equipment size (particularly the UA value for the multistream heat exchangers), give overdimensioned designs. Instead, the trade-off between equipment size and thermodynamic efficiency is better captured through a total annualized cost analysis. The authors also recommended optimizing long-term expenditures to obtain maximum profit from the liquefaction plant. Khan *et al.* [78] optimized the specific compression power and total UA using multi-objective optimization for a DMR process. Aspen HYSYS was used for process modeling, whereas MATLAB was used for finding the Pareto-optimal solutions. The results show that multi-objective optimization decreases the specific compressor power and total heat exchanger conductance (UA) by 13% and 3% respectively compared to the base case. Another optimization study was done by Hwang *et al.* [79] on a DMR process using Aspen HYSYS for process simulation and a hybrid optimization method combining a genetic algorithm with sequential quadratic programming (SQP). Process optimization resulted in a 34% reduction in total compression power compared to the original design. Morin *et al.* [80] optimized an SMR and a DMR process using an evolutionary search method and sequential quadratic programming. SQP was shown to obtain better results on average, particularly for the SMR process. However, it struggled to converge successfully for the DMR process without significant tuning, and SQP was found to be highly sensitive to the problem formulation. The evolutionary search method, on the other hand, required relatively little tuning and was faster than SQP for the DMR process. Furthermore, it obtained solutions within 3.12% of the SQP solution. The authors therefore suggest using a hybrid optimization strategy, where an evolutionary search method would be used for obtaining a good starting point for the SQP algorithm. Such a hybrid optimization strategy was employed by another study by Hwang *et al.* [41], which synthesized the DMR process by considering 27 different liquefaction configurations optimized with respect to the total shaft work. Flowsheet models were developed in Aspen HYSYS, and an external solver called EzOptimizer [81] that combine stochastic search (GA) with an SQP solver was employed. The optimized liquefaction cycle offered a 7% reduction in shaft work compared to the original design [82]. Additional optimization studies of DMR processes are reviewed in Austbø *et al.* [53] and He *et al.* [54]

Chapter 4

Simulation of Single Mixed Refrigerant processes using a nonsmooth framework

Abstract

The previous chapter introduced different processes for natural gas liquefaction. Large temperature spans and small temperature differences in the heat exchangers make these processes challenging to simulate and optimize, and limitations in the implementation of multistream heat exchangers in commercial process simulation tools, encourages the use of custom models. Different multistream heat exchanger models were presented. However, these suffer in terms of scaling, as most of them rely on binary variables for modeling phase changes, and can only enforce a minimum temperature difference in combination with flowsheet optimization. A nonsmooth multistream heat exchanger model was presented that use a hybrid flowsheet strategy, where a large portion of the flowsheet operations are nested in subroutines to improve the overall scaling of the model. Here the multistream heat exchanger model is used to develop flowsheet simulation models for more complex single mixed refrigerant processes. Accuracy of the current implementation is highlighted through comparisons with existing simulation software, with the purpose of showing how this alternative modeling strategy can be seen as a replacement of current software, offering significant improvements in robustness and versatility.

This chapter is based on the publication:

- M. Vikse, H. A. J. Watson, T. Gundersen, and P. I. Barton. Versatile simulation method for complex single mixed refrigerant natural gas liquefaction processes. *Industrial & Engineering Chemistry Research*, 57(17):5881-5894, 2018.

Different multistream heat exchanger models were introducted in Chapter 3 for the optimization of natural gas liquefaction processes. Scalability remain a considerable challenge with using these models as a large number of auxiliary variables are needed to model phase changes in the heat exchanger. As a result, the models have thus far only been tested for the relatively simple PRICO process, which consist of a single MHEX for cooling the natural gas. Moreover, the implementation of the models are done in such a fashion that a minimum temperature difference (and thus the compliance with the second law of thermodynamics) is only enforced in relation to flowsheet optimization, whereas the task of process simulation is diverted to existing commercial process simulation software. In fact, enforcing a minimum temperature difference, and thus a feasible operating point, is a feature that is lacking in current simulation tools. This is credited to a difficulty in MHEX operation with phase changes, as the minimum approach temperature may occur at any interior points of the heat exchanger. The simulation of complex SMR processes, as well as DMR and C3MR process designs is still carried out using commerical software, sometimes followed by flowsheet optimization using either an external derivative based or derivative free solver.

A nonsmooth multistream heat exchanger model was presented in Chapter 3, which solves a system of three nonsmooth equations to yield a feasible operation for the heat exchanger. Unlike the other MHEX models, which employ a fully equation oriented framework, the nonsmooth model nests large portions of the flowsheet operations, i.e. the flash calculations, in subroutines that are solved using a sequential modular approach upon every flowsheet iteration. This does not only improve the robustness, as all flash routines remain fully converged throughout, but also improves scalability such that the MHEX can be embedded in larger models.

Until now, the nonsmooth multistream heat exchanger model has been used to successfully develop a simulation model for the PRICO process, yet it remains to be implemented in more complicated liquefaction models. In this chapter, three different SMR processes are studied. The first example deals with an SMR liquefaction process consisting of a spiral wound heat exchanger (SWHX) with two hot and two cold refrigerant streams working in different temperature ranges. The second example looks at an extended PRICO process with two MHEXs and NGL extraction after precooling. The third example considers a hybrid version of the two previous processes that considers both multiple refrigerant streams and NGL ex-

traction after precooling. All simulations are carried out using the Peng-Robinson EOS with property parameter values taken from Aspen Plus. The models are written in the Julia v0.6.0 programming language and run on a Dell Latitude E5470 laptop in the Ubuntu v16.10 environment with an Intel Core i7-6820HQ CPU at 2.7 GHz and 8.2 GB RAM. Five stream segments are used for representing the physical streams in single-phase vapor/liquid regions and 20 stream segments for the two-phase region. The latter was chosen carefully to ensure accurate representation of the two-phase region [69]. The tolerance for flowsheet convergence was set to $\|\mathbf{y}\|_\infty < 10^{-6}$, where $\mathbf{y}$ are the equation residuals, and the tolerance for the flash calculations was set to $\|\mathbf{y}\|_\infty < 10^{-8}$.

Case studies are performed to investigate whether the models are robust enough to obtain feasible solutions for different sets of unknown variables. Two cases are considered in the first two examples, whereas in the last example, three cases are studied. The variables considered in the analysis are the outlet temperatures of the high and low pressure refrigerant streams, pressure levels, refrigerant compositions, minimum temperature difference in the MHEXs, heat exchanger areas, and the NGL extraction temperature. Some of these variables, such as the refrigerant composition and NGL extraction temperature, are more difficult to solve for as they influence several parts of the flowsheets. For the last two examples, validation of the results are performed in Aspen Plus using the same property parameters and thermo-physical property package. Comparisons are also done with results from Aspen HYSYS. However, it is important to observe that this does not mean that Aspen could have performed these simulations. Actually, Aspen Plus fails to converge for any of the following cases with the design specifications and initial guesses provided for Examples 2 and 3. Their MHEX models are limited to one degree of freedom from solving the overall energy balance and can thus only handle a single unknown variable. The nonsmooth MHEX model, on the other hand, provides either two or three degrees of freedom depending on whether area calculations are included. Moreover, a ΔT_{min} or UA-value can be specified in the model, something that is not available for simulations in Aspen Plus, which instead calculates these parameters automatically for the given composite curves. Therefore, Aspen Plus is merely used for validating the physical feasibility of the solutions by providing the data from the results of the nonsmooth simulation, with the exception of the outlet temperature of the low pressure refrigerant (LPR) stream in each MHEXs, which is calculated by Aspen Plus or Aspen HYSYS from the energy balance. The following nomenclature is used for the parameters and variables related to the MR streams in the model:

- Pressure level of the high pressure refrigerant: P_{HP}.

- Pressure level of the low pressure refrigerant: P_{LP}.
- Inlet/outlet temperatures of the high pressure refrigerant: $T_{\text{HP}}^{\text{IN/OUT}}$.
- Inlet/outlet temperatures of the low pressure refrigerant: $T_{\text{LP}}^{\text{IN/OUT}}$.
- Molar flowrate of the refrigerant: F_{MR}.
- Molar flowrate of refrigerant component i: $f_{\text{MR},i}$.

4.1 A single mixed refrigerant process with a SWHX (Example 1)

In this example, a modified PRICO process is considered in which the high pressure refrigerant (HPR) is separated into a liquid and vapor branch. The liquid branch (Branch 1) is subcooled to a temperature $T_{\text{HP,1}}^{\text{OUT}}$ before it is throttled to pressure level P_{LP} and mixed with the LPR stream to provide precooling. The vapor branch (Branch 2), on the other hand, is condensed and subcooled to a temperature $T_{\text{HP,2}}^{\text{OUT}}$ and then throttled to the same pressure P_{LP} to provide cooling at the cold end of the MHEX. Figure 4.1 shows the flowsheet of this modified PRICO process. The configuration of a spiral-wound heat exchanger (SWHX) is similar to that of the MHEX. The SWHX is a cryogenic heat exchanger, commonly used in dual mixed refrigerant (DMR) processes, that consists of one or several stream bundles wound around a mandrel. Separate tubes are used for the hot refrigerant and natural gas streams, whereas the cold refrigerant is flowing countercurrently outside the bundles. Furthermore, different refrigerants may be used to provide cooling at different temperature levels, which results in less refrigerant that is circulated in the cold end of the heat exchanger. As a consequence, the heat transfer area required to cool the same quantity of natural gas is comparatively smaller.

The SWHX is modeled as a single five-stream MHEX; a cold stream in the hot and cold end of the heat exchanger in addition to the three hot streams. The first LPR stream corresponds to the cold end of the SWHX and will have the same composition and flowrate as the vapor stream in Branch 2. This stream will leave the cold end of the SWHX at a temperature $T_{\text{LP,1}}^{\text{OUT}}$ where it is mixed with the liquid stream from Branch 1 to form the second LPR stream. This stream provides necessary precooling for the hot streams in the hot end of the SWHX and will exit the heat exchanger to enter the compressor at $T_{\text{LP,2}}^{\text{OUT}}$. The sets of unknown variables considered for this example are:

- **Case I - variable set**: P_{HP}, P_{LP}, UA.

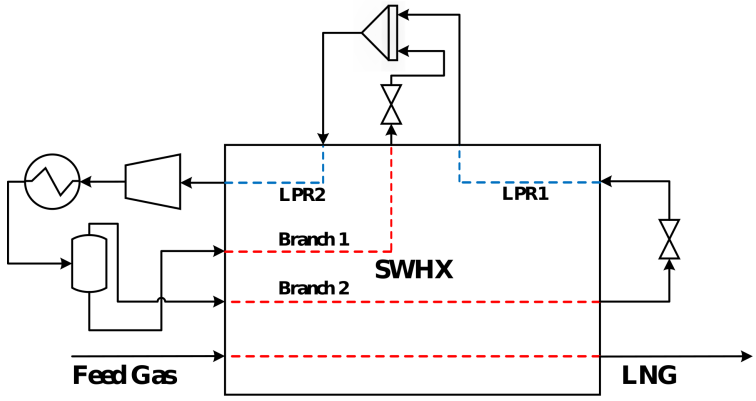

Figure 4.1 SMR process with a SWHX.

- **Case II - variable set**: $f_{\text{MR,ethane}}$, $T_{\text{LP,2}}^{\text{OUT}}$, ΔT_{min}.

Table 4.1 provides the initial guesses for the unknown variables and the values of the known parameters in the simulations. The model consists of 43 variables: the three variables solved for in each case as well as the temperatures for each stream segment in the subcooled and superheated regions determined by $s_i(n_{\text{sup}} + n_{\text{sub}} - 2)$, where s_i are the number of streams in the MHEX and n_{sup} and n_{sub} are the number of segments for the superheated and subcooled regions. The temperatures for the segments in the two-phase region are solved sequentially in the nested subroutines and thus do not appear in the overall model. Nevertheless, only the parameters presented in Table 4.1 need to be provided by the user, while the remaining temperatures are calculated through an automatic initialization procedure that assumes a linear relationship between enthalpy and temperature in the subcooled and superheated phase regions [69]. For comparison, the PRICO model from Watson *et al.* [69] consists of 27 variables. The data for the natural gas stream are presented in Table 4.2 and are assumed fixed throughout this example. No tear equations are required in this model as the pressure levels, material flows and compositions are set for the high and low pressure refrigerant streams similar to an equation oriented approach. In addition, the temperature is fixed after the cooler. The results of the simulations are discussed for each of the two variable sets below.

Case I. Here, the minimum approach temperature ΔT_{min} remains fixed at 1.5 K while varying the pressure levels of the refrigerant and the UA value. The high pressure level affects the split fraction in the separator and hence the refrigerant composition in the two branches. Consequently, it affects the shape of the com-

Table 4.1 MHEX and refrigerant stream data for Example 1. Initial guesses for the unknown variables are placed in brackets.

Property	**Set I**	**Set II**
UA [MW/K]	[10.00]	10.00
ΔT_{min} [K]	1.50	[1.50]
F_{MR} [kmol/s]	2.928	[2.928]
P_{HP} [MPa]	[1.7129]	1.7129
P_{LP} [MPa]	[0.202]	0.202
$T_{\text{HP}}^{\text{IN}}$ [K]	298.15	298.15
$T_{\text{HP,1}}^{\text{OUT}}$ [K]	240.15	240.15
$T_{\text{HP,2}}^{\text{OUT}}$ [K]	112.15	112.15
$T_{\text{LP,2}}^{\text{OUT}}$ [K]	280.15	[280.15]
$T_{\text{LP,1}}^{\text{OUT}}$ [K]	230.00	230.00
Composition [mol %]:		
Nitrogen	5.82	[5.82]
Methane	20.62	[20.62]
Ethane	39.37	[39.37]
n-Butane	34.19	[34.19]

Table 4.2 Natural gas stream data for Example 1.

Property	**Natural gas**
Flowrate [kmol/s]	1.00
Pressure [MPa]	5.50
Inlet temperature [K]	295.15
Outlet temperature [K]	110.15
Composition [mol %]	
Nitrogen	1.00
Methane	91.60
Ethane	4.93
Propane	1.71
n-Butane	0.35
iso-Butane	0.4
iso-Pentane	0.01

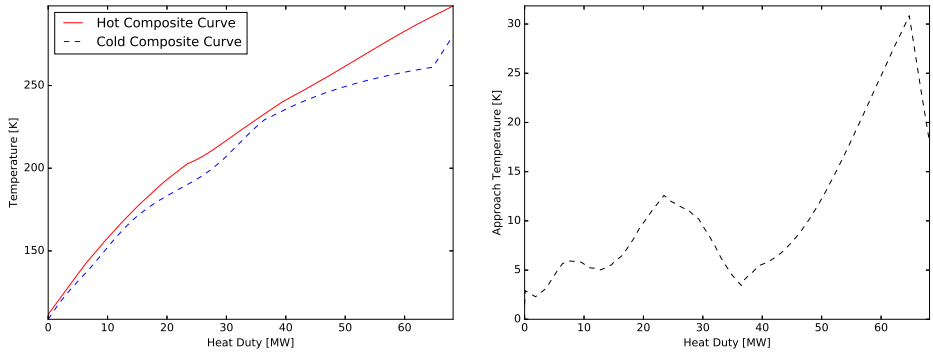

(a) **(b)**

Figure 4.2 (**a**) Composite curves for Example 1, Case I. (**b**) Corresponding driving force plot.

posite curves and is more strenuous to solve for than in the original PRICO process. Flowsheet convergence was reached after 3 iterations and a total simulation time of 20.97 seconds including initialization. A solution is found with $P_{\text{HP}} = 1.5326$ MPa, $P_{\text{LP}} = 0.1855$ MPa and $UA = 9.29$ MW/K, which corresponds to a required isentropic compression power of 15.81 MW. Figure 4.2(a) shows the composite curves for the process and Figure 4.2(b) presents the driving force plot. The driving force plot shows that the process is constrained mainly in the cold end and at the point of mixing, which results in smaller driving forces compared to what was observed for the PRICO process [69]. The corresponding compression power is therefore significantly smaller. It should be stated here that this is only a feasible solution resulting from simulating the process, and that flowsheet optimization is not carried out in this chapter.

Case II. Here, the composition of the refrigerant mixture, the inlet temperature to the compressor and the minimum approach temperature are varied while keeping the UA-value fixed at 10 MW/K. The model solves for the refrigerant composition by varying the molar flowrate of component i, here ethane, and then resolve the mole fractions $z_{\text{MR},i}$ from $f_{\text{MR},i} = z_{\text{MR},i}F_{\text{MR}}$. The simulation converged after 4 iterations requiring 31.2 seconds to solve including initialization of the stream variables. A solution is obtained with $T_{\text{LP,2}}^{\text{OUT}} = 271.30$ K, $\Delta T_{\text{min}} = 1.59$ K, and a new refrigerant composition with 5.89 % nitrogen, 20.88 % methane, 38.63 % ethane and 34.62 % n-butane. The total MR flowrate is also changed from 2.928 to 2.892 kmol/s as a result of varying the component flowrate of ethane. The solution resulted in an isentropic compression power of 15.22 MW. Figure 4.3(a) shows the

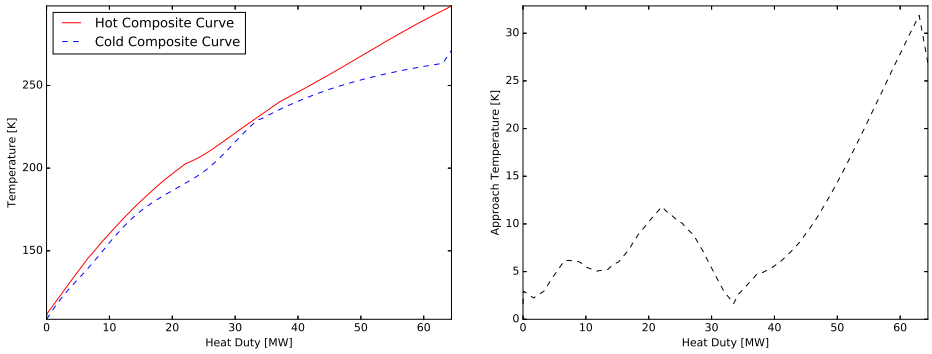

(a) **(b)**

Figure 4.3 (**a**) Composite curves for Example 1, Case II. (**b**) Corresponding driving force plot.

composite curves for the process and Figure 4.3(b) presents the driving force plot. A summary of the simulation results from the two cases are presented in Table 4.3.

Example 1 represents a compact way of formulating the SWHX model, which is ideal when studying larger processes that include one or several SWHXs. The compact formulation reduces the number of variables in the model compared to using two separate MHEXs as required by Aspen HYSYS. A drawback with this formulation, however, is that the model only provides three degrees of freedom compared to six when using two MHEXs. As a consequence, more model parameters must be specified prior to simulation, thus removing some of the flexibility in the model. A similar process using two MHEXs that includes NGL extraction at intermediate temperatures is considered in Example 3.

4.2 A PRICO process with intermediate NGL extraction (Example 2)

For LNG production that handles unprocessed feed gas, a key decision is whether to have integrated or upstream natural gas liquids (NGL) extraction. Heavier hydrocarbons freeze out at cold temperatures, which can cause plugging of process equipment. The LNG is also subject to quality constraints that may require heating value adjustments by removing heavier components. In addition, liquefied petroleum gas (LPG), i.e. propane and butane, is a valuable commodity and is therefore normally sold separately. This example deals with a modified PRICO process with two MHEXs and integrated extraction of natural gas liquids (NGLs). A rich natural gas is first precooled in MHEX 1 before separating the NGLs at an intermediate

Table 4.3 Summary of simulation results for Example 1.

Property	Case I	Case II
Compression power [MW]	15.81	15.23
UA [MW/K]	9.29	10.00
ΔT_{min} [K]	1.50	1.57
F_{MR} [kmol/s]	2.928	2.890
P_{HP} [MPa]	1.5326	1.7129
P_{LP} [MPa]	0.1855	0.202
$T_{\text{LP,2}}^{\text{OUT}}$ [K]	280.15	271.30
Composition [mol %]:		
Nitrogen	5.82	5.89
Methane	20.62	20.87
Ethane	39.37	38.63
n-Butane	34.19	34.61

temperature to ensure an appropriate LNG composition. Figure 4.4 presents the process flowsheet. Unlike the process studied in Example 1, this model considers only one refrigerant composition in both exchangers.

The simulations in Example 2 use the same initial refrigerant composition, flowrate and low pressure level as Example 1. Again, this is not intended to indicate that these are optimal operation conditions, but rather to demonstrate the general simulation capabilities of the model. Other relevant process data are summarized in Table 4.4. An MHEX model solving only Equations (3.2) and (3.4) was used for MHEX 1. Specifying either the UA-value or ΔT_{min} as a parameter in this heat exchanger is challenging as they are dependent of the process conditions in MHEX 2 and vice versa. The MHEX design is also less critical for the precooler, where temperature driving forces are larger. Thus, an efficient approach is to use the two-equation MHEX model to first identify the approach temperature for a set of initial conditions, while calculating the required heat exchanger area subsequently. Then, in detailed design, the three-equation model can be employed to iterate around the initial area value as desired.

The model contains 53 variables, ten more than the model in Example 1. Table 4.5 presents the property data for the natural gas stream, which are held fixed in the simulations. A richer composition is used compared to Example 1 and the pressure is lowered from 5.5 MPa to 3.5 MPa to ensure adequate separation after precooling. In practical applications, the natural gas and hot refrigerant streams leave the MHEX at approximately the same temperature to avoid excessive subcooling of the refrigerant. Therefore, due to limited degrees of freedom in the simulation

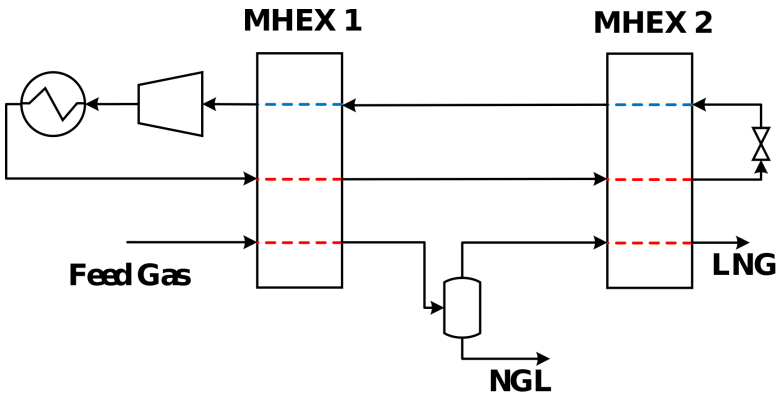

Figure 4.4 SMR process with NGL extraction.

Table 4.4 MHEX and refrigerant stream data for Example 2. Initial guesses for the unknown variables are placed in brackets.

Property	Set I	Set II
F_{MR} [kmol/s]	[2.928]	2.928
P_{HP} [MPa]	1.513	[1.513]
P_{LP} [MPa]	[0.270]	[0.270]
MHEX 1:		
$\Delta T_{\text{min},1}$ [K]	[5.00]	[5.00]
$T^{\text{IN}}_{\text{HP},1}$ [K]	298.15	298.15
$T^{\text{OUT}}_{\text{HP},1}$ [K]	220.15	220.15
$T^{\text{OUT}}_{\text{LP},1}$ [K]	290.15	290.15
MHEX 2:		
UA_2 [MW/K]	[9.50]	9.50
$\Delta T_{\text{min},2}$ [K]	2.50	[2.50]
$T^{\text{OUT}}_{\text{HP},2}$ [K]	120.15	120.15
$T^{\text{OUT}}_{\text{LP},2}$ [K]	[215.15]	[215.15]
Composition [mol %]		
Nitrogen	[5.82]	5.82
Methane	[20.62]	20.62
Ethane	[39.37]	39.37
n-Butane	[34.19]	34.19

Table 4.5 Natural gas stream data for Example 2.

Property	Natural gas
Flowrate [kmol/s]	1.00
Pressure [MPa]	3.50
Inlet temperature [K]	295.15
Outlet temperature [K]	120.15
Composition [mol %]	
Nitrogen	1.00
Methane	81.60
Ethane	9.93
Propane	1.71
n-Butane	0.35
iso-Butane	0.4
iso-Pentane	0.01

models, rather than varying the outlet temperatures of the natural gas stream and HPR refrigerant streams independently, they are assigned to the same temperature variable. With two equations provided by MHEX 1 and three by MHEX 2, the model can solve for five variables involved in the heat exchangers. The following two cases are studied in this chapter:

- **Case I - variable set**: $f_{\text{MR,n-butane}}$, $\Delta T_{\text{min,1}}$, P_{LP}, $T_{\text{LP,2}}^{\text{OUT}}$, UA_2.
- **Case II - variable set**: P_{LP}, $\Delta T_{\text{min,1}}$, P_{HP}, $T_{\text{LP,2}}^{\text{OUT}}$, $\Delta T_{\text{min,2}}$.

Case I. In this case, the refrigerant composition, the minimum approach temperature in MHEX 1, the low pressure level, the LPR temperature out of MHEX 2, and the UA value in MHEX 2 are varied, while keeping the approach temperature in MHEX 2 fixed. The flowsheet converged after 24.5 seconds and 4 iterations to a solution with $\Delta T_{\text{min,1}} = 8.00$ K, $P_{\text{LP}} = 0.202$ MPa, $T_{\text{LP,2}}^{\text{OUT}} = 209.91$ K and $UA_2 = 7.57$ MW/K, resulting in an isentropic compression power of 15.19 MW. The new refrigerant composition and flowrate was found to be 5.96 % nitrogen, 21.12 % methane, 40.33 % ethane and 32.58 % n-butane with $F_{\text{MR}} = 2.916$ kmol/s. Furthermore, the natural gas composition after extraction is 1.18 % nitrogen, 90.35 % methane, 6.66 % ethane, 1.74 % propane, 0.03 % n-butane, 0.04 % iso-butane and 0.00 % iso-pentane. A UA_1-value of 3.07 MW/K was calculated during post-processing.

Figures 4.5 and 4.6 present the composite curves and the driving force plots for Case I. The driving force plot also includes results for the same case from simula-

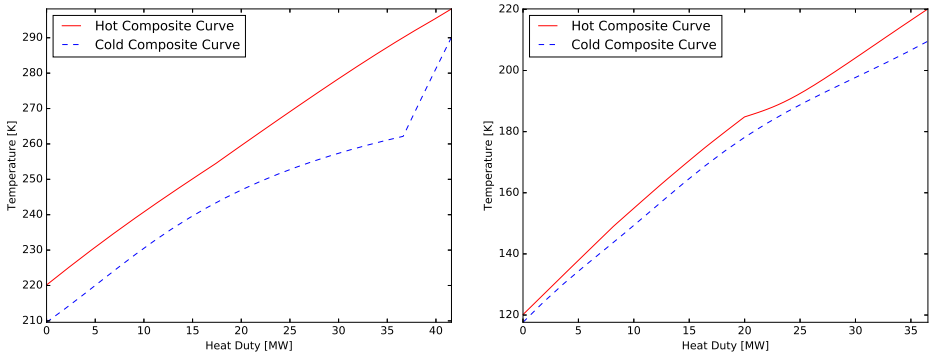

(a) **(b)**

Figure 4.5 (**a**) Composite curves for MHEX 1 in Example 2, Case I. (**b**) Corresponding for MHEX 2.

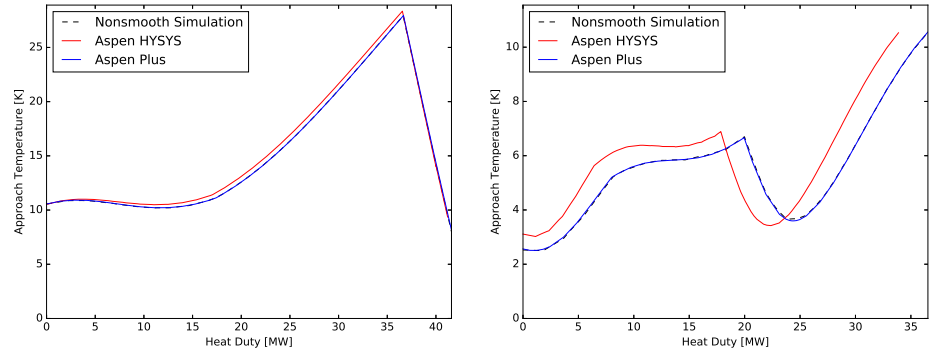

(a) **(b)**

Figure 4.6 (**a**) Driving force plot for MHEX 1 in Example 2, Case I. (**b**) Corresponding for MHEX 2.

tions in Aspen Plus v9 and Aspen HYSYS v9 using 30 segments for each MHEX. As was mentioned earlier, both simulations were performed using the result from the nonsmooth model as a starting point and allowing the outlet temperature of the LPR stream in each MHEX to vary. Stream pressures cannot be selected as variables in the MHEX models in Aspen, and consequently they fail to solve for Case I and II in this example since fixing $T_{\text{HP,1}}^{\text{OUT}}$ and $T_{\text{LP,1}}^{\text{OUT}}$ would over-specify MHEX 1. Aspen Plus and the nonsmooth model obtain the same driving force distribution at the solution. In addition, the isentropic compression power, $UA_{1/2}$ and $\Delta T_{\text{min,2}}$ all lie within <1% of the results of the nonsmooth model, whereas $\Delta T_{\text{min,1}}$ lies within <2%. A clear similarity can also be observed between the nonsmooth model and the solution from Aspen HYSYS, particularly in Figure 4.6(a) where the curves are almost identical. Nevertheless, the duty in MHEX 2 in HYSYS is shifted as a result of different ideal gas enthalpy correlations. HYSYS uses the Cavett equation for ideal gas enthalpy calculations, whereas Aspen Plus and the nonsmooth model both employ the ideal gas heat capacity equation (DIPPR 107) by Aly and Lee [83]. The effect of these enthalpy calculations are likely to be more critical at lower temperatures where a higher liquid content is present and the correlations are extrapolated. The temperature after the low temperature valve is 0.6 K lower compared to Aspen Plus and the nonsmooth simulation. HYSYS found the isentropic compression power to be 15.11 MW, a <1% deviation from the result of the nonsmooth model. Larger deviations were observed for the two UA-values, particularly for UA_2. The large deviation in calculated UA-value for MHEX 2 is due to the shift in the driving force distribution curves and a larger driving force at the low temperature side of the exchanger (see Figure 4.6(b)). Table 4.7 presents the resulting MHEX and compressor data for the HYSYS simulation.

Case II. The second case solves for both pressure levels of the refrigerant, the minimum approach temperature in both MHEXs and the LPR temperature out of MHEX 2. The model converged after 5 iterations and a total simulation time (including initialization) of 24.9 seconds to the solution $\Delta T_{\text{min,1}} = 8.00$ K, $\Delta T_{\text{min,2}} = 2.33$ K, $P_{\text{LP}} = 0.2064$ MPa, $P_{\text{HP}} = 1.355$ MPa and $T_{\text{LP,2}}^{\text{OUT}} = 211.72$ K. After post-processing, the UA-value of MHEX 1 was calculated to 3.68 MW/K. This solution requires 14.38 MW of isentropic compression power. Figures 4.7 and 4.8 show the composite curves and driving force plots for the solution. The driving force plots show that the solution of Case II exhibits comparatively smaller driving forces in MHEX 2 than Case I, resulting in the observed drop in compression power.

As in Case I, the model was simulated using Aspen Plus and Aspen HYSYS with the results from the nonsmooth model as inputs and letting the outlet temperature of the LPR vary. Figure 4.8 presents the driving force plots for both MHEXs, which display the same trend that was observed for Case I. Aspen Plus simulations

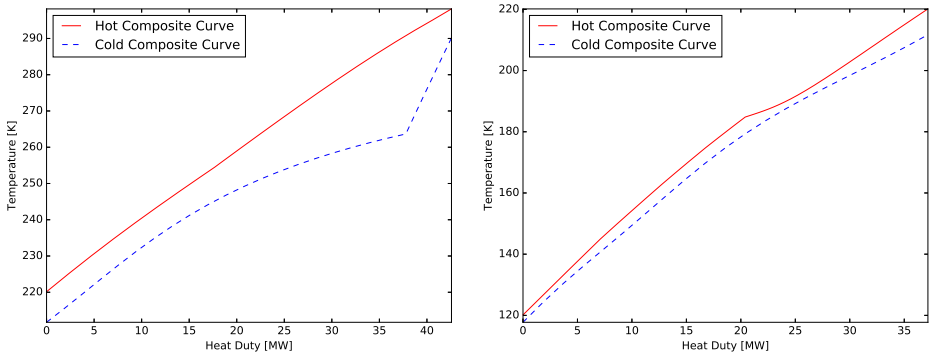

(a) **(b)**

Figure 4.7 (**a**) Composite curves for MHEX 1 in Example 2, Case II. (**b**) Corresponding for MHEX 2.

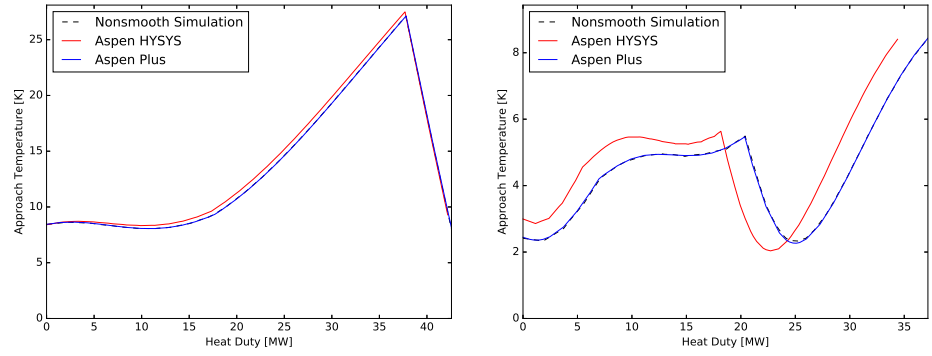

(a) **(b)**

Figure 4.8 (**a**) Driving force plot for MHEX 1 in Example 2, Case II. (**b**) Corresponding for MHEX 2.

Table 4.6 Summary of simulation results for Example 2.

Property	Case I	Case II
Compression power [MW]	15.19	14.38
F_{MR} [kmol/s]	2.858	2.928
P_{HP} [MPa]	1.513	1.355
P_{LP} [MPa]	0.202	0.2065
MHEX 1:		
UA_1 [MW/K]	3.07	3.68
$\Delta T_{\text{min,MHEX1}}$ [K]	8.00	8.00
MHEX 2:		
UA_2 [MW/K]	7.57	9.50
$\Delta T_{\text{min,2}}$ [K]	2.50	2.03
$T_{\text{LP,2}}^{\text{OUT}}$ [K]	209.91	211.72
Composition [mol %]		
Nitrogen	5.96	5.82
Methane	21.12	20.62
Ethane	40.33	39.37
n-Butane	32.58	34.19

obtain identical driving force curves as for the nonsmooth model. Aspen HYSYS shows good agreement with the nonsmooth model at high temperatures. However, the curves are again shifted relative to one another in MHEX 2 as a result of the different ideal gas enthalpy calculation methods. The Aspen Plus validation results in a required isentropic compression power of 14.37 MW. In addition, the UA-values were calculated to be $UA_1 = 3.674$ MW/K and $UA_2 = 9.52$ MW/K, both within 1% of the results of the nonsmooth model. The minimum approach temperatures were $\Delta T_{\text{min,1}} = 8.06$ K and $\Delta T_{\text{min,2}} = 2.27$ K.

The simulation results for the two cases in Aspen HYSYS are summarized in Table 4.7. As explained in more detail for Case I, Aspen HYSYS uses different correlations for ideal gas enthalpy calculations leading to shifted driving force distributions compared to Aspen Plus and the nonsmooth model. As observed in Figures 4.6 and 4.8, the shift is especially prominent at low temperatures and is likely due to the extrapolation of the enthalpy correlations. The same trend can also be observed in Table 4.7, in which the calculated UA_{MHEX2}-value deviates considerably from the value obtained by the nonsmooth model.

Table 4.7 Summary of results from Aspen HYSYS for Example 2.

Property	Case I	Case II
Compression power [MW]	15.11	14.31
UA_1 [MW/K]	2.95	3.54
$\Delta T_{\text{min},1}$ [K]	9.34	8.33
UA_2 [MW/K]	6.59	8.49
$\Delta T_{\text{min},2}$ [K]	3.02	2.04

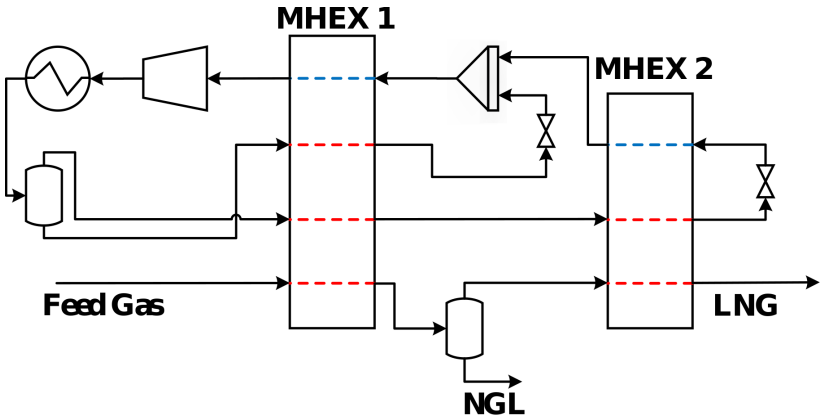

Figure 4.9 Hybrid process.

4.3 A single mixed refrigerant process with split refrigerant streams and intermediate NGL extraction (Example 3)

The last example looks at a hybrid version of the two previous processes. As in Example 1, the refrigerant stream is separated at the inlet of the first MHEX and the liquid product is subcooled to $T_{\text{HP},1}^{\text{OUT}}$, throttled and used for precooling the natural gas and the vapor product. The vapor product, on the other hand, is precooled and condensed to $T_{\text{HP},2}^{\text{OUT}}$, throttled and used for cooling the natural gas after NGL extraction. The LPR product from MHEX 2 is mixed with the refrigerant stream from MHEX 1 and used for precooling. The process flowheet is presented in Figure 4.9.

The refrigerant stream and MHEX data are given in Table 4.8. Example 3 uses the same initial refrigerant composition, high and low pressure levels and molar flowrate as in the first example. Furthermore, a rich natural gas composition is chosen to demonstrate the effect of NGL extraction. The model contains 61 vari-

Table 4.8 MHEX and refrigerant stream data for Example 3. Initial guesses for the unknown variables are placed in brackets.

Property	Set I	Set II	Set III
F_{MR} [kmol/s]	2.928	[2.928]	[2.928]
P_{HP} [MPa]	[1.713]	[0.829]	[2.500]
P_{LP} [MPa]	[0.260]	0.202	0.202
MHEX 1:			
$\Delta T_{\text{min,1}}$ [K]	[10.00]	5.00	5.00
$T^{\text{IN}}_{\text{HP,1}}$ [K]	298.15	298.15	298.15
$T^{\text{OUT}}_{\text{HP,1}}$ [K]	[230.15]	250.15	[260.15]
$T^{\text{OUT}}_{\text{LP,1}}$ [K]	290.15	[320.15]	[265.15]
MHEX 2:			
UA_2 [MW/K]	9.00	[6.50]	8.50
$\Delta T_{\text{min,2}}$ [K]	1.20	0.75	1.50
$T^{\text{OUT}}_{\text{HP,2}}$ [K]	120.15	120.15	120.15
$T^{\text{OUT}}_{\text{LP,2}}$ [K]	[230.15]	[245.15]	[248.15]
Composition [mol %]			
Nitrogen	5.82	[5.82]	5.82
Methane	20.62	[20.62]	20.62
Ethane	39.37	[39.37]	39.37
n-Butane	34.19	[34.19]	34.19

ables, 8 variables more than the process in Example 2 and 18 variables more than the process in Example 1. The model size increases only moderately with additional heat exchangers and refrigerant streams. This is due to the flash calculations and the stream segments in the two-phase region being solved separately from the overall model. Table 4.9 gives the full set of natural gas stream data used in the simulations. In the model, all hot streams are set to exit the MHEX at the same temperature. Equations (3.2) and (3.4) are used to model MHEX 1 as before, whereas Equation (3.3) is solved subsequently during post-processing. As a consequence, the MHEX models can be used to solve for five unknown variables in the process, where the following are considered in the analysis:

- **Case I - variable set**: $T^{\text{OUT}}_{\text{HP,1}}$, $\Delta T_{\text{min,1}}$, P_{HP}, P_{LP}, $T^{\text{OUT}}_{\text{LP,2}}$.
- **Case II - variable set**: $f_{\text{MR,n-butane}}$, $T^{\text{OUT}}_{\text{LP,1}}$, P_{HP}, $T^{\text{OUT}}_{\text{LP,2}}$, UA_2.
- **Case III -variable set**: $T^{\text{OUT}}_{\text{HP,1}}$, $T^{\text{OUT}}_{\text{LP,1}}$, P_{HP}, $T^{\text{OUT}}_{\text{LP,2}}$, F_{MR}.

Table 4.9 Natural gas stream data for Example 3.

Property	**Natural gas**
Flowrate [kmol/s]	1.00
Pressure [MPa]	3.50
Inlet temperature [K]	295.15
Outlet temperature [K]	120.15
Composition [mol %]	
Nitrogen	1.00
Methane	83.60
Ethane	7.93
Propane	3.71
n-Butane	1.90
iso-Butane	1.30
iso-Pentane	0.56

Case I. In this case, the minimum approach temperature, the HPR and thus NG temperature out of MHEX 1 (NGL extraction temperature), the high and low pressure levels of the refrigerant as well as the LPR temperature out of MHEX 2 are varied, while keeping the approach temperature and the UA value in MHEX 2 fixed. Changing the NGL extraction temperature is an interesting albeit challenging problem as it determines the LNG composition in MHEX2. The problem is also interesting from an optimization viewpoint as LNG specifications can place constraints on the optimum LNG/NGL split ratio. A solution is obtained with $T_{\text{HP,1}}^{\text{OUT}} = 234.99$ K, $\Delta T_{\text{min,1}} = 1.93$ K, $P_{\text{HP}} = 1.393$ MPa, $P_{\text{LP}} = 0.239$ MPa and $T_{\text{LP,2}}^{\text{OUT}} = 233.79$ K. The model converged to the solution after 6 iterations and a total simulation time (including initialization) of 38.5 seconds. This solution requires the UA-value for MHEX 1 to be $UA_1 = 6.43$ MW/K. The resulting isentropic compression power for the nonsmooth solution was 13.30 MW.

Figure 4.10 presents the hot and cold composite curves in each MHEX. A direct comparison with the results from Example 1 is not possible as the HPR temperature out of MHEX 1 is treated implicitly in the first example. Moreover, the model only solves for three variables, compared to five variables in this case, and thus two additional stream variables must be fixed in Example 1. Nevertheless, the composite curves show a similar trend as for the results in Figures 4.2(a) and 4.3(a). The curves for MHEX 2 approach one-another at three distinct locations resulting in the two peaks in Figure 4.11(b) that can also be observed in Figures 4.2(b) and 4.3(b).

The same process was simulated with Aspen Plus and Aspen HYSYS using the solution from the nonsmooth model as input and letting the LPR outlet temper-

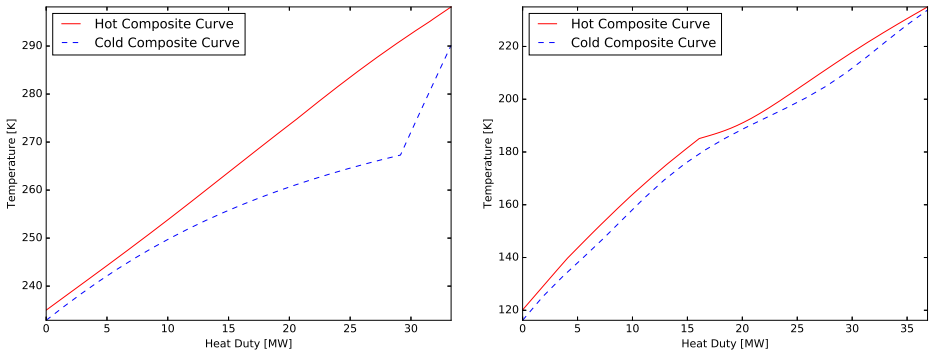

(a) **(b)**

Figure 4.10 (**a**) Composite curves for MHEX 1 in Example 3, Case I. (**b**) Corresponding for MHEX 2.

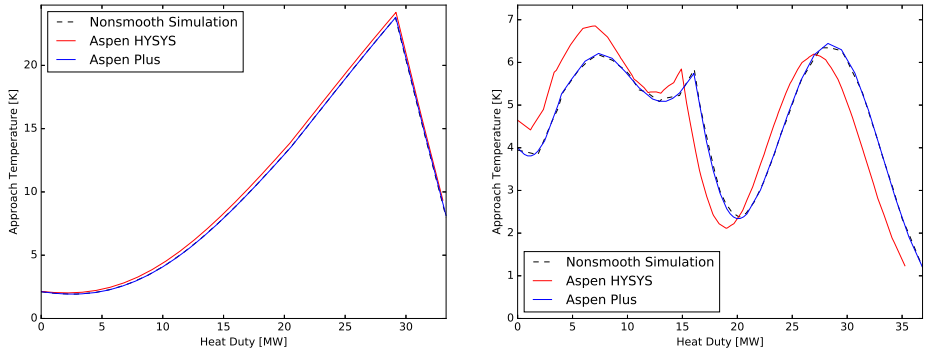

(a) **(b)**

Figure 4.11 (**a**) Driving force plot for MHEX 1 in Example 3, Case I. (**b**) Corresponding for MHEX 2.

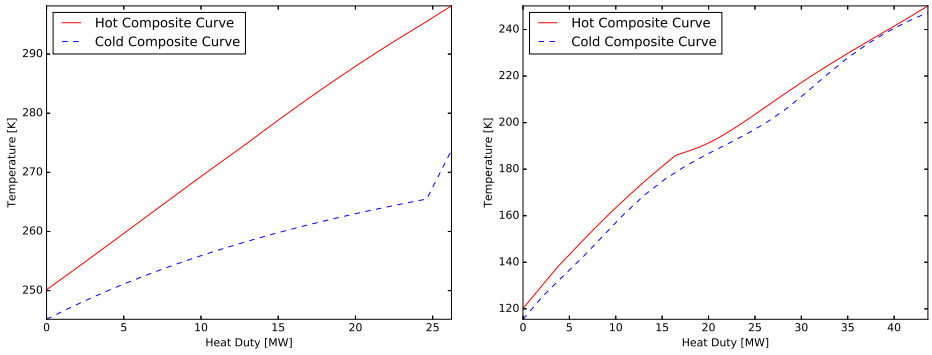

(a) **(b)**

Figure 4.12 (**a**) Composite curves for MHEX 1 in Example 3, Case II. (**b**) Corresponding for MHEX 2.

ature vary in both MHEXs. The driving force plots are presented along with the results from the nonsmooth simulation in Figure 4.11. Simulations in Aspen Plus resulted in an isentropic compression power requirement of 13.29 MW. The UA-values are $UA_1 = 6.44$ MW/K and $UA_2 = 9.04$ MW/K, both within 1% of the values determined by the nonsmooth model. Furthermore, $\Delta T_{\text{min},1} = 1.93$ K and $\Delta T_{\text{min},2} = 1.21$ K, whereas the respective values for the nonsmooth model are $\Delta T_{\text{min},1} = 1.93$ K and $\Delta T_{\text{min},2} = 1.20$ K. A summary of the HYSYS results is found in Table 4.11.

Case II. The second case varies the refrigerant composition, temperature into the compressor, the high pressure level, the LPR temperature out of MHEX 2 and the UA_2-value. The approach temperatures were set to $\Delta T_{\text{min},1} = 5.00$ K and $\Delta T_{\text{min},2} = 0.75$ K. The model converged after 6 iterations and a total simulation time (with initialization) of 48.1 seconds to a solution with $T_{\text{LP},1}^{\text{OUT}} = 273.72$ K, $T_{\text{LP},2}^{\text{OUT}} = 247.29$ K, $P_{\text{HP}} = 1.352$ MPa and $UA_2 = 13.75$ MW/K. At the specified approach temperature in MHEX 1, the UA_1-value was calculated to be 2.01 MW/K. The new refrigerant composition consists of 5.51 % nitrogen, 19.52 % methane, 37.27 % ethane and 37.70 % n-butane with $F_{\text{MR}} = 3.093$ kmol/s. Figure 4.12 presents the hot and cold composite curves for the process. This solution resulted in an isentropic compression power of 14.35 MW.

Figure 4.13 presents the driving force plots for the nonsmooth, Aspen Plus and Aspen HYSYS simulations in Case II. As before, Aspen Plus and the nonsmooth model obtain nearly identical results. The isentropic power requirement is 14.34 MW. In addition, the UA values of the two MHEXs are $UA_1 = 2.01$ MW/K and

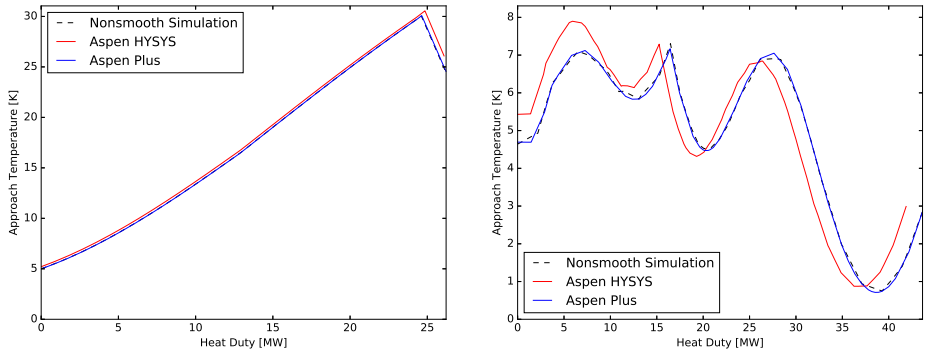

(a) **(b)**

Figure 4.13 (**a**) Driving force plot for MHEX 1 in Example 3, Case II. (**b**) Corresponding for MHEX 2.

$UA_2 = 14.236$ MW/K. The corresponding values for the nonsmooth model are $UA_1 = 2.01$ MW/K and $UA_2 = 13.75$ MW/K. The approach temperatures in the two MHEXs are $\Delta T_{\text{min},1} = 4.99$ K compared to 5.00 K fixed in the nonsmooth model and $\Delta T_{\text{min},2} = 0.71$ K compared to 0.75 K for the nonsmooth model. The results from Aspen HYSYS are presented in Table 4.11.

Case III. The last case solves for the HPR and thus NG temperature out of MHEX 1, the temperature into the compressor, the HPR pressure level, the LPR temperature out of MHEX 2 as well as the refrigerant flowrate. The flowsheet converged after 57.5 seconds and 9 iterations to a solution with $T^{\text{OUT}}_{\text{HP, 1}} = 245.80$ K, $T^{\text{OUT}}_{\text{LP,1}} = 284.74$ K, $P_{\text{HP}} = 1.565$ MPa, $T^{\text{OUT}}_{\text{LP,2}} = 243.66$ K and $F_{\text{MR}} = 2.808$ kmol/s. In addition, the UA_1 value at the solution is 2.15 MW/K, and the required isentropic compression power is 14.85 MW. The composite curves for the process are provided in Figure 4.14. A summary of the results for the three simulation cases is presented in Table 4.10.

The driving force plots for the nonsmooth model along with the results from Aspen Plus and Aspen HYSYS model are provided in Figure 4.15. The graphs show similar tendencies to what was observed in the two previous cases. Aspen Plus displays a nearly identical driving force distribution as the nonsmooth model, whereas the solution from Aspen HYSYS deviates from the other models at low temperatures. Aspen Plus calculates an isentropic compression power requirement of 14.84 MW. The UA-values are $UA_1 = 2.15$ MW/K and $UA_2 = 8.63$ MW/K, with $\Delta T_{\text{min},1} = 4.99$ K and $\Delta T_{\text{min},2} = 1.45$ K. The corresponding values for the nonsmooth model are $UA_1 = 2.15$ MW/K, $UA_2 = 8.50$ MW/K, $\Delta T_{\text{min},1} = 5.00$

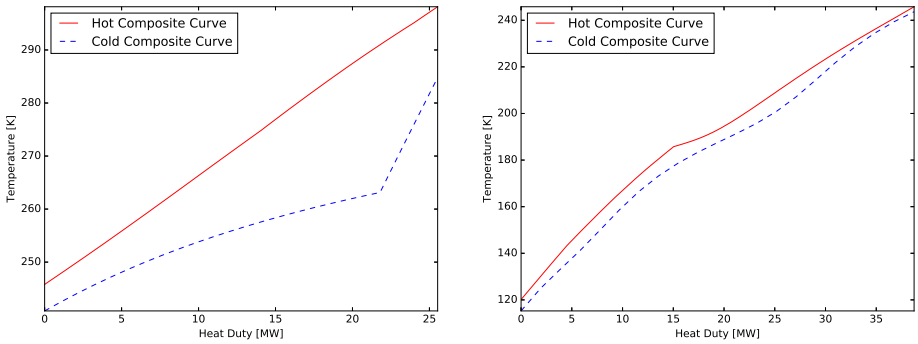

(a) **(b)**

Figure 4.14 (**a**) Composite curves for MHEX 1 in Example 3, Case III. (**b**) Corresponding for MHEX 2.

K and $\Delta T_{\text{min},2} = 1.50$ K.

Table 4.11 presents the results of the three cases in Aspen HYSYS. As in Example 2, Aspen HYSYS calculates a different driving force distribution than Aspen Plus and the nonsmooth model, which is a result of different correlations used for ideal gas enthalpy calculations. This mostly affect the calculations at low temperatures.

4.4 Conclusions

This chapter applied the nonsmooth multistream heat exchanger model to develop flowsheet models of three single mixed refrigerant processes of different complexity. Different cases for each process were analyzed, and the simulations were performed with the Peng-Robinson equation of state, by solving an algebraic equation system with a hybrid nonsmooth Newton solver as presented in Section 2.2. Various sets of unknown variables were considered in the analysis to study whether the nonsmooth models converged to feasible solutions. Few iterations were required to solve for each case and the results correlate well with values obtained from Aspen Plus. The nonsmooth model also managed to locate feasible solutions for more challenging problems, such as varying the refrigerant compositions that impact large portions of the flowsheet. On the other hand, both Aspen Plus and Aspen HYSYS were unable to solve these cases with the initial conditions given, instead only being able to validate the results of the nonsmooth simulation. This versatility makes the software suitable for simulation, as well as providing good initial starting points for flowsheet optimization. Validations performed by Aspen HYSYS achieved similar results as the nonsmooth model at high temperatures but

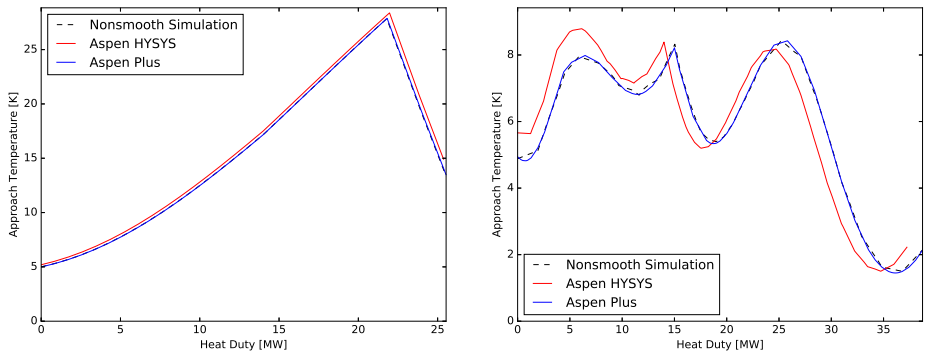

(a) **(b)**

Figure 4.15 (**a**) Driving force plot for MHEX 1 in Example 3, Case III. (**b**) Corresponding for MHEX 2.

Table 4.10 Summary of simulation results for Example 3.

Property	**Case I**	**Case II**	**Case III**
Compression power [MW]	13.30	14.35	14.85
F_{MR} [kmol/s]	2.928	3.093	2.808
P_{HP} [MPa]	1.393	1.352	1.565
P_{LP} [MPa]	0.239	0.202	0.202
MHEX 1:			
UA_1 [MW/K]	6.43	2.01	2.15
$\Delta T_{\text{min},1}$ [K]	1.93	5.00	5.00
$T_{\text{HP},1}^{\text{OUT}}$ [K]	234.99	250.15	245.80
$T_{\text{LP},1}^{\text{OUT}}$ [K]	290.15	273.72	284.79
MHEX 2:			
UA_2 [MW/K]	9.00	13.75	8.50
$\Delta T_{\text{min},2}$ [K]	1.20	0.75	1.50
$T_{\text{LP},2}^{\text{OUT}}$ [K]	233.79	247.29	243.66
Composition [mol %]			
Nitrogen	5.82	5.51	5.82
Methane	20.62	19.52	20.62
Ethane	39.37	37.27	39.37
n-Butane	34.19	37.70	34.19

Table 4.11 Summary of results from Aspen HYSYS for Example 3.

Property	**Case I**	**Case II**	**Case III**
Compression power [MW]	13.23	14.27	14.76
UA_1 [MW/K]	6.07	1.95	2.07
$\Delta T_{\text{min},1}$ [K]	2.02	5.21	5.19
UA_2 [MW/K]	8.68	12.70	8.08
$\Delta T_{\text{min},2}$ [K]	1.24	0.88	1.51

deviated from the solution at lower temperatures. The disparity in the solutions is caused by the nonsmooth models and Aspen Plus using another ideal gas enthalpy correlation than Aspen HYSYS. In particular, this affected the total duty and calculated area of the low temperature MHEX in the models, which emphasizes the importance of matching the physical property correlations before comparing simulation and optimization results from different models. In particular, this becomes a problem when comparing process performance to other studies that perhaps use the same EOS but other physical property correlations. As stream segments for the two-phase region are handled separately in nested subroutines and the size of the pinch location algorithm remains unchanged irrespective of the number of stream segments, the model size increases only moderately with additional streams and heat exchangers. This makes the nonsmooth framework suitable for handling larger and more complex LNG liquefaction processes. Although the single mixed processes here are more complex than the original PRICO process, with additional MHEXs and/or split refrigerant streams to better approximate the cooling curve of natural gas, they still feature a relatively simple and necessarily inefficient design that is only suitable for small-scale LNG production. Therefore, the ability of this new flowsheeting strategy of also developing robust simulation models for large-scale processes is paramount in the effort of avoiding the dependency on commercial simulation tools. The next chapter presents the development of nonsmooth simulation models for two different dual mixed refrigerant processes.

Chapter 5

Nonsmooth simulation models for complex Dual Mixed Refrigerant processes

Abstract

In this chapter, liquefaction processes suitable for large-scale production of liquefied natural gas, more specifically dual mixed refrigerant processes, are discussed. Simulation models for two different dual mixed refrigerant processes are covered in detail. The first features a simple configuration of two PRICO processes in cascade, whereas the second is a configuration of the AP-DMR process with and without NGL extraction, but with single stage compression for the two refrigeration cycles.

This chapter is based on the following publications:

- M. Vikse, H. A. J. Watson, T. Gundersen, and P. I. Barton. Simulation of dual mixed refrigerant natural gas liquefaction processes using a nonsmooth framework. *Processes*, 6(10):193, 2018.

- M. Vikse, H. A. J. Watson, P. I. Barton, and T. Gundersen. Simulation of a Dual Mixed Refrigerant LNG Process using a Nonsmooth Framework. *Computer Aided Chemical Engineering*, 44:391-396, 2018.

In the preceeding chapter, the nonsmooth simulation framework was used to develop and analyze different single mixed refrigerant (SMR) models under conditions for which the commercial simulator Aspen Plus failed to obtain results. In particular, the additional two unknowns computed by Equations (3.3) and (3.4) add versatility, making it possible to obtain feasible operating points in cases where more than one operating parameter is unknown to the designer. Moreover, the ability to solve for other process conditions than the inlet/outlet temperatures of the exchanger, such as pressure levels and compositions, made it easier to find feasible operating points without having to resort to flowsheet optimization. Nevertheless, single-mixed refrigerant processes, despite more complex than the PRICO, consist of relatively few auxilary components, refrigerant mixtures and MHEXs. The processes are primarily suitable for small-scale LNG liquefaction, and larger and more complex configurations are necessary to achieve additional energy savings. Dual mixed refrigerant processes serve as an interesting alternative that offer higher efficiencies and a lower equipment count than alternative processes for large-scale processes for natural gas. This chapter develops simulation models for two different DMR processes. The first example constitutes a simple design with two PRICO cycles that are organized in cascade. Furthermore, a natural gas liquid (NGL) separator is added for the extraction of heavier hydrocarbons. The second DMR process is a version of the AP-DMR process [52], where a PRICO cycle is used for precooling the natural gas upstream of a spiral wound heat exchanger. The main focus here is on the liquefaction part of the process, and thus, not the compression scheme. Therefore, only a single-stage compression with aftercooling is included in the model. Different case studies are presented, each solving for different sets of unknown variables. The variables considered in the analysis are the high and low pressure levels, refrigerant flowrates, inlet and outlet temperatures from the MHEXs, and refrigerant compositions for the warm and cold mixed refrigerant. For the MHEX specifications, both the minimum temperature difference and the heat exchanger conductance have been included. The following nomenclature is used for the parameters and unknown variables in the models:

- Pressure level of the (warm/cold) high pressure refrigerant: $P_{\text{HP,(W/C)}}$.
- Pressure level of the (warm/cold) low pressure refrigerant: $P_{\text{LP,(W/C)}}$.
- Inlet/outlet temperatures of the high pressure refrigerant (equal to the natural gas stream): $T_{\text{HP}}^{\text{IN/OUT}}$.
- Inlet/outlet temperatures of the low pressure refrigerant: $T_{\text{LP}}^{\text{IN/OUT}}$.
- Molar flowrate of the (warm/cold) refrigerants: $F_{\text{(W/C)}}$.

- Molar flowrate of component i in (warm/cold) refrigerants: $f_{(\mathrm{W/C}),i}$.

The models were written using Julia v0.6.0 and run on a Dell Latitude E5470 laptop in the Ubuntu v16.10 environment with an Intel Core i7-6820HQ CPU at 2.7 GHz and 8.2 GB RAM. Simulations were done for the Peng–Robinson equation of state where the property parameters were taken from Aspen Plus [9]. The same partitioning of the single-phase and two-phase substreams as in Chapter 4 were used to ensure an accurate representation of the process streams. Moreover, the overall flowsheet convergence tolerance was set to $\|\mathbf{y}\|_\infty < 10^{-5}$, whereas the tolerance for the individual flash calculations was set to $\|\mathbf{y}\|_\infty < 10^{-8}$.

5.1 A simple DMR process with cascading PRICO cycles (Example 1)

The first DMR process studied in this paper is a simple configuration with cascading PRICO cycles for the warm and cold mixed refrigerants. This cascaded cycle consists of two MHEXs as well as an NGL separator for the extraction of heavier hydrocarbons. The feed gas is sent to the process at 295.15 K where it is precooled by a warm mixed refrigerant cycle consisting of ethane, propane, and n-butane. The feed gas and the refrigerants exit the heat exchanger at a temperature of $T_{\mathrm{HP,1}}^{\mathrm{OUT}}$. The feed gas is then sent to the NGL separator, where heavier hydrocarbons are extracted for further fractionation and/or export, before the gas enters MHEX 2 for liquefaction. The cold mixed refrigerant consists of a lighter refrigerant mixture consisting of nitrogen, methane, ethane, and propane for the liquefaction of the natural gas. Along with the feed gas, the cold mixed refrigerant (CMR) is precooled in the warm mixed refrigerant (WMR) PRICO cycle before it enters the cold heat exchanger. A process flowsheet of the DMR process is presented in Figure 5.1.

The parameter values and initial guess values for the unknown variables are provided in Table 5.1. The parameter values were selected such that Aspen Plus failed to converge to a feasible solution using its standard MHEX model with one equation. Essentially, the Aspen Plus model only solves the overall energy balance in Equation (3.2) for a single unknown temperature (chosen here as the inlet temperatures to the compressors). Refrigerant compositions and pressures cannot be handled as unknown variables in these models. This results in less versatility in cases where pressure, compositions, and multiple temperatures must be adjusted to find a feasible design.

The model contains 61 unknowns, five of which are provided by the solution of the MHEX equations. The remaining 56 variables are the temperatures of the in-

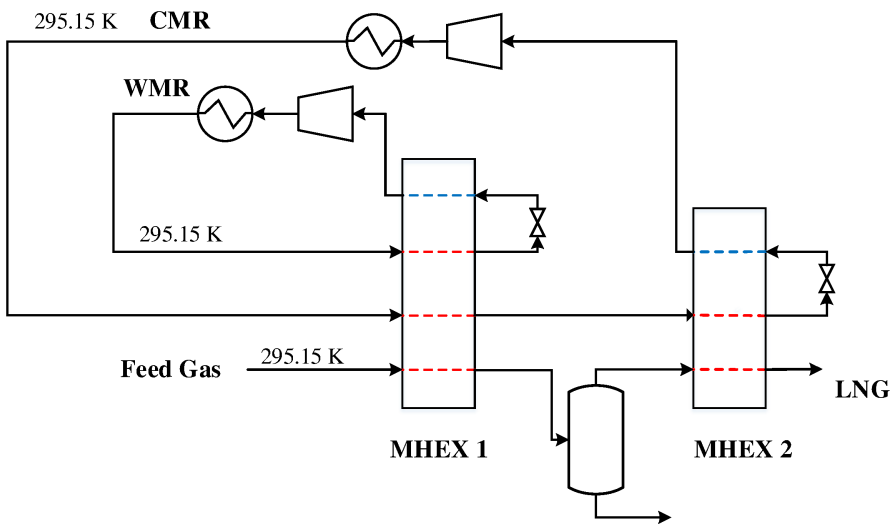

Figure 5.1 The dual mixed refrigerant (DMR) model with cascading PRICO cycles for the warm and cold mixed refrigerant streams.

termediate stream segments for the single phase regions. As flash calculations are decoupled and solved separately, the model size is independent of the number of stream segments in the two-phase region. A two-equation model is used for MHEX 1 as the UA-value depends on the stream results from MHEX 2. Fixing the area prior to simulation can therefore be challenging. Therefore, the heat exchanger conductance value is instead calculated through post-processing. The simulations were carried out for a rich feed gas composition with 1.00 mol % nitrogen, 85.60 mol % methane, 4.93 mol % ethane, 3.71 mol % propane, 2.90 mol % n-butane, 1.30 mol % i-butane, and 0.56 mol % n-pentane at a pressure of 4 MPa and flowrate of 1.0 kmol/s where both the refrigerant mixtures and the feed gas enter the precooling MHEX at a temperature of 295.15 K, as indicated in Figure 5.1. Two simulation cases were constructed, solving for different sets of unknown variables:

- **Case I:** $P_{\text{LP,W}}$, $P_{\text{HP,C}}$, $f_{\text{W,propane}}$, $T_{\text{LP,2}}^{\text{OUT}}$, UA_2.
- **Case II:** $P_{\text{HP,W}}$, $P_{\text{LP,C}}$, F_{C}, $\Delta T_{\text{min,1}}$, $\Delta T_{\text{min,2}}$.

Case I: This case is solved for a variable WMR composition, an unknown inlet temperature to the CMR compressor, the heat exchanger conductance in MHEX 2, as well as the low pressure level P_{LPW} and high pressure level P_{HPC} of the warm and cold mixed refrigerants, respectively. The refrigerant composition was

Table 5.1 Multistream heat exchanger (MHEX) and refrigerant stream data for Example 1. For unknown variables, the value listed is an initial guess.

Property	Value	Property	Value
η	0.8	UA_2 (MW/K)	3.0
$\Delta T_{\text{min},1}$ (K)	3.0	$\Delta T_{\text{min},2}$ (K)	3.0
F_{W} (kmol/s)	1.65	F_{C} (kmol/s)	1.55
$P_{\text{HP,W}}$ (MPa)	1.67	$P_{\text{HP,C}}$ (MPa)	4.30
$P_{\text{LP,W}}$ (MPa)	0.42	$P_{\text{LP,C}}$ (MPa)	0.25
$T^{\text{OUT}}_{\text{HP},1}$ (K)	245.15	$T^{\text{OUT}}_{\text{HP},2}$ (K)	120.15
$T^{\text{OUT}}_{\text{LP},1}$ (K)	290.15	$T^{\text{OUT}}_{\text{LP},2}$ (K)	240.15
Composition (mol %):			
Ethane	47.83	Nitrogen	10.00
Propane	34.17	Methane	43.80
n-Butane	18.00	Ethane	35.20
		Propane	11.00

changed in the model by varying the component molar flowrate of propane $f_{\text{W,propane}}$. A solution was obtained after four iterations and a total simulation time of 62.7 s, including initialization. The model converged to a solution with $P_{\text{LP,W}} = 0.57$ MPa, $P_{\text{HP,C}} = 6.53$ MPa and $T^{\text{OUT}}_{\text{LP},2} = 242.15$ K. The design resulted in a total compression work of 21.33 MW, with heat exchanger conductance values of $UA_1 = 2.69$ MW/K and $UA_2 = 1.89$ MW/K. The work distribution of the two compressors was 16.79 MW for compressing the CMR and 4.54 MW for compressing the WMR. A new WMR composition was obtained consisting of 53.30 mol % ethane, 26.64 mol % propane and 20.06 mol % n-butane with a corresponding molar flowrate of 1.48 kmol/s. Figure 5.2 presents the composite curves and driving force plot for the solution.

Case II: This case is solved for the flowrate of the CMR, the minimum approach temperatures in both MHEXs, and the high pressure and low pressure levels of the warm and cold refrigerant mixtures, respectively. A solution was obtained after 13 iterations with $P_{\text{HP,W}} = 1.58$ MPa, $P_{\text{LP,C}} = 0.388$ MPa, $F_{\text{C}} = 1.952$ kmol/s, and minimum approach temperatures of 5.00 K and 3.15 K for MHEX 1 and 2, respectively. The design resulted in a total compressor work of 20.56 MW, and a heat exchanger conductance value UA_1 of 2.04 MW/K. Compressing the CMR required a total of 14.10 MW, whereas compressing the WMR required only 6.46 MW. The total simulation time, including initialization of the model, was 102.5 s. The composite curves and driving force plot for the process are presented in

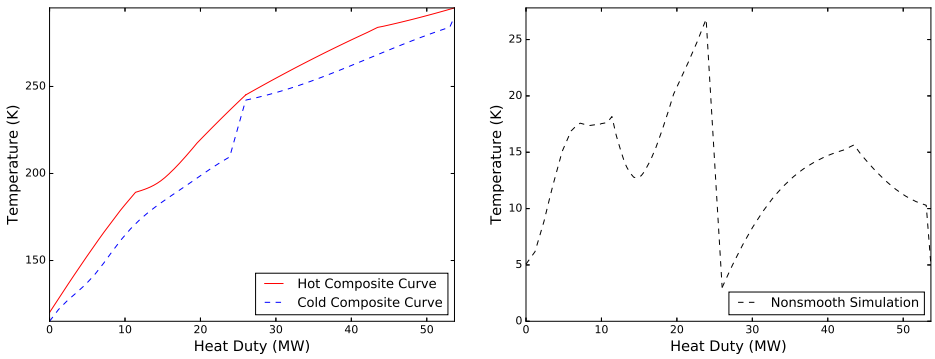

(a) **(b)**

Figure 5.2 (**a**) Composite curves for the feasible design in Case I. (**b**) The corresponding driving force plot.

Figure 5.3. As can be seen, both solutions have a similar trend, although the cold low pressure refrigerant superheating is noticeably larger in Case I. This results in lower driving forces in MHEX 1, but also introduces a larger temperature difference at the cold end of the process, leading to a higher compression power. A discussion on superheating and its effect on design of DMR processes was made by Kim and Gundersen [84].

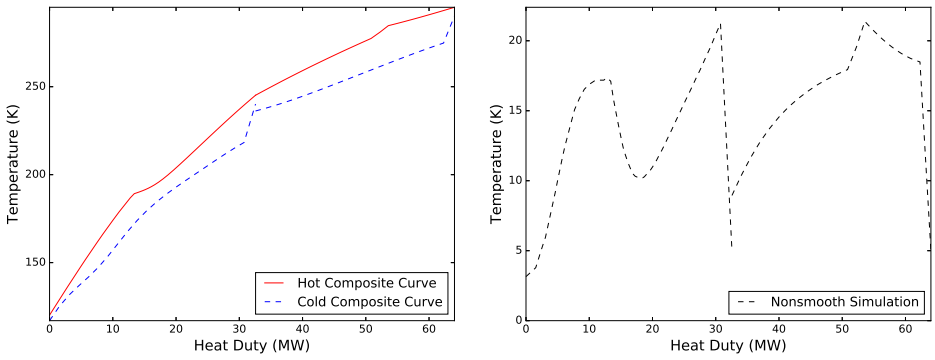

(a) **(b)**

Figure 5.3 (**a**) Composite curves for the feasible design in Case II. (**b**) The corresponding driving force plot.

5.2 The AP-DMR process (Example 2)

A more complex DMR design is presented in Figure 5.4. Instead of having two cascading PRICO cycles, this design features a SWHX (represented by MHEX 2 and MHEX 3 in Figure 5.4) for the CMR where the refrigerant is separated after precooling to provide cooling at different temperature levels. The vapor product, which consists mainly of the light components nitrogen and methane, is liquefied, subcooled and throttled to provide cooling in the cold MHEX 3. At the same time, the liquid product is subcooled, throttled and mixed with the low pressure refrigerant from MHEX 3 and used to cool the feed gas in the intermediate MHEX 2. Since part of the refrigerant mixture only circulates in the warm end of the SWHX, the overall molar flowrate and thus the required heat transfer area decrease.

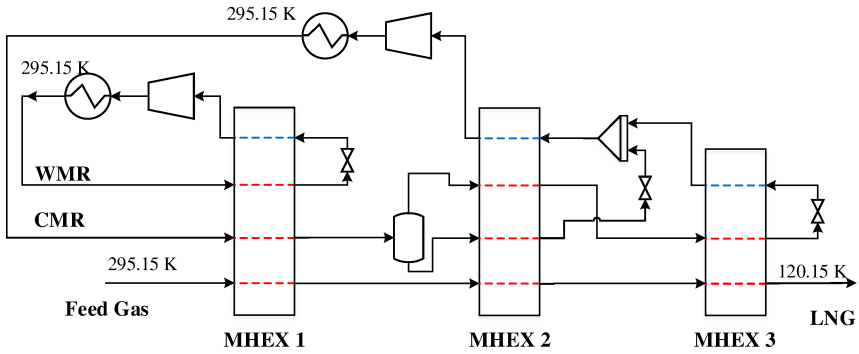

Figure 5.4 The DMR process with a spiral-wound heat exchanger (SWHX) for the cold mixed refrigerant.

The refrigerant streams and MHEX data for the DMR model are given in Table 5.2. Again, the parameter values were selected such that a solution could not be obtained using the commercial simulation tool Aspen Plus. A feed gas with 1.00 mol % nitrogen, 91.60 mol % methane, 4.93 mol % ethane, 1.71 mol % propane, 0.35 mol % n-butane, 0.40 mol % i-butane, and 0.01 mol % i-pentane at a pressure of 5.5 MPa and a flowrate of 1.0 kmol/s was used in the simulations.

The simulation model with three MHEXs consists of 96 variables and exhibits seven unknowns. Again, these unknowns may be used to solve for any process stream variable such as pressure, composition, flowrate, or temperature, as well as important MHEX data such as the minimum temperature difference and the heat exchanger conductance. Specifying the UA-value in MHEXs 1 and 2 is challenging as it depends on the solution of MHEX 3. Therefore, as for Example 1, the UA-values are calculated during post-processing to make problem specification easier. Two simulation cases were constructed solving for the following sets of

Table 5.2 MHEX and refrigerant stream data for Example 2. For unknown variables, the value listed is an initial guess.

Property	**Value**	**Property**	**Value**
η	1.0	$\Delta T_{\text{min,1}}$ (K)	4.0
UA_3 (MW/K)	0.3	$\Delta T_{\text{min,2}}$ (K)	11.0
		$\Delta T_{\text{min,3}}$ (K)	4.0
F_{W} (kmol/s)	1.55	F_{C} (kmol/s)	1.45
$P_{\text{HP,W}}$ (MPa)	1.67	$P_{\text{HP,C}}$ (MPa)	4.85
$P_{\text{LP,W}}$ (MPa)	0.50	$P_{\text{LP,C}}$ (MPa)	0.25
$T^{\text{OUT}}_{\text{HP,1}}$ (K)	240.15	$T^{\text{OUT}}_{\text{HP,2}}$ (K)	170.15
$T^{\text{OUT}}_{\text{HP,3}}$ (K)	120.15	$T^{\text{OUT}}_{\text{LP,1}}$ (K)	280.15
$T^{\text{OUT}}_{\text{LP,2}}$ (K)	230.15	$T^{\text{OUT}}_{\text{LP,3}}$ (K)	145.15
Composition (mol %):			
Ethane	47.83	Nitrogen	7.00
Propane	34.17	Methane	41.80
n-Butane	18.00	Ethane	33.20
		Propane	18.00

unknown variables:

- **Case I:** $P_{\text{LP,W}}$, $P_{\text{HP,W}}$, P_{LPC}, $T^{\text{OUT}}_{\text{HP,2}}$, $T^{\text{OUT}}_{\text{LP,3}}$, F_{C}, $\Delta T_{\text{min,2}}$.
- **Case II:** $P_{\text{LP,W}}$, $P_{\text{HP,C}}$, $T^{\text{OUT}}_{\text{HP,2}}$, $T^{\text{OUT}}_{\text{LP,3}}$, $f_{\text{W, ethane}}$, $\Delta T_{\text{min,2}}$, UA_3.

Case I: This case is solved for both pressure levels of the WMR, the low pressure level and refrigerant flowrate of the CMR, the feed gas and high pressure refrigerant temperatures out of MHEX 2, the low pressure refrigerant temperature out of MHEX 3, as well as the minimum approach temperature in MHEX 2. A solution was obtained after six iterations and a total simulation time of 83.0 s with $P_{\text{LPW}} = 0.43$ MPa, $P_{\text{HP,W}} = 1.62$ MPa, $P_{\text{LP,C}} = 0.27$ MPa, $T^{\text{OUT}}_{\text{HP,2}} = 155.34$ K, $T^{\text{OUT}}_{\text{LP,3}} = 151.34$ K, $F_{\text{C}} = 1.42$ kmol/s, and $\Delta T_{\text{min,2}} = 6.68$ K. The UA-values were calculated to be 1.99 MW/K and 2.12 MW/K for MHEXs 1 and 2, respectively. The obtained feasible design resulted in a combined compression work of 14.40 MW, where 9.76 MW was needed to compress the CMR, and 4.64 MW was used to compress the WMR. Figure 5.5 presents the composite curves and driving force distribution in the MHEXs at the solution.

Case II: This case is solved for the low pressure level of the WMR, high pressure

level of the CMR, the natural gas and high pressure refrigerant temperatures out of MHEX 2, the low pressure refrigerant temperature out of MHEX 3, the composition of the WMR, the minimum temperature difference in MHEX 2, and the heat exchanger conductance value for MHEX 3. The model converged after three iterations and a total simulation time of 64.2 s to a solution with $P_{\text{LP,W}} = 0.44$ MPa, $P_{\text{HP,C}} = 4.59$ MPa, $T^{\text{OUT}}_{\text{HP,2}} = 161.03$ K, $T^{\text{OUT}}_{\text{LP,3}} = 157,03$ K, $\Delta T_{\text{min,2}} = 7.88$ K, and $UA_3 = 0.33$ MW/K. A new WMR composition was obtained with 49.24 mol % ethane, 33.24 mol % propane, and 17.51 mol % n-butane and a total molar flowrate of 1.59 kmol/s. The feasible design required a total compression power of 14.85 MW, where 10.08 MW was spent compressing the CMR and 4.76 MW was used to compress the WMR. The heat exchanger conductance values were calculated during post-processing to be $UA_1 = 2.02$ MW/K and $UA_2 = 1.84$ MW/K, respectively. The composite curves and driving force plot for the process are presented in Figure 5.6.

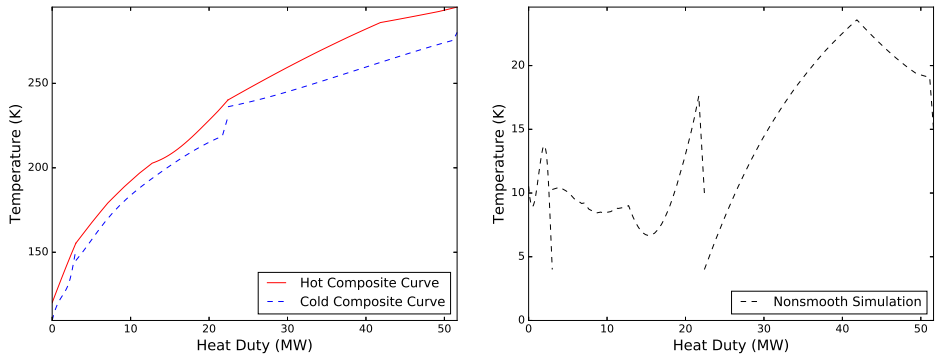

(a) **(b)**

Figure 5.5 (**a**) Composite curves for the feasible design in Case I. (**b**) The corresponding driving force plot.

Case III: This case included an NGL separator for the extraction of heavier hydrocarbons (see Figure 5.7). The case solved for the same set of variables as in Case I and with the same initial guesses and parameter values as given in Table 5.2. As for the previous examples, the model was solved from an initial guess at which Aspen Plus obtained no feasible solutions with the built-in MHEX module. Rich feed gas compositions at a reduced pressure of 4.0 MPa were used to ensure adequate separation. Simulations were carried out at three different compositions with varying methane contents (Table 5.3).

Driving force distributions for the three solutions are provided in Figure 5.8. Solu-

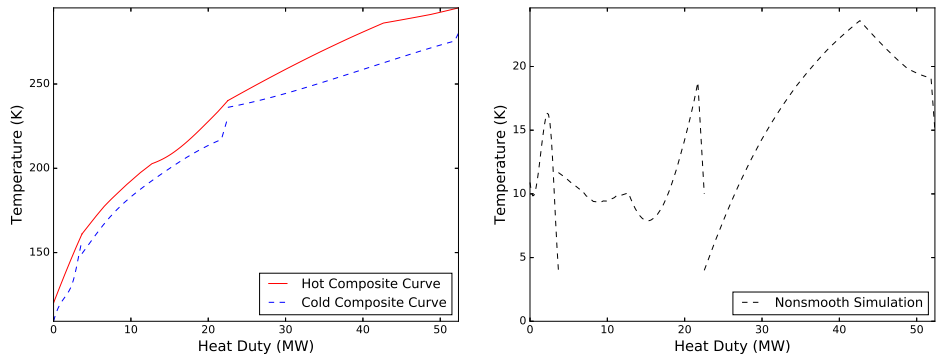

(a) **(b)**

Figure 5.6 (**a**) Composite curves for the feasible design in Case II. (**b**) The corresponding driving force plot.

Table 5.3 Natural gas compositions for Case III.

	Compostion I:	**Composition II:**	**Composition III:**
Nitrogen (mol %)	2.00	2.00	2.00
Methane (mol %)	85.60	87.60	89.60
Ethane (mol %)	6.93	5.93	4.93
Propane (mol %)	3.71	2.71	1.71
n-Butane (mol %)	1.35	1.35	1.35
i-Butane (mol %)	0.40	0.40	0.40
i-Pentane (mol %)	0.01	0.01	0.01

tions were obtained for all three cases within a few iterations. The first two feed gas compositions converged after seven iterations and total simulation times of 85.6 s and 86.4 s for compositions I and II, respectively. The third case converged after six iterations and a total simulation time of 82.1 s. All three solutions exhibited similar driving force profiles, with temperature differences varying mainly in the intermediate MHEX. The same trend can also be seen from the simulation results in Table 5.4, where the main differences between the three solutions are the UA and $\Delta T_{\min}$ values for the intermediate MHEX.

5.3 Conclusions

This chapter developed simulation models for two different dual mixed refrigerant processes using a nonsmooth framework and the multistream heat exchanger

Table 5.4 Simulation results for the DMR process with NGL extraction.

	Comp. I:	**Comp. II:**	**Comp. III:**
Total work (MW)	14.99	15.11	15.13
W_{C} (MW)	10.26	10.40	10.43
W_{H} (MW)	4.73	4.71	4.70
UA_1 (MW/K)	2.07	2.05	2.03
UA_2 (MW/K)	2.63	2.87	3.41
P_{LPW} (MPa)	0.43	0.43	0.43
P_{HPW} (MPa)	1.66	1.66	1.65
P_{LPC} (MPa)	0.26	0.25	0.25
$T_{\mathrm{HP,2}}^{\mathrm{OUT}}$ (K)	158.22	157.95	157.50
$T_{\mathrm{LP,3}}^{\mathrm{OUT}}$ (K)	154.22	153.95	153.50
F_{C} (kmol/s)	1.46	1.47	1.48
$\Delta T_{\mathrm{min,2}}$ (K)	3.69	3.14	2.20
LNG comp. (mol %):			
Nitrogen	2.08	2.05	2.03
Methane	88.04	89.24	90.61
Ethane	6.50	5.68	4.81
Propane	2.67	2.15	1.48
n-Butane	0.52	0.65	0.81
i-Butane	0.19	0.23	0.27
i-Pentane	0.00	0.00	0.00
F_{LNG} (kmol/s)	0.96	0.97	0.98

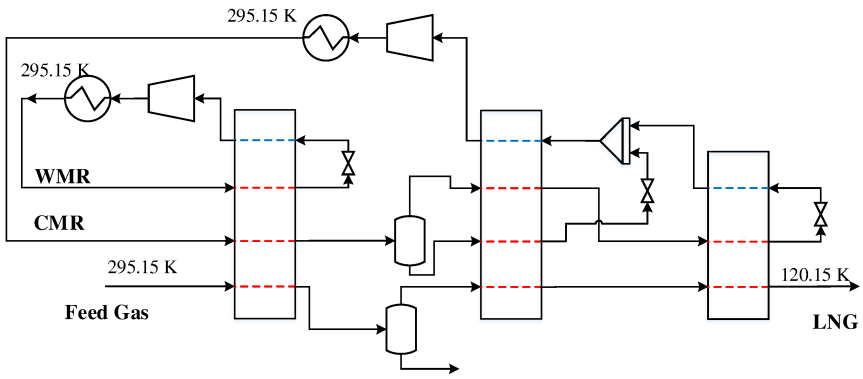

Figure 5.7 The DMR process in Example 2 with natural gas liquid (NGL) extraction.

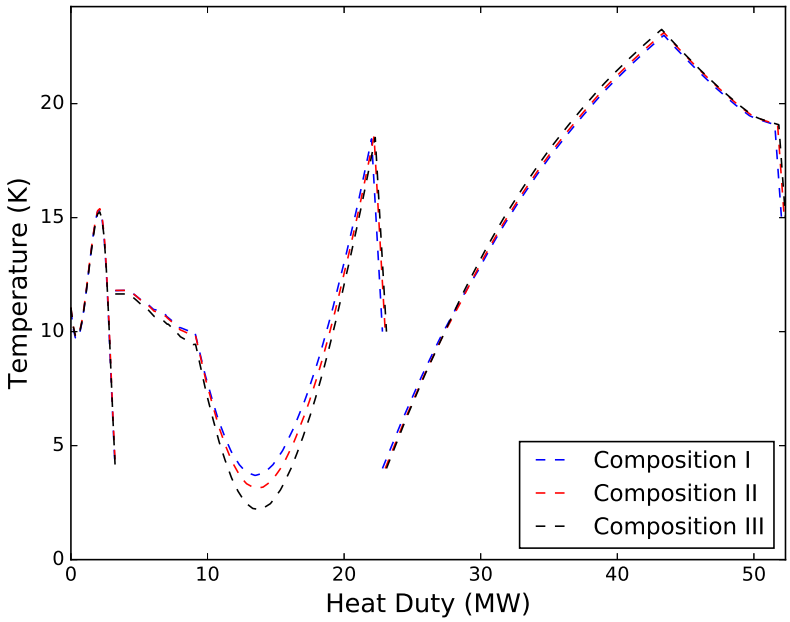

Figure 5.8 Driving force distributions for the DMR process with NGL extraction.

model from Chapter 3. Different operating variables were studied in the simulation cases, such as pressure levels, component molar flowrates, temperatures, minimum approach temperature and heat exchanger conductance. Although the processes are significantly more complex than in the previous chapter, the relative size of the models are still manageable, something that can be accredited to

the implementation of a hybrid framework, where large portions of the operations are diverted to subroutines that are converged at every iteration. As a result, these more complex models consist of 61 unknowns in Example 1, and 96 unknowns for Example 2. The conventional approach in the literature for simulating large-scale liquefaction processes has been to rely on commerical process simulators such as Aspen HYSYS (see Chapter 3), and the custom multistream heat exchanger models have so far only been implemented in relatively simple SMR processes. This work, thus presents a first attempt at looking beyond to more commercially interesting designs. All the cases successfully converged within a total simulation time of 100 s, including initialization of the models. Furthermore, each case was constructed such that Aspen Plus failed to obtain a feasible solution using the same starting point and initial values as the nonsmooth model. The use of additional unknowns and the possibility of varying ostensibly difficult process stream variables, such as compositions makes the tool more versatile and capable of handling even complex LNG liquefaction processes.

So far, process simulation has been of main concern in this thesis, with flowsheet models developed for both small-scale and large-scale liquefaction plants. Process simulation represents a powerful tool for the engineer to study different feasible operations, as well as for conducting sensitivity analysis around the current design point. Nevertheless, flowsheet optimization is essential in order to obtain significant improvement in design and operating points. Optimization of the different single mixed refrigerant processes was carried out in parallel and is summarized in a publication by Watson *et al.* [65]. Using IPOPT [85] as a solver, with sensitivities provided as part of the automatic differentiation procedure for nonsmooth functions that is embedded in the flowsheet models, improvements were made to all three models. In addition, the simulation results provided good starting points for the optimizer, thus improving convergence. The next chapter will conclude the LNG part of the thesis by conducting flowsheet optimization for the AP-DMR process.

Chapter 6

Optimization of a Nonsmooth Dual Mixed Refrigerant Model

Abstract

With flowsheet models now constructed for dual mixed refrigerant processes, what remains is to apply flowsheet optimization. In this chapter, the primal-dual interior point algorithm IPOPT supplied with the sensitivity information given by the LD-derivatives, is used to optimize the configuration of the AP-DMR process from Chapter 5. The results are compared with those obtained using the current state-of-the-art tools for handling large-scale liquefaction cycles, namely a commercial simulator connected to an external stochastic search algorithm.

This chapter is based on the publication:

- M. Vikse, H. A. J. Watson, D. Kim, P. I. Barton, and T. Gundersen. Optimization of a dual mixed refrigerant process using a nonsmooth approach. *In review*.

Until now, the main concern in this thesis has been on flowsheet simulation using a nonsmooth equation solver to obtain values for a set of unknown process variables. Simulation is indeed an important task allowing for the study of different operating points, as well as leaving the designer with powerful insight into the different driving mechanisms in the design. More importantly, however, the simulation model provides a basic design of which further improvements can be explored through optimization. The ability of conducting optimization on existing flowsheet models is essential in any process simulation tool, as relations between different variables remain shrouded in large models, making manual optimization difficult. Optimization of the single mixed refrigerant models presented in Chapter 4 was addressed in a publication by Watson *et al.* [65] using the primal-dual interior point algorithm IPOPT [85]. As indicated in Chapter 3, model size remains an important issue in multistream heat exchanger models. An inflation in the number of binary variables or complementarity constraints for handling phase detection and enforcing the second law have resulted in these models only being used for studying the relatively simple PRICO process. For larger and more complex processes, literature still rely on commercial simulation tools, e.g. Aspen HYSYS, sometimes with an external optimizer, accompanied with the limitations these entail. The hybrid nature of the nonsmooth modeling framework, however, allowed for the construction of relatively complex models of dual mixed refrigerant processes while retaining a favorable scaling. As a result, feasible operating points could be obtained even for these complex cycles without a large increase in solver time. Here, the optimization of the AP-DMR model in Chapter 5 is presented. Optimization studies of these processes have mainly relied on derivative free solvers. Others have used SQP, although it suffers from a low success rate, and require significant fine tuning of the model [80]. Optimization cases with constraints on the total heat exchanger conductance $UA_{\max}$ and minimum approach temperature $\Delta T_{\min}$ are considered in the analysis, and the performance of the algorithm is compared with the state-of-the-art, i.e. using Aspen HYSYS together with particle swarm optimization (PSO) [86, 87].

6.1 The Dual Mixed Refrigerant process

A flowsheet of the dual mixed refrigerant process optimized in this chapter is provided in Figure 6.1, along with the decision variables considered for optimization. A feasible process design is used as an initial point for the optimizer. The operating point is obtained through process simulation with the following unknown variables: $T^{\text{OUT}}_{\text{HP,1}}$, $T^{\text{OUT}}_{\text{HP,2}}$, $T^{\text{OUT}}_{\text{LP,3}}$, $P_{\text{LP,C}}$, F_{C}, $f_{\text{W, ethane}}$ and $\Delta T_{\text{min,2}}$ [88].

The model converged to a solution within three iterations and a total simulation time of 68.7 s. At an isentropic efficiency of 0.8 for the compressors, the ba-

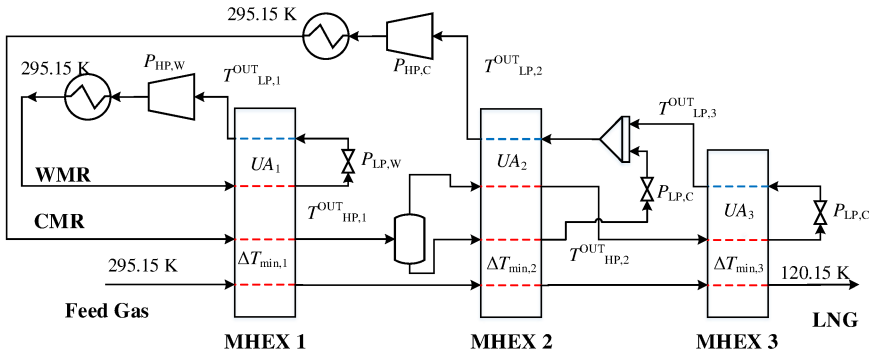

Figure 6.1 Flowsheet of the DMR process.

sic design required 17.34 MW in total compression power for the two refrigerant cycles. The results of the base case is presented in Table 6.1 and will be used as a future reference for the optimization studies. The variables solved for in the model are presented in italic, for which the individual compressor duties ($W_{W/C}$) and the $UA_{1/2}$-values are calculated during post-processing. Compressor duties are calculated using thermodynamic property calculations adjusted by the specified isentropic efficiency, and the UA-values are calculated for MHEX 1 and 2 using Equation (3.3). The warm mixed refrigerant composition changes in the simulation as a result of varying the component molar flowrate of ethane ($f_{W,ethane}$). The corresponding natural gas composition, flowrate and pressure level are specified in Table 6.2.

6.2 Optimization of the Dual Mixed Refrigerant process

6.2.1 Formulation of the optimization problem

Appropriate formulation of the optimization problem is imperative when analyzing LNG liquefaction processes, especially concerning the establishment of key parameters to promote smart design decisions that capture the trade-off between improved energy efficiency and excessive capital costs. The optimal design depends on the parameters provided and using the wrong criteria for driving the optimizer can have detrimental effects on the solution. Design of heat exchanger networks frequently impose a lower bound on the minimum approach temperature ΔT_{min} as a measure of the level of heat integration in the process. A smaller ΔT_{min} results in more heat integration at the expense of a larger total heat transfer area and thus higher capital costs. Therefore, by placing constraints on the minimum approach temperature in the process one can manipulate the trade-off between energy consumption and the required heat transfer area. The same reasoning has been ex-

Table 6.1 Process data for the base case. Calculated values are presented in italic.

Property		**Property**	
Total work [MW]	*17.34*	UA_3 [MW/K]	0.3
η	0.8	$UA_{\max}$ [MW/K]	5.39
W_{W} [MW]	*6.36*	$\Delta T_{\min,1}$ [K]	4.0
W_{C} [MW]	*10.98*	$\Delta T_{\min,2}$ [K]	*3.55*
$T_{\mathrm{HP},1}^{\mathrm{OUT}}$ [K]	*238.11*	$\Delta T_{\min,3}$ [K]	4.0
$T_{\mathrm{HP},2}^{\mathrm{OUT}}$ [K]	*150.96*	$T_{\mathrm{LP},1}^{\mathrm{OUT}}$ [K]	280.15
UA_1 [MW/K]	*1.93*	$T_{\mathrm{LP},2}^{\mathrm{OUT}}$ [K]	230.15
UA_2 [MW/K]	*3.16*	$T_{\mathrm{LP},3}^{\mathrm{OUT}}$ [K]	*146.96*
WMR:		**CMR:**	
F_{W} [kmol/s]	1.62	F_{C} [kmol/s]	*0.99*
$P_{\mathrm{HP,W}}$ [MPa]	1.67	$P_{\mathrm{HP,C}}$ [MPa]	4.85
$P_{\mathrm{LP,W}}$ [MPa]	0.42	$P_{\mathrm{LP,C}}$ [MPa]	*0.31*
Composition [mol %]:		Composition [mol %]:	
Ethane	*50.16*	Nitrogen	7.00
Propane	*32.64*	Methane	41.80
n-Butane	*17.20*	Ethane	33.20
		Propane	18.00

Table 6.2 Natural gas stream data for the DMR process.

Property	**Natural gas**
Flowrate [kmol/s]	1.00
Pressure [MPa]	5.50
Inlet temperature [K]	295.15
Outlet temperature [K]	120.15
Composition [mol %]	
Nitrogen	1.00
Methane	91.60
Ethane	4.93
Propane	1.71
n-Butane	0.35
iso-Butane	0.4
iso-Pentane	0.01

trapolated to the design and optimization of LNG processes. However, thermodynamic irreversibilities increase with both increasing driving forces and decreasing operating temperature [89, 90], of which the latter prevails in natural gas liquefaction processes due to heat transfer at cryogenic temperature levels where the exergy of a given amount of heat can be larger than the amount of heat. As a result, the distribution of driving forces in MHEXs plays a more influential role in LNG optimization than in the design of above ambient heat exchanger networks. In fact, Jensen and Skogestad [91] showed that using a minimum temperature approach when optimizing LNG processes led to sub-optimal utilization of the heat exchanger conductance. Later, Austbø and Gundersen showed that a problem formulation constraining the heat exchanger conductance rather than ΔT_{min}, resulted in an overall better driving force distribution in the heat exchanger [90]. Kim and Gundersen [84] later expanded the results to optimization of dual mixed refrigerant processes, though here the total UA-value should be used rather than the heat exchanger conductance values for the individual MHEXs.

Another important consideration in optimization of LNG processes is the degree of superheating for the low pressure refrigerant. A certain degree of superheating is always required to avoid the formation of liquid droplets in the compressor and excessive compressor wear. However, large safety margins may degrade the optimal solution. Kim and Gundersen [84] plotted the specific compression power as a function of the minimum superheating value, and found that the solution was more sensitive to the minimum degree of superheating when using a ΔT_{min} approach. Furthermore, they discovered that the optimal superheating values for the WMR and CMR when using area constraints for the DMR process were 10 K and 12 K, respectively. A minimum superheating of 5 K is used for all optimization cases presented in this chapter. The overall optimization formulation is similar to that of SMR processes [65]:

$$\begin{aligned} \min_{\mathbf{x}} \quad & W_{\text{W}}(\mathbf{x}) + W_{\text{C}}(\mathbf{x}) \\ \text{s.t.} \quad & \mathbf{h}(\mathbf{x}) = \mathbf{0}, \\ & UA_1(\mathbf{x}) + UA_2(\mathbf{x}) + UA_3(\mathbf{x}) \leq UA_{\text{max}}, \\ & \Delta T_{\text{sup}} \geq \Delta T_{\text{sup,min}}, \\ & \mathbf{x}^{\text{LB}} \leq \mathbf{x} \leq \mathbf{x}^{\text{UB}}, \end{aligned} \tag{6.1}$$

where ΔT_{sup} is the degree of superheating for the two compressors and $\mathbf{h}$ is a set of equations describing the DMR model (see Section 3.3). This set includes Equations (3.2) and (3.4), as well as energy balances for the individual stream segments. As the two-phase stream variables, as well as auxiliary equipment such as valves, mixers and compressors, are solved using nested flash calculations, their

functions are not included in $\mathbf{h}$, but are instead resolved at every iteration. The functions in $\mathbf{h}$ are inherently nonsmooth with nonsmooth operators such as min, max and mid for modeling phase changes, and the minimum approach temperature in the MHEXs. The individual UA functions are given by Equation (3.3).

Nonsmooth optimization algorithms exist in the literature [92]. In particular, solvers can be divided into two main categories; subgradient methods and bundle solvers. Subgradient-based methods work similar to smooth methods (e.g. the steepest descent method) but where the gradient is replaced by an arbitrary subgradient of the function. Subgradient methods are advantageous in that they exhibit low storage requirements and are relatively easy to implement. However, convergence of the algorithms can be slow, there exists no rigorous stopping condition, and the selection of step size is challenging, predominantly due to the possibility of having nondecending step directions [93]. Rather than using an arbitrary subgradient at each point, bundle methods approximate the subdifferential of the function. This is achieved by gathering the subgradients obtained at previous iterations into a bundle. Different bundle methods have been proposed [93]; the proximal bundle solver [94], bundle Newton method [95] and a limited memory bundle method [96, 97]. Implementations of the bundle Newton method for linearly constrained optimization and the limited memory bundle method for bound constraints exist. The proximal bundle method [94] is suitable for nonsmooth constrained optimization problems. Tests conducted on different convex and nonconvex nonsmooth optimization problems favored the proximal bundle method both in regards to efficiency and reliability [93]. However, attempts at using the MPBNGC v2.0 [94] solver for the nonsmooth single mixed refrigerant processes were unsuccessful [65]. Surprisingly, the interior-point optimizer, IPOPT [85], proved to be more suitable for optimizing the nonsmooth flowsheet models, despite its assumption that the objective function and constraints are twice continuously differentiable. However, some issues remain regarding the use of IPOPT for optimizing the nonsmooth models, particularly in relation to the termination criteria [65]. Specifically, no implementation currently exists of the nonsmooth analog for the dual feasibility calculations in IPOPT, such that termination at points of nondifferentiability is problematic [65]. However, Watson *et al.* [65] showed that the termination issues are avoided with the dual feasibility tolerance selected suitably high. The authors also provided a list of changes to the default settings, which empirically was shown to provide better performance for the nonsmooth models. The full list of non-default settings is provided in Table 6.3 and is used for optimizing the DMR process.

Table 6.3 Non-default settings for IPOPT used in this work.

tol	0.1
constr_viol_tol	10^{-6}
bound_push	10^{-9}
bound_frac	10^{-9}
recalc_y_feas_tol	10^{-2}
max_iter	500
mu_strategy	adaptive
hessian_approximation	limited-memory
limited_memory_max_history	number of decision variables

6.2.2 Optimization of the base case with a maximum heat exchanger conductance formulation

The first example looks at improving the operation of the feasible design from Table 6.1 by varying the pressure levels, refrigerant compositions, and intermediate temperatures for the same maximum total heat exchanger conductance ($UA_{\max}$). Optimization is done using both the nonsmooth approach and PSO together with the process simulator Aspen HYSYS. However, as pointed out in Chapter 4, different thermophysical property models are embedded in Aspen HYSYS and Aspen Plus, where the latter's property package has been implemented in the nonsmooth models. Therefore, simulations performed in Aspen Plus showed close correlation to results from the nonsmooth models, whereas results in Aspen HYSYS deviated significantly at lower temperatures [98]. In particular, this was accredited to Aspen HYSYS using different ideal gas enthalpy correlations than Aspen Plus and the nonsmooth models. As it turns out, however, Aspen HYSYS also includes the possibility of loading property models directly from Aspen Plus. Therefore, simulations in Aspen HYSYS are here done with underlying property models from Aspen Plus to better compare the results from PSO with the nonsmooth models. Termination criteria for the PSO algorithm were set to 500 maximum iterations, a function tolerance of 10^{-8} and a maximum number of stall iterations of 40, otherwise defined as the number of iterations resulting in a smaller relative change in objective function than the overall function tolerance, before termination.

The optimization model uses the same partitioning of the process streams with five segments for representing the single-phase behavior and 20 stream segments for the two-phase region in each MHEX. Moreover, as the two-phase stream variables remain nested in the model, and are not described explicitly in the program (6.1), they are resolved at each iteration instead of being elevated to decision variables in the model. Consequently, the optimization model consists of 108 variables,

Table 6.4 Decision variables and bounds for the DMR model.

Variable	Bounds	Variable	Bounds
$f_{\text{C,Nitrogen}}$	$[0, 0.35]$	$f_{\text{W,Ethane}}$	$[0.1, 1.0]$
$f_{\text{C,Methane}}$	$[0.1, 1.0]$	$f_{\text{W,Propane}}$	$[0.1, 1.0]$
$f_{\text{C,Ethane}}$	$[0.1, 1.0]$	$f_{\text{W,n-Butane}}$	$[0, 0.8]$
$f_{\text{C,Propane}}$	$[0.1, 0.6]$	$P_{\text{LP,C}}$	$[0.15, 0.33]$
$f_{\text{C,n-Butane}}$	$[0, 0.2]$	$P_{\text{HP,C}}$	$[2.5, 5.0]$
$P_{\text{LP,W}}$	$[0.2, 0.7]$	$T^{\text{OUT}}_{\text{LP,1}}$	$[250.0, 400.0]$
$P_{\text{HP,W}}$	$[1.0, 3.0]$	$T^{\text{OUT}}_{\text{LP,2}}$	$[220.0, 250.0]$
$\Delta T_{\text{min,1}}$	$[1.0, 4.0]$	$T^{\text{OUT}}_{\text{LP,3}}$	$[130.0, 160.0]$
$\Delta T_{\text{min,2}}$	$[1.0, 4.0]$	$T^{\text{OUT}}_{\text{HP,1}}$	$[230.0, 260.0]$
$\Delta T_{\text{min,3}}$	$[0.5, 5.0]$	$T^{\text{OUT}}_{\text{HP,2}}$	$[150.0, 170.0]$

of which $\sum_{i=1}^{3} s_i(n_{\text{sup}} + n_{\text{sub}} - 2) = 88$ (where s_i are the number of process streams in MHEX i and $n_{\text{sup/sub}}$ are the number of segments for the superheated and subcooled regions) are the temperatures of the individual stream segments and the remaining 20 variables are other decision variables such as composition, pressure levels and intermediate stream temperatures. Variable bounds for the decision variables are presented in Table 6.4. Upper and lower bounds on the temperature of the individual stream segments are set to 350 K and 100 K, respectively.

An optimal solution to the DMR process was obtained with IPOPT after 135 iterations and a total run time (including the time needed for initializing and simulating the DMR model to obtain the initial feasible design) of 1173 s. The optimal solution results in a total compression work of 14.84 MW, which corresponds to a 14.4% reduction. Composite curves and driving force plots for both the initial feasible design and the optimized solution are presented in Figure 6.2. The composite curves in the optimal design are significantly closer in MHEX 3, though slightly less so in the intermediate MHEX. The result is a design where the overall temperature difference is closer to being proportional to the operating temperature, thus reducing the exergetic losses due to irreversible heat transfer as discussed by Austbø and Gundersen [90]. Lower refrigerant flowrates and a higher degree of separation before the intermediate MHEX also result in less self refrigeration and a smaller overall heat exchanger duty.

The DMR model was also optimized using PSO with the same model built in Aspen HYSYS. The same initial feasible design and variable bounds were used to compare the performance of the two optimization strategies. A total run time of 20.9 hrs was needed before the algorithm obtained a solution with a total compression work of 15.11 MW, 1.8% higher than the solution with the nonsmooth

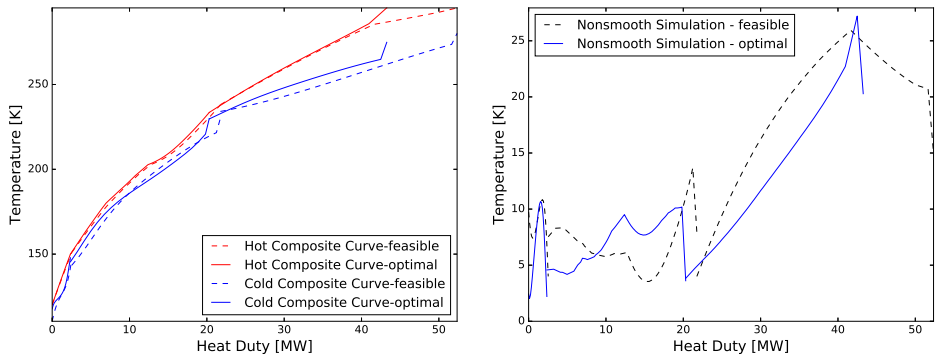

(a) **(b)**

Figure 6.2 (**a**) Composite curves for the initial feasible and the optimized design in the base case (**b**) The corresponding driving force plots.

model (NM). PSO obtains a process with larger approach temperatures in all three MHEXs. The high pressure level of the cold mixed refrigerant is also significantly higher than what was obtained with the nonsmooth model. Morin *et al.* reported a similar difference in objective values between using the evolutionary search method and SQP for optimization of DMR processes [80]. Optimization results from the two optimization methods are presented in Tables 6.5 and 6.6 along with the data from the initial feasible design. The $UA_{\max}$ calculated from the simulation, is used as an upper bound on the total heat exchanger conductance. Consequently, any improvements must come from a redistribution of the available heat transfer area in the individual MHEXs.

Next, the DMR model is optimized for a set of different maximum total heat exchanger conductance values, using the nonsmooth approach as well as PSO for comparison. Variable bounds and IPOPT settings remain the same as in Tables 6.3 and 6.4, with maximum total heat exchanger conductance values of 6, 9 and 12 MW/K, respectively. Solutions were obtained for the nonsmooth model in the three cases. However, as the initial point is the base case in Table 6.1 with a $UA_{\max} = 5.39$ MW/K, the optimal design will differ considerably from the initial design for larger heat exchanger conductance values. As a result, the number of iterations and hence the total solution time is larger. The first case converged after 106 iterations and a total run time of 838 s. The second case required 221 iterations to solve, resulting in a total run time (including the time needed for initialization and simulation to obtain the initial feasible design) of 2067 s. For the last case, with a $UA_{\max} = 12$ MW/K, a solution was obtained in 137 iterations,

Table 6.5 Process optimization results for the base case.

Property	Feasible design	NM	PSO
Total work [MW]	17.34	14.84	15.11
W_{W} [MW]	6.36	5.74	5.17
W_{C} [MW]	10.98	9.10	9.94
UA_1 [MW/K]	1.93	2.19	2.01
UA_2 [MW/K]	3.16	2.74	2.76
UA_3 [MW/K]	0.3	0.46	0.62
UA_{max} [MW/K]	5.39	5.39	5.39
$\Delta T_{\mathrm{min},1}$ [K]	4.0	3.83	3.22
$\Delta T_{\mathrm{min},2}$ [K]	3.55	3.61	4.55
$\Delta T_{\mathrm{min},3}$ [K]	4.0	2.03	4.04
$T^{\mathrm{OUT}}_{\mathrm{HP},1}$ [K]	238.11	233.53	237.86
$T^{\mathrm{OUT}}_{\mathrm{HP},2}$ [K]	150.96	150.04	150.89
$T^{\mathrm{OUT}}_{\mathrm{LP},1}$ [K]	280.15	271.47	282.1
$T^{\mathrm{OUT}}_{\mathrm{LP},2}$ [K]	234.11	226.88	232.80
$T^{\mathrm{OUT}}_{\mathrm{LP},3}$ [K]	146.96	145.10	148.2

Table 6.6 Warm and cold mixed refrigerant optimization results for the base case.

Property	Feasible design	NM	PSO
WMR:			
F_{W} [kmol/s]	1.62	1.07	1.34
$P_{\mathrm{HP,W}}$ [MPa]	1.67	1.26	1.70
$P_{\mathrm{LP,W}}$ [MPa]	0.42	0.20	0.34
Composition [mol %]:			
Ethane	50.16	42.43	36.75
Propane	32.64	34.95	49.16
n-Butane	17.20	22.62	14.08
CMR:			
F_{C} [kmol/s]	0.99	1.17	1.34
$P_{\mathrm{HP,C}}$ [MPa]	4.85	2.72	3.96
$P_{\mathrm{LP,C}}$ [MPa]	0.31	0.19	0.30
Composition [mol %]:			
Nitrogen	7.00	0.84	3.20
Methane	41.80	37.64	41.79
Ethane	33.20	44.90	40.60
Propane	18.00	14.57	14.38
n-Butane	0.0	2.05	0.02

Table 6.7 Process optimization results for different $UA_{\max}$ values.

Property	6 MW/K	9 MW/K	12 MW/K
Total work [MW]	14.49	13.56	13.11
W_{W} [MW]	5.60	5.21	5.05
W_{C} [MW]	8.89	8.36	8.06
UA_1 [MW/K]	2.47	3.65	4.88
UA_2 [MW/K]	3.04	4.63	6.18
UA_3 [MW/K]	0.49	0.72	0.94
$UA_{\max}$ [MW/K]	6.0	9.0	12.0
$\Delta T_{\min,1}$ [K]	3.44	2.32	1.34
$\Delta T_{\min,2}$ [K]	3.77	2.43	1.38
$\Delta T_{\min,3}$ [K]	1.87	1.18	0.79
$T_{\mathrm{HP},1}^{\mathrm{OUT}}$ [K]	233.38	233.59	233.14
$T_{\mathrm{HP},2}^{\mathrm{OUT}}$ [K]	150.00	150.00	150.00
$T_{\mathrm{LP},1}^{\mathrm{OUT}}$ [K]	278.10	282.14	280.56
$T_{\mathrm{LP},2}^{\mathrm{OUT}}$ [K]	229.60	230.77	231.77
$T_{\mathrm{LP},3}^{\mathrm{OUT}}$ [K]	148.03	148.76	149.21

corresponding to a total run time (including initialization) of 1158 s. Results for the three cases are presented in Tables 6.7 and 6.8. The driving force plots for the three cases are shown in Figure 6.3. As can be observed, the driving force profiles show a similar shape for the three cases, although, with increasing heat exchanger conductance values, the obtained designs become tighter with smaller driving force temperatures throughout the process.

The three cases were also optimized using Aspen HYSYS with PSO. For $UA_{\max} = 6$ MW/K, a solution was obtained after 22.3 hrs with an objective function value of 14.84 MW, which is 2.4% higher than what was obtained by the nonsmooth model. In the second case, PSO obtained a design after 25.3 hrs with a total compression power of 13.79 MW, or 1.7% higher than the corresponding nonsmooth solution. PSO obtained a solution with 13.26 MW for the third case, which corresponds to 1.1% additional compressor power than the design obtained by the nonsmooth model. The optimization algorithm required 23.9 hrs to solve this case. It should be mentioned that PSO terminated after reaching the maximum number of iterations in all cases above. Consequently, no local optima were obtained, and the PSO algorithm terminated with the best known solution within 500 iterations. A greater function tolerance of 10^{-6} was also tested. However, in that case the PSO algorithm converged to significantly suboptimal points compared to the nonsmooth models.

Table 6.8 Warm and cold mixed refrigerant optimization results for different $UA_{\max}$ values.

Property	6 MW/K	9 MW/K	12 MW/K
WMR:			
F_{W} [kmol/s]	1.04	1.01	1.04
$P_{\mathrm{HP,W}}$ [MPa]	1.240	1.236	1.406
$P_{\mathrm{LP,W}}$ [MPa]	0.200	0.216	0.264
Composition [mol %]:			
Ethane	23.70	25.10	31.72
Propane	45.96	39.26	32.81
n-Butane	30.34	35.64	35.47
CMR:			
F_{C} [kmol/s]	1.17	1.18	1.18
$P_{\mathrm{HP,C}}$ [MPa]	2.720	2.780	2.795
$P_{\mathrm{LP,C}}$ [MPa]	0.195	0.232	0.251
Composition [mol %]:			
Nitrogen	0.91	1.36	1.56
Methane	37.62	37.55	37.70
Ethane	44.71	45.08	45.25
Propane	14.47	13.58	13.14
n-Butane	2.28	2.44	2.35

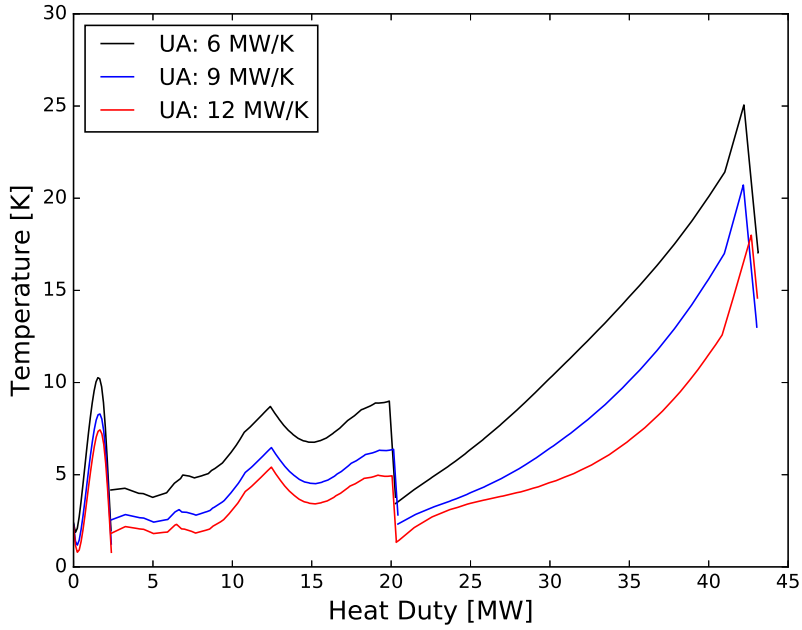

Figure 6.3 Driving force plots of the optimal DMR process with different heat exchanger conductance values.

6.2.3 Optimization of the base case using a minimum temperature approach formulation

The importance of a correct formulation of the optimization problem is here demonstrated by replacing the constraint on the overall heat exchanger conductance with a minimum temperature specification. The feasible design in Table 6.1 is again used as a starting point for the optimizer, with the same bounds as specified in Table 6.4. The minimum approach temperature was specified to 3.50 K in all three MHEXs. IPOPT obtained a solution for the DMR model with a ΔT_{min} formulation after 188 iterations and a total run time of 2363 s. The solution requires a total compressor work of 14.51 MW and a total heat exchanger conductance of 11.54 MW/K. By comparison, optimization using the UA_{max} formulation with a corresponding UA_{max} of 11.54 MW/K, i.e same as for the optimal design with a ΔT_{min} specification, resulted in a total compression power of 13.16 MW or 9.3% less than the solution predicted by the ΔT_{min} formulation. Thus, energy is saved without extra investment, just by using a different problem formulation inspired by thermodynamics that utilizes the heat exchanger area more efficiently. The same

argument can be obtained from studying the composite curves and driving force plot in Figure 6.4. A minimum temperature specification will result in more parallel composite curves as driving forces are distributed more evenly across the three MHEXs. Consequently, more heat exchanger area are allocated to the precooling section of the process, where the benefits of smaller driving forces do not compensate for the additional required heat exchanger area. The optimal solution for the nonsmooth model with the $\Delta T_{\min}$ and $UA_{\max}$ formulations are summarized in Table 6.9.

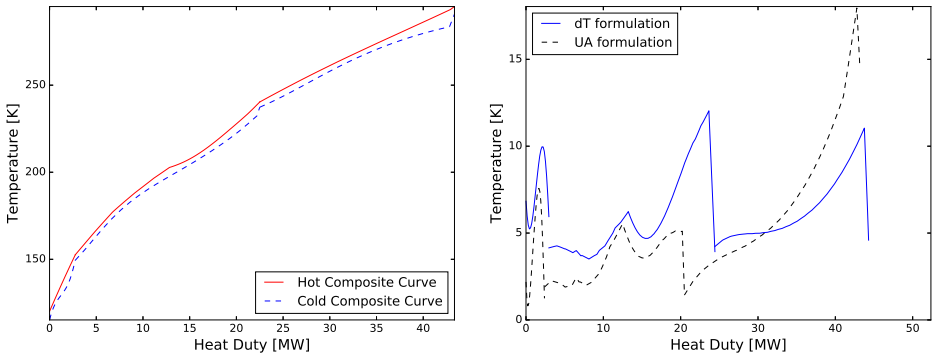

(a) **(b)**

Figure 6.4 (**a**) Composite curves for the optimized solution with a $\Delta T_{\min}$ of 3.50 K. (**b**) The driving force plot for the optimal solutions with $\Delta T_{\min}$ and $UA_{\max}$ constraints.

6.2.4 Optimization of the Dual Mixed Refrigerant process with NGL extraction

Depending on the feed composition of the natural gas and sales specifications for the LNG product, integrated NGL extraction may be necessary. The last case looks at such a situation, where natural gas liquids are extracted between the natural gas precooler (MHEX 1) and the liquefaction and subcooling part (MHEX 2 and 3) (see Figure 6.5). The same process configuration was previously simulated for the different feed gas compositions in Table 6.10. Here, however, richer feed compositions are considered, placing constraints on the separator to only return solutions with a satisfactory lean product with a methane content greater than 89 mol %. Optimization is done using the formulation in (6.1) with a $UA_{\max}$ specification. As the natural gas stream data remain fixed in the optimization, and extraction rate and product specifications can be determined through solving for the outlet temperature of MHEX 1, the number of optimization variables will be unchanged from the previous model.

Table 6.9 Process optimization results for the base case with a ΔT_{min} and UA_{max} formulation.

Property	ΔT_{min}	UA_{max}	**Property**	ΔT_{min}	UA_{max}
Total work [MW]	14.51	13.16	**WMR:**		
W_{W} [MW]	3.80	5.05	F_{W} [kmol/s]	0.95	1.05
W_{C} [MW]	10.71	8.10	$P_{\text{HP,W}}$ [MPa]	1.41	1.43
			$P_{\text{LP,W}}$ [MPa]	0.36	0.27
UA_1 [MW/K]	3.36	4.68	Composition [mol %]		
UA_2 [MW/K]	7.45	5.96	Ethane	31.58	32.52
UA_3 [MW/K]	0.73	0.90	Propane	35.40	33.14
UA_{max} [MW/K]	11.54	11.54	n-Butane	33.02	34.34
			CMR:		
$\Delta T_{\text{min,1}}$ [K]	4.23	1.41	F_{C} [kmol/s]	1.39	1.19
$\Delta T_{\text{min,2}}$ [K]	3.50	1.00	$P_{\text{HP,C}}$ [MPa]	3.56	2.79
$\Delta T_{\text{min,3}}$ [K]	5.24	0.81	$P_{\text{LP,C}}$ [MPa]	0.27	0.25
			Composition [mol %]:		
$T^{\text{OUT}}_{\text{HP,1}}$ [K]	246.14	233.40	Nitrogen	4.62	1.63
$T^{\text{OUT}}_{\text{HP,2}}$ [K]	153.36	150.00	Methane	35.77	37.77
$T^{\text{OUT}}_{\text{LP,1}}$ [K]	290.56	280.61	Ethane	41.67	45.50
$T^{\text{OUT}}_{\text{LP,2}}$ [K]	242.21	232.04	Propane	15.38	12.56
$T^{\text{OUT}}_{\text{LP,3}}$ [K]	147.42	148.76	n-Butane	2.56	2.54

Table 6.10 Feed gas compositions considered for the DMR process with NGL extraction.

Composition [mol %]	**Case I**	**Case II**	**Case III**
Nitrogen	2.00	2.00	2.00
Methane	87.60	85.60	83.60
Ethane	5.93	4.93	5.93
Propane	2.71	3.71	4.71
n-Butane	1.35	2.35	2.35
i-Butane	0.4	1.4	1.4
n-Pentane	0.01	0.01	0.01

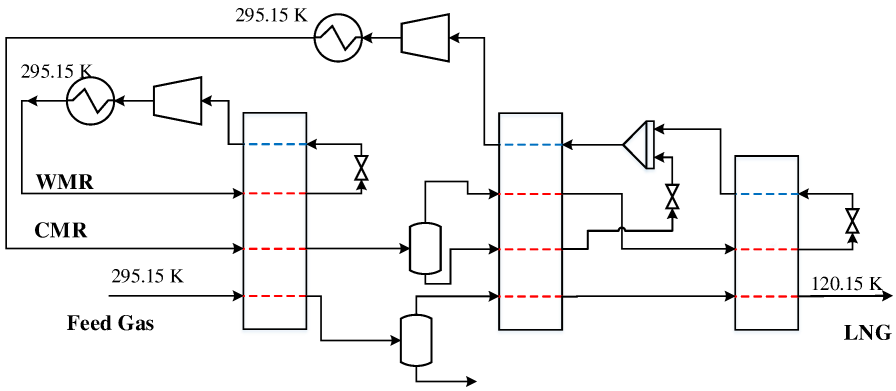

Figure 6.5 Flowsheet of the DMR model with NGL extraction.

Flowsheet simulation is used to obtain feasible starting points for the optimizer. The following unknown variables were solved for in the simulation model: $T_{\mathrm{HP,1}}^{\mathrm{OUT}}$, $T_{\mathrm{HP,2}}^{\mathrm{OUT}}$, $T_{\mathrm{LP,3}}^{\mathrm{OUT}}$, $P_{\mathrm{LP,C}}$, $P_{\mathrm{LP,W}}$, $P_{\mathrm{HP,C}}$, and UA_3. A warm mixed refrigerant composition with 47.83% ethane, 34.17% propane and 18.00% n-butane was used for all three feed compositions, with a corresponding molar flowrate of 1.55 kmol/s. The cold mixed refrigerant flowrate and composition also remained constant for the three cases with 7% nitrogen, 41.80% methane, 33.20% ethane and 18.00% propane and a molar flowrate of 1.45 kmol/s. Outlet temperatures of the low pressure mixed refrigerant in MHEX 1 and 2 were specified as 290.15 K and 225.15 K, and the minimum approach temperature in the three MHEXs were selected as 4.0 K, 4.0 K and 7.0 K, respectively. The solutions of the simulation model for the different feed compositions are given in Table 6.11.

As for the previous cases, optimization was done using the simulation results as a starting point, with the calculated $UA_{\max}$ providing an upper bound on the total heat exchanger conductance. Most of the variable bounds are changed from the base case, however, and are given in Table 6.13 for clarification.

The first case considers a relatively light natural gas composition with 87.60% methane content. IPOPT obtained a solution after 300 iterations and a total run time of 2684 s including the time needed for initialization and simulation. Significant improvements in compressor duties were achieved in the optimized design, which at a total power consumption of 15.57 MW, represents a 20.9% reduction compared to the initial feasible design. NGL extraction is performed at a temperature of 220 K, resulting in a methane content of 91.7% for the end product, well above the specification of at least 89% methane in the LNG. At this extraction temperature, approximately 9% of the feed gas is sectioned off in the separator to

Table 6.11 Nonsmooth simulation results for the DMR model with NGL extraction. Calculated values are presented in italic.

Property	I	II	III	Property	I	II	III
Total work [MW]	*19.68*	*18.88*	*18.39*	**WMR:**			
W_{W} [MW]	*7.34*	*6.77*	*6.56*	F_{W} [kmol/s]	1.55	1.55	1.55
W_{C} [MW]	*12.34*	*12.12*	*11.83*	$P_{\mathrm{HP,W}}$ [MPa]	1.67	1.67	1.67
η	0.8	0.8	0.8	$P_{\mathrm{LP,W}}$ [MPa]	*0.35*	*0.39*	*0.40*
UA_1 [MW/K]	2.21	2.29	2.32	Comp. [mol %]			
UA_2 [MW/K]	2.27	2.15	2.18	Ethane	47.83	47.83	47.83
UA_3 [MW/K]	0.34	0.37	0.38	Propane	34.17	34.17	34.17
UA_{max} [MW/K]	*4.82*	*4.81*	*4.87*	n-Butane	18.00	18.00	18.00
$\Delta T_{\mathrm{min,1}}$ [K]	4.0	4.0	4.0	**CMR:**			
$\Delta T_{\mathrm{min,2}}$ [K]	4.0	4.0	4.0	F_{C} [kmol/s]	1.45	1.45	1.45
$\Delta T_{\mathrm{min,3}}$ [K]	7.0	4.0	4.0	$P_{\mathrm{HP,C}}$ [MPa]	*3.49*	*3.64*	*3.79*
$T^{\mathrm{OUT}}_{\mathrm{HP,1}}$ [K]	*233.77*	*236.89*	*238.02*	$P_{\mathrm{LP,C}}$ [MPa]	*0.19*	*0.21*	*0.23*
$T^{\mathrm{OUT}}_{\mathrm{HP,2}}$ [K]	*171.93*	*174.87*	*174.81*	Comp. [mol %]			
$T^{\mathrm{OUT}}_{\mathrm{LP,1}}$ [K]	290.15	290.15	290.15	Nitrogen	7.00	7.00	7.00
$T^{\mathrm{OUT}}_{\mathrm{LP,2}}$ [K]	225.15	225.15	225.15	Methane	41.80	41.80	41.80
$T^{\mathrm{OUT}}_{\mathrm{LP,3}}$ [K]	*164.93*	*167.87*	*167.81*	Ethane	33.20	33.20	33.20
				Propane	18.00	18.00	18.00

Table 6.12 LNG product of the DMR model with NGL extraction.

Property	Case I	Case II	Case III
F_{LNG} [kmol/s]	0.96	0.91	0.89
Compositon [mol %]			
Nitrogen	2.08	2.18	2.21
Methane	90.00	90.77	89.66
Ethane	5.48	4.26	5.04
Propane	1.83	1.93	2.30
n-Butane	0.44	0.48	0.44
i-Butane	0.16	0.38	0.35

Table 6.13 Changed variable bounds for the DMR model with NGL extraction.

Variable	Bounds	Variable	Bounds
$f_{\text{C,Nitrogen}}$	$[0, 0.30]$	$P_{\text{HP,W}}$	$[0.9, 3.0]$
$f_{\text{C,Methane}}$	$[0.1, 0.8]$	$P_{\text{LP,W}}$	$[0.13, 0.7]$
$f_{\text{C,Ethane}}$	$[0.1, 0.8]$	$P_{\text{LP,C}}$	$[0.13, 0.33]$
$f_{\text{W,Ethane}}$	$[0, 0.7]$	$P_{\text{HP,C}}$	$[1.3, 5.0]$
$f_{\text{W,Propane}}$	$[0.1, 0.7]$	$T^{\text{OUT}}_{\text{HP,1}}$	$[220.0, 260.0]$
$f_{\text{W,n-Butane}}$	$[0.1, 0.6]$	$T^{\text{OUT}}_{\text{HP,2}}$	$[150.0, 180.0]$
$\Delta T_{\text{min,1}}$	$[1.5, 6.0]$	$T^{\text{OUT}}_{\text{LP,1}}$	$[260.0, 400.0]$
$\Delta T_{\text{min,2}}$	$[1.5, 5.0]$	$T^{\text{OUT}}_{\text{LP,2}}$	$[170.0, 230.0]$
$\Delta T_{\text{min,3}}$	$[1.0, 7.0]$	$T^{\text{OUT}}_{\text{LP,3}}$	$[140.0, 170.0]$

be exported as NGL liquids or otherwise undergo further fractionation into separate products. A richer composition with 85.6% methane content is used in the second case. The model converged after 600 s and 62 iterations to a solution with a total power requirement of 14.90 MW, which corresponds to a 21.1% decrease compared to the initial design. A higher NGL extraction temperature was used in this case, thus the final LNG composition of 92.4% methane is comparably lighter. Richer feed gas composition also led to a slight increase in the extraction rate of NGL liquids, with 13% of the gas sectioned off as NGL product. In the third case, a rich natural gas composition with 83.6% methane content is assumed where significant NGL separation is necessary to obtain a satisfactory compliance with the LNG specification. A solution was obtained after 1794 s and 173 iterations, at which 14.42 MW is required by the two compressors, a 21.6% decrease from the feasible design. At this solution, the extraction temperature is again 220 K, resulting in a final methane content of 92.3% in the LNG. The NGL from the separator in this case equal around 18% of the feed gas flowrate. The results for the three cases are summarized in Table 6.14. As more of the feed gas is extracted after the precooler for the heavier compositions, the compressor duties are correspondingly smaller. It also explains the relative small difference in heat exchanger conductance values between the three designs.

Driving force plots of the three cases are presented in Figure 6.6.

6.2.5 Convergence characteristics

A nonconvex dependence on composition, pressure levels and temperatures on the cooling curve for the mixed refrigerants makes optimization of LNG processes difficult. This property together with the large model size and multiple refrigeration stages often used in dual mixed refrigerant processes, make DMR processes

Table 6.14 Nonsmooth optimization results of the DMR process with NGL extraction.

Property	I	II	III	Property	I	II	III
Total work [MW]	15.57	14.90	14.42	Propane	1.12	1.24	1.18
W_{W}	7.53	7.55	7.76	n-Butane	0.18	0.24	0.16
W_{C}	8.05	7.35	6.67	i-Butane	0.07	0.20	0.14
UA_1 [MW/K]	2.41	2.34	2.52	**WMR:**			
UA_2 [MW/K]	2.09	2.16	2.05	F_{W} [kmol/s]	1.10	1.07	1.08
UA_3 [MW/K]	0.32	0.31	0.29	$P_{\mathrm{HP,W}}$ [MPa]	1.348	1.214	1.316
UA_{max} [MW/K]	4.82	4.81	4.86	$P_{\mathrm{LP,W}}$ [MPa]	0.130	0.131	0.130
$\Delta T_{\mathrm{min},1}$ [K]	4.32	4.39	3.90	Comp. [mol %]			
$\Delta T_{\mathrm{min},2}$ [K]	2.85	2.50	2.70	Ethane	27.46	22.77	27.04
$\Delta T_{\mathrm{min},3}$ [K]	1.43	1.76	1.34	Propane	44.13	46.71	41.53
$T_{\mathrm{HP},1}^{\mathrm{OUT}}$ [K]	220.00	223.97	220.00	n-Butane	28.41	30.52	31.43
$T_{\mathrm{HP},2}^{\mathrm{OUT}}$ [K]	150.00	150.02	150.00	**CMR:**			
$T_{\mathrm{LP},1}^{\mathrm{OUT}}$ [K]	281.87	280.18	279.45	F_{C} [kmol/s]	1.03	0.98	0.90
$T_{\mathrm{LP},2}^{\mathrm{OUT}}$ [K]	217.15	221.47	217.30	$P_{\mathrm{HP,C}}$ [MPa]	1.986	1.992	1.869
$T_{\mathrm{LP},3}^{\mathrm{OUT}}$ [K]	148.57	148.26	148.66	$P_{\mathrm{LP,C}}$ [MPa]	0.143	0.135	0.133
LNG:				Comp. [mol %]			
F_{LNG} [kmol/s]	0.91	0.87	0.82	Nitrogen	0.18	0.11	0.0
Comp. [mol %]				Methane	36.65	35.01	35.74
Nitrogen	2.17	2.27	2.38	Ethane	52.96	53.25	52.66
Methane	91.73	92.40	92.28	Propane	9.74	10.26	11.07
Ethane	4.73	3.66	3.87	n-Butane	0.47	1.37	0.53

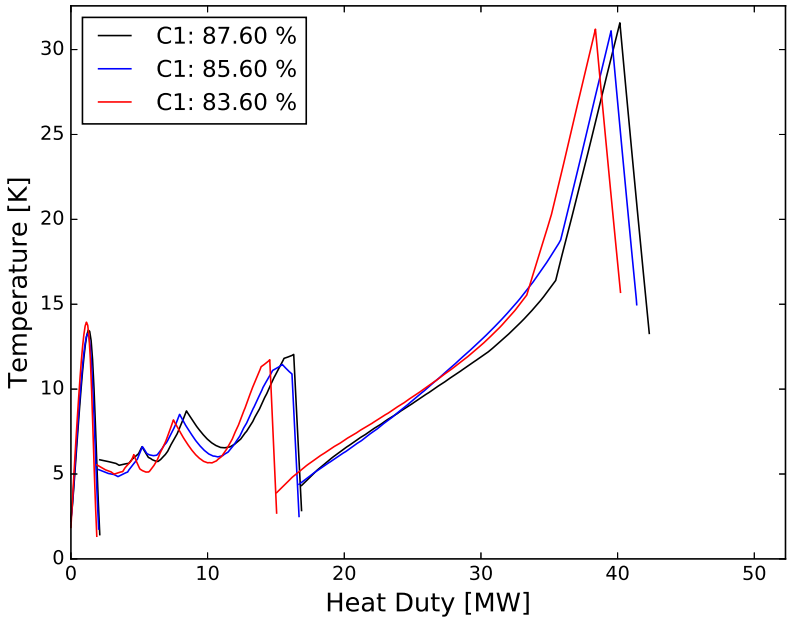

Figure 6.6 Driving force plots for the DMR model with NGL extraction.

significantly more challenging to analyze than SMR processes. Derivative based methods in particular tend to struggle to converge, mainly due to the large number of nonlinear constraints and inflated model size. Morin *et al.* [80] came to a similar conclusion using an SQP algorithm for optimizing a DMR process in Aspen HYSYS. Tuning the algorithm for the particular model required great attention from the designer, making it an arduous and time consuming task. However, once properly set up it achieved about a 3% decrease in objective function value compared to using a stochastic search method. The nonsmooth modeling framework presented here serve as a stand-alone simulation and optimization tool tailored for LNG processes, and consequently, does not require fine tuning for each instance. However, it relies on the validity of IPOPT, or more specifically on the issue with computing the termination criterion. The dual feasibility calculations are not valid at nonsmooth points [65], which can cause the algorithm not to converge and instead iterate in a negligibly small search space. Although, ideally this termination criterion should be extended to also hold true for nonsmooth functions, here it is resolved by raising the dual feasibility tolerance. Global optimality cannot be guaranteed for the solutions seeing as IPOPT is strictly a local solver. As the problem is inherently nonconvex, nothing prevents IPOPT converging to a locally optimal

point, and so, global optimality can only be confirmed once it is included in a branch and bound solver for global optimization. Nevertheless, multistart can help asserting the quality of the results by examining solutions obtained from a set of different initial starting conditions. Multistart using 15 runs from randomly generated (and possibly infeasible) starting points was done for the cases with variable UA_{max} values. Results show that none of the converged solutions were better than the one provided using the feasible starting point. For the case with a UA_{max} value of 6 MW/K, multistart yields four runs converging to the same solution, two cases converging to suboptimal designs, and the remaining nine runs not converging at all. This corresponds to a success rate of 27%, while Austbø and Gundersen [90] reported a success rate in the 10-20% range with UA_{max} constraints for the PRICO process. It should be noted however, that the DMR model is considerably larger than what would be required for modeling the PRICO process, and that a success rate of 83% were obtained with the nonsmooth PRICO model [65]. For the cases with heat exchanger conductances of 8 MW/K and 15 MW/K, six of the runs converged to the same improved solution, whereas two runs converged to suboptimal solutions. This corresponds to a success rate of 40%. A slightly higher success rate was obtained with the ΔT_{min} formulation, where 45% of the runs converged to the best known solution. Therefore, a possible strategy would be to relax the UA_{max} constraint first, and use the solution as an initial guess before optimizing the driving force distribution in the MHEXs.

Setting bounds for the optimization variables is challenging for the DMR process due to the large number of constraints and decision variables in the model. In particular, finding a good set of bounds on component molar flowrates, refrigerant pressure levels and minimum approach temperatures is tedious, and may influence the convergence. Simulation provides good initial points to the optimizer, and aid the user in setting bounds that increase the convergence rate. In the case studies performed here, the pressure, ΔT_{min} and temperature bounds are relaxed to encompass solutions of different case studies. Significant improvements to the convergence can be made, therefore, through stricter bounds tailored for the specific case. The latter becomes easier by first considering the initial feasible design, and adjusting the bounds accordingly. As no other tuning is necessary for IPOPT besides the settings provided in Table 6.3, finding bounds and optimizing the models is still less time-consuming and yield better results than running Aspen HYSYS with stochastic search methods such as PSO. In the optimization studies, some of the decision variables ended up on their respective lower bounds. As the bounds were relaxed further, the model experienced failures in the flash calculations, as the model approached regions for which no solution was obtained using the inside-out flash algorithm. Consequently, it imposes a limitation on the current implementation. Developing an alternative model formulation or heuristics for handling these

extreme flash conditions to prevent failures in the overall model, is therefore a necessary next step.

6.3 Conclusions

Several stand-alone models for LNG processes have been reported in the literature, and these have been tested for single mixed refrigerant processes. However, these models often involve solving either a mixed integer nonlinear program or a nonlinear program with a large number of variables and constraints. Dual mixed refrigerant processes feature designs with small temperature differences, several multistream heat exchangers, intermediate throttling, and separation. The models are therefore significantly larger and more complex than single mixed refrigerant processes, and as a result, optimization studies in the literature tend to use commercial process simulators such as Aspen HYSYS along with a derivative based or stochastic search method. The nonsmooth flowsheet models presented here are stand-alone tools for both simulation and optimization of LNG processes, where functioning models already have been developed for different single mixed refrigerant processes. In this chapter, the nonsmooth flowsheeting strategy is used for developing a simulation and optimization model for dual mixed refrigerant processes.

Different cases were studied using both ΔT_{min} and UA_{max} constraints, and optimization was done with IPOPT using sensitivity information provided by LD-derivatives. Optimization resulted in a 14.4 % decrease in total compression power for the DMR process and 20.9-21.6 % for the DMR process with NGL extraction. The nonsmooth optimization model also obtained 1.1-2.4 % more energy efficient operating points than PSO in 25-80 times less solution time. Multistart for several of the cases showed that IPOPT obtained the best (known) solution when using a feasible starting point. Furthermore, the model achieved a higher success rate with a UA_{max} constraint than what was reported by Austbø and Gundersen for the basic PRICO process [90].

Chapter 7

Mathematical optimization for targeting and synthesis of work and heat exchange networks

Abstract

This chapter explores a new field in process integration that looks at the interaction of two modes of energy transfer that commonly occurs in chemical processes, namely work and heat, and how these can be combined in a work and heat exchange network (WHEN) that enhances work and heat integration in such a way that the overall thermodynamic losses in the process are minimized.

The chapter is structured as follows. First, an introduction to pinch analysis is provided, followed by the introduction of mathematical programming for enhancing heat recovery. Here, an introduction to various pinch location algorithms found in the literature is given, along with pros and cons with choosing a specific model. Then different superstructures for targeting and synthesis of WHENs are covered, followed by a discussion on the different models with regards to exergy targeting.

This chapter is based on the publication:

- M. Vikse, C. Fu, P. I. Barton, and T. Gundersen. Towards the use of mathematical optimization for work and heat exchange networks. *Chemical Engineering Transactions*, 61:1351-1356, 2017.

Liquefaction processes for natural gas are particular subproblems belonging to the category of work and heat exchange networks (WHENs). In particular, heat and work are the two main modes of energy transfer in most chemical processes, and studying the interaction between the two is essential in improving the overall energy efficiency. Early work isolated heat transfer with the objective of reducing waste heat. However, studying one without the other will in most cases yield suboptimal networks where further improvements are possible. In the case of LNG processes, the problem is simplified to minimizing net compression work. This is only made possible since thermodynamic losses in the process must be covered by additional compression power to drive the refrigeration system. The direct translation between work and heat is not always as apparent, however, requiring the use of other key performance parameters to capture the relation between work and heat on the overall performance of the process. One such key performance parameter is exergy, which allows for a 1:1 comparison between work and heat by comparing the quality rather than quantity of energy transfer. As process integration gradually migrated towards simultaneous work and heat integration, it brought with it a library of new superstructures for the optimization and synthesis of WHENs. Although a few of these models were considering exergy and, in particular the exergy destruction, as a measure of the degree of integration in the process, most were developed based on a total annualized cost analysis. Certainly, the choice of superstructure will depend on its usage and applicability for a specific problem. It is therefore important to categorize the different superstructures by mapping their individual advantages and disadvantages, to better provide an overview on which models are suitable for a given application. As thermodynamic efficiency is at a forefront in this thesis, this chapter attempts to dissect each superstructure and find out how well it complies with theorems for appropriate placement of compressors and expanders.

7.1 Pinch analysis and the correct integration of pressure changing equipment in heat exchanger networks

The concept of pinch analysis was introduced in the 1970s as an attempt to establish a framework for improving efficiency of process systems in view of resource scarcity and cost. At first, the focus was on enhanced heat integration with pioneering work from Hohman [99] and Rudd and co-workers [100–102]. Later the identification of a process pinch point as a bottleneck to feasible heat recovery was presented by Linnhoff and Flower [103, 104] and Linnhoff *et al.* [105], which culminated in the development of the pinch design method by Linnhoff and Hindmarsh [106]. Since then the pinch concept has been extended to include other resources such as mass integration [107] and wastewater minimization [108].

In the aspect of heat integration, the point with the smallest temperature difference $\Delta T_{\min}$ between the hot and cold composite curves is known as the process pinch point. At this point, the process is most constrained, and further improvements in heat recovery is only obtainable by relaxing this constraint. Moreover, at minimum utility consumption, the composite curves are decomposed at the pinch point, where the region above pinch suffer from a net heat deficit that must be satisfied by an external utility, whereas the region below pinch experience a heat surplus. Consequently, any design that allow for net heat transfer across the pinch point will require additional hot and cold utilities, and should be prevented for minimum energy targeting. The final objective with the pinch design method is to develop a heat exchanger network (HEN) of maximum energy recovery (i.e. an MER design). Extensive early reviews on HEN synthesis have been provided by Gundersen and Naess [109] and Furman and Sahinidis [110], and later by Klemeš and Kravanja [111].

Heat exchangers only make up a small portion of most chemical processes. Additional equipment comprising of stream separation (i.e. distillation columns and flash vessels), reactors, heat engines, heat pumps, and pressure-changing units (i.e. compressors, expanders, valves, etc.), all affect the overall design, hence influencing the stream temperatures, and thus the available heat recovery in the process. Arbitrary integration of process equipment in the HEN can be detrimental to heat recovery and should be avoided. For this reason, the concept of appropriate placement [112], also commonly referred to as correct integration, serves as a fundamental principle in pinch analysis. It provides guidelines or rules dictating how different equipment should be integrated in the HEN to obtain maximum enhanced heat recovery. Appropriate placement rules of various equipment such as heat engines, heat pumps, reactors and distillation columns in HENs are already well documented [113]. Integration of pressure-changing equipment is considerably more complex, however, as it involves simultaneous work and heat transfer. Characterizing the nature of the relationship between these two modes of energy transfer is essential for identifying advantageous integration schemes, which in some cases contradict already established rules of thumb or engineering know-how. Traditionally, compression is done from low temperatures to minimize the work input, whereas expansion is done at high temperatures to maximize the work output. Although this strategy works well in terms of minimizing shaft work (or in the case of expansion: maximize the work output), it disregards the impact of pressure manipulations on the overall heat recovery for the process.

Huang and Fan [114] extended the concept of heat exchanger networks to that of work exchange networks (WENs), where work is transferred from high pressure to low pressure streams using flow work exchangers. Later, Razib *et al.* [115]

developed a model for WEN synthesis, where compressors and expanders are matched using single shaft turbine compressors (SSTCs). The model also included utility compressors and expanders, as well as valves. Heat integration is not considered in their WEN synthesis problem. Instead, rather than looking at these two problems separately, they should be optimized simultaneously, in what is known as work and heat exchange networks. With enhanced work and heat integration in mind, however, the integration scheme for pressure changing equipment such as compressors and expanders can be very different from that in WENs.

Yu et al. formulated the WHENs problem [116] as follows: "Given a set of process streams with supply and target states (temperature and pressure) as well as utilities for heating, cooling and power; design a Work and Heat Exchange Network consisting of heat transfer equipment such as heat exchangers, heaters and coolers, as well as pressure changing equipment such as compressors, expanders, pumps and valves, in a way that minimizes Exergy consumption or Total Annualized Cost". A first attempt at providing a set of guidelines for the integration of compressors and expanders in HENs was made by the ExPAnD methodology [117]. It established a set of heuristic rules stating that as compression adds heat to the system and expansion provide cooling, compression should be done above pinch where there exists a net heat deficit, and expansion should preferably be done below pinch where there is a heat surplus. Later, Gundersen *et al.* [118] reformulated the heuristics, stating that compression and expansion should both be done at pinch. A difficulty with developing rules for appropriate placement of pressure changing equipment such as compressors and expanders is that work and heat are of different qualities and should not be compared on a 1:1 basis. Exergy provides a suitable measure of different modes of energy transfer based on their quality to produce useful work [119]. From the definition, the exergy of work is equal to the work itself. Exergy of heat, on the other hand, is dependent on the temperature level; where temperatures far from the ambient temperature have a higher potential for useful work. Results of the ExPAnD methodology were included in the superstructure used for optimization of Work and Heat Exchange Networks by Wechsung *et al.* [58], where exergy rather than energy was used for targeting in these models. However, the heuristic rules are of limited validity, however, as was later confirmed by a series of theorems for appropriate placement of compressors and expanders in above ambient and subambient heat recovery networks [120–123]. Exergy targeting proved that for minimum exergy destruction in the network, compression/expansion should start at pinch, ambient, or cold/hot utility temperatures depending on the design problem. In particular, the integration scheme is dependent on the availiable heat or cooling as determined by the grand composite curve (GCC), and stream splitting is sometimes necessary to provide heating or cooling as most suited. The results of the theorems are summarized in Table 7.1 for above ambient networks. The

Table 7.1 Appropriate placement of compressors and expanders in above ambient networks.

Theorem	Expansion	Compression
Theorem 1:	$Q_{\text{ex,PI}} \leq Q_{\text{C,min}}$ $T_{\text{ex,HU}} > T_0$ Pinch expansion	$Q_{\text{co,PI}} \leq Q_{\text{H,min}}$ $T_{\text{co,0}} < T_{\text{HU}}$ Pinch compression
Theorem 2:	$Q_{\text{ex,PI}} > Q_{\text{C,min}}$ $T_{\text{ex,HU}} \geq T_{\text{PI}}$ Maximize pinch expansion Expand rest from T_0 or T_{HU}	$Q_{\text{co,PI}} > Q_{\text{H,min}}$ $T_{\text{co,0}} \leq T_{\text{PI}}$ Maximimize pinch compression Compress rest from T_0
Theorem 3:	$Q_{\text{ex,PI}} > Q_{\text{C,min}}$ $T_0 < T_{\text{ex,HU}} < T_{\text{PI}}$ Increase HU expansion Reduce pinch expansion	$Q_{\text{co,PI}} > Q_{\text{H,min}}$ $T_{\text{PI}} < T_{\text{co,0}} < T_{\text{HU}}$ Increase ambient compression Reduce pinch compression
Theorem 4:	$T_{\text{ex,HU}} \leq T_0$ HU expansion	$T_{\text{co,0}} \geq T_{\text{HU}}$ Ambient compression

theorems are symmetrical for subambient networks (see [122, 123])

In addition to the theorems for integration of compressors and expanders in heat exchanger networks, the authors developed a manual design procedure for WHENs using the grand composite curve as a design tool. The procedure is iterative in nature, and revolves around identifying suitable integration temperatures to minimize exergy destruction in the network. It starts with a grand composite curve, and thus a pinch point, for the background process. The theorems state that initially, integration should start from this point, though if the available heat of compression (or cooling from expansion) surpass that of which can readily be absorbed by the background process, a stream split, and hence pressure manipulation from different temperature levels will be necessary to avoid excessive losses. Manual iterations where the individual branch flowrates are varied to provide a best fit for the overall grand composite curve are therefore necessary [120–123]. The manual design procedure was applied to the design of an air separation unit [124].

7.2 Pinch location algorithms

Introduction of computers in process systems engineering was accompanied by an alternative approach to process integration. Although the pinch design method received initial praise for its ability in enhancing process design, it suffered from inherent limitations regarding the problem size and considerations of economic trade-offs due to its manual design procedure. Instead, a separate school developed

starting with the transshipment model by Papoulias and Grossmann [125] that relied on mathematical programming for performing heat integration. Rather than manually develop a heat cascade or construct composite curves to determine the pinch point, the transshipment model formulated the heat integration target as a linear program (LP) that partitioned the streams into individual temperature intervals and calculated the heat residual from each node. Necessary utility consumption would thus be calculated as the amount needed for which the individual heat residuals are equal to or greater than zero, with the constraint being active at minimum utility consumption. Although simple in nature, the LP model provided a mathematically tractable approach to heat integration, that with auspicious scalability, made it possible to analyze larger systems. However, the transshipment model lacked generality especially with regards to variable process streams. In particular, the algorithm was unsuitable for the integration of equipment such as reactor systems, which requires stream temperatures as decision variables to be optimized simultaneous with the heat exchanger network. Instead, to solve these types of problems, a two-stage approach was required, where stream temperatures had to be optimized independently following the solution of the transshipment model [16].

Simultaneous work and heat integration requires the optimization model to handle variable stream conditions. Appropriate placement rules for compressors and expanders necessitates that compression and expansion temperatures are made variables to be determined as part of the integration problem. However, the sequential nature of the transshipment model when handling variable process conditions makes it unsuitable for solving these types of problems. Instead, a simultaneous optimization and heat integration algorithm was proposed by Duran and Grossmann [16] (see Section 2.1.3). It presented the first pinch location algorithm handling variable supply and target temperatures, using nonsmooth equations to quantify the contributions of individual streams above a given pinch point candidate. Although the algorithm achieved a favorable polynomial scaling with the number of integration streams, it still suffered in terms of computation, primarily due to presence of nonsmooth points. Smooth approximations were suggested for handling these constraints, although that too experience certain limitations, especially in regards to the conditioning of the problem. As a result, another algorithm exploiting the development of rigorous MINLP solvers was proposed by Grossmann *et al.* [18]. It replaced the nonsmooth constraints with a disjunctive formulation that used binary variables for assigning stream contributions relative to the pinch candidates. Big-M constraints were needed for handling the disjunctive constraints, and with three binary variables needed for each pair of stream and pinch candidate, the algorithm is exponential in nature. Nevertheless, the availability of applicable solvers for handling MINLP problems generated a lot of attention to the

disjunctive pinch location algorithm, which has since been used in for instance the WHEN superstructure by Wechsung *et al.* [58].

Other pinch location algorithms have been presented in the literature. Anantharaman *et al.* [67] proposed an alternative formulation that instead of locating all possible pinch candidates, determines how inlet temperature of hot streams or the outlet temperature of cold streams are located relative to an intermediate temperature representing the process pinch point. Although big-M constraints are still needed to quantify the individual stream contributions, the alternative model avoids the use of binary variables for describing each stream-pinch candidate pair, and thus achieves a better scaling, though still being exponential in nature. Navarro-Amorós *et al.* [68] proposed a pinch location algorithm based on the transshipment model and an implicit ordering of stream temperatures using shifted temperature intervals. Logical constraints are then used for locating the relative position of process streams to a given temperature interval. The resulting model required additional variables and constraints compared to the formulation by Grossmann *et al.* [18]. However, prepossessing resulted in a considerable reduction in size from the initial problem, making it comparable in both solution time and total relaxation gap [68]. A disjunctive reformulation of the Duran and Grossmann model was suggested by Quirante *et al.* [19] by applying the convex hull reformulation of the max-term provided in Section 2.1.4. The resulting model obtains better scaling than the algorithm by Grossmann *et al.* [18], i.e. two binary variables versus three binary variables for the latter model, in addition to a lower overall relaxation gap. Nielsen and Barton [17] recently proposed a general nonsmooth process integration operator (see Section 2.1.3), formulating the pinch location problem as two nonsmooth equations. No optimization is required for finding the process pinch point, but is instead replaced by a nonsmooth equation solve, making the problem size comparably much smaller than for other pinch location methods in the literature (see Table 7.2).

Scalability is important when implementing the pinch location algorithm as part of the work and heat integration problem. Depending on the choice of superstructure, and thus a specific integration scheme for pressure changing equipment, several streams may have unknown supply or target temperatures, and if allowing for stream splits, unknown heat capacity flowrates. Efficient solution of the overall model depends on the choice of pinch location algorithm, hence the size of the model, and the availability of efficient solvers. Table 7.2 provides an overview of the available pinch location methods in the literature. In particular, the transshipment method and the model by Duran and Grossmann are advantageous with regards to size as no binary variables are involved, and as a result, a polynomial scaling with the number of streams in the model is obtained. However,

both these models suffer from numerical issues; the first concerning the limitation of fixed process conditions, the second due to the presence of nondifferentiable points that can provide numerical instability for derivative based optimization solvers. Nielsen and Barton [17] arguably obtains the best scaling of all the pinch location models, although with two equations, it can only solve for two unknowns. Therefore, if additional unknown process variables are required for describing the problem, a nonsmooth NLP must be solved instead. On the other hand, the disjunctive models obtain an exponential scaling, which is disadvantageous with regards to problem size. However, the generality of these models make it easy to include additional requirements for the network (e.g. forbidden matches, SSTC setup or bypass). Moreover, there exist several solvers on the market that handle these types of models efficiently, even for a relatively large number of variables and constraints [24, 25].

7.3 Superstructures for targeting and synthesis of work and heat exchange networks

Simultaneous work and heat integration requires a strategy for the interaction between heat exchange and pressure manipulating units. The theorems for appropriate placement of pressure changing equipment in HENs accentuated the difficulty to comply with a streamlined approach to WHENs targeting, owing to the trade-off between work and heat and the difference in quality between the two modes of energy transfer. Instead, there exist sets of subproblems for which different integration schemes should be applied (see Table 7.1). A manual design procedure was developed for exergy targeting and synthesis of WHENs. However, it relies on a sequential integration procedure that requires repeated calculations of the grand composite curve, which is time-consuming even for small problems. A mathematical programming based optimization approach overcomes this restriction by solving the work and heat integration problem simultaneously using a mathematical model. Such a model can be formulated using a superstructure, which clearly highlights alternative integration strategies by using graphical means. It compiles different flowsheet decisions; whether it is multistage compression, variable heat capacity flowrates, and/or stream splits, in one exhaustive graph/model that is optimized for a specific objective. A rich superstructure provides a large number of possible configurations, and therefore has the capability of obtaining good solutions. In return, exhaustive superstructures result in large-size models that can become prohibitive for larger problems. More importantly, optimal WHEN design, and thus the choice of superstructure, can only be discussed in connection with a specific objective. Different objective functions are selected for WHEN targeting and synthesis, the most frequently used being total

Table 7.2 Different pinch location algorithms in the literature.

Pinch location method	Model	Process streams	Stream classification	Scalability
Papoulias and Grossmann [125]	LP	Fixed	Fixed	O(n)
Duran and Grossmann [16]	NLP	Variable	Fixed	O(n)
Grossmann *et al.* [18]	MINLP	Variable	Fixed	O(n^2)
Anantharaman *et al.* [67]	MINLP	Variable	Fixed	O(n^2)
Navarro-Amorós *et al.* [68]	MINLP	Variable	Fixed	O(n^2)
Quirante *et al.* [19]	MINLP	Variable	Fixed	O(n^2)
Quirante *et al.* [126]	MINLP	Variable	Variable	O(n^2)
Yu *et al.* [116]	MINLP	Variable	Variable	O(n^2)
Nielsen and Barton [17]	Nonsmooth equation system	Variable	Fixed	2

annualized cost (TAC) and exergy destruction. As this chapter is discussing the use of mathematical optimization for targeting and synthesis of WHENs, the focus lies with obtaining the exergy targets for the network, i.e. a WHEN design equivalent to the MER in heat integration.

A first attempt at developing a superstructure for WHENs synthesis, specifically targeting sub-ambient networks with applications within the LNG field was presented by Wechsung et al. [58]. A state space approach [60] was employed for modeling the interaction between pressure-changing equipment and heat integration, in which the two are separated into different operations. There is a pinch operator that locates the pinch point(s) and calculates the minimum external utility requirements for the process, in addition to preventing temperature crossovers in the multistream heat exchanger. Compression and expansion are included through a pressure operator, and are linked with the pinch operator through the utilization of compressor heat and expansion cooling. The objective of the model is to minimize exergy consumption, i.e. the thermodynamic irreversibilities in the process. Wechsung et al. [58] also considered several alternative objective functions during their studies of the offshore LNG process, such as the minimum nitrogen flowrate yielding a net power output. Onishi *et al.* [127] conducted a total annual cost (TAC) analysis using the same superstructure together with additional operators for the coupling of compressors and expanders, and for selecting valves or turbines. Later, they used the same superstructure in a retrofit design task of WHENs at subambient process conditions [128]. The streams in the model are classified as either fixed or variable (see Figure 7.1). Fixed streams are streams that do not undergo any pressure change, and thus only interact with the pinch operator. The variable streams, on the other hand, are the set of streams that undergo pressure change, and therefore will interact with both pinch and pressure operators. Wechsung et al. [58] employed the ExPAnD methodology in the development of a compression/-expansion scheme. Their focus was on cryogenic processes, more specifically offshore natural gas liquefaction, where cooling is the primary objective. As a result, the proposed superstructure has a distinct compression/expansion scheme that was found to be heuristically favorable for subambient processes. A hot stream undergoing compression should first be cooled to pinch, compressed, followed by additional cooling to pinch to recover any heat from compression. At pinch, the stream should then be expanded, thereby exploiting the cooling from expansion as it is reheated back to pinch, before it is finally compressed and cooled to target. Similarly, for cold streams undergoing expansion with the same number of stages: heating, expansion, heating, compression, cooling, expansion and heating to target temperature. Stream segments are used for each of the different pressure-stages in the model, with variable supply and target temperatures. Hence, the model requires a pinch location algorithm that is capable of handling variable supply/target

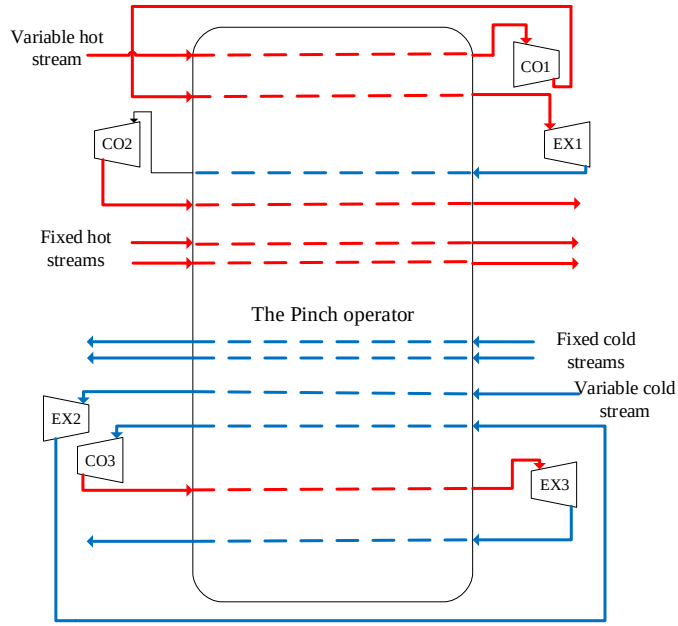

Figure 7.1 A superstructure by Wechsung *et al.* for WHENs targeting.

temperatures. Their original implementation applied the pinch location algorithm by Grossmann *et al.* [18], though any of the above listed algorithms can be used. The compression/expansion scheme causes stream identity changes to occur in the model. For instance, the variable hot stream is temporarily a cold stream after expander EX1, before changing back to being a hot stream after compressor CO2. Similarly, the variable cold stream turns into a hot stream after compressor CO3 before returning to be a cold stream after expander EX3. However, since these stream identity changes are predictable, and will always occur, no extensions to the pinch location method for handling unclassified process streams are required.

Huang and Karimi [129] proposed an alternative superstructure that, similar to the one by Wechsung et al. [58], divides the problem into HEN and pressure operators, respectively. The compression/expansion part is formulated as a WEN problem, employing a similar superstructure to that suggested by Razib *et al.* [115], thus allowing for pressure recovery from using companders (i.e. a unit with both expansion and compression) as well as bypass of a pressure stage. Unlike the previous superstructure, however, greater attention was directed towards the specific compressor and turbine setup, distinguishing between utility and SSTC equipment, and coming up with a design that enhances the total pressure recovery. Effects from

the placement of pressure-changing equipment in relation to the HEN is not investigated here. Instead, rather than reducing the exergy consumption, the objective of the model is to minimize total annualized cost of the process. The result is the multi-stage superstructure shown in Figure 7.2, where the pressure-changing streams pass through both the HEN and WEN at each pressure stage.

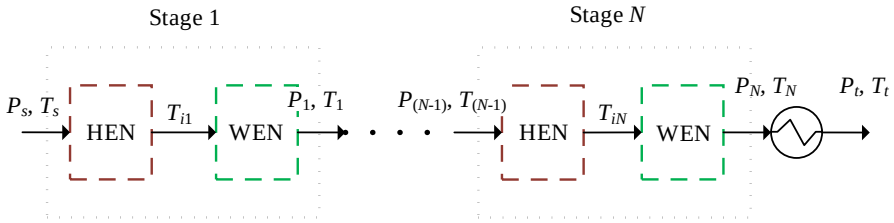

Figure 7.2 The multi-stage superstructure by Huang and Karimi.

In Figure 7.2 P_s and T_s are the supply pressure and temperature, T_{in} is the intermediate temperature at pressure stage n (where $n = 1, \ldots, N$), and P_t and T_t are the target pressure and temperature. Rather than using the compression/expansion scheme of Wechsung *et al.* [58], the model distinguishes between high-pressure (HP) and low-pressure (LP) streams, where HP streams are expanded and LP streams are compressed. The model also includes throttling valves for the HP streams as well as the possibility of bypassing pressure-changing stages. Figure 7.3 shows the WEN compression and expansion stage in detail.

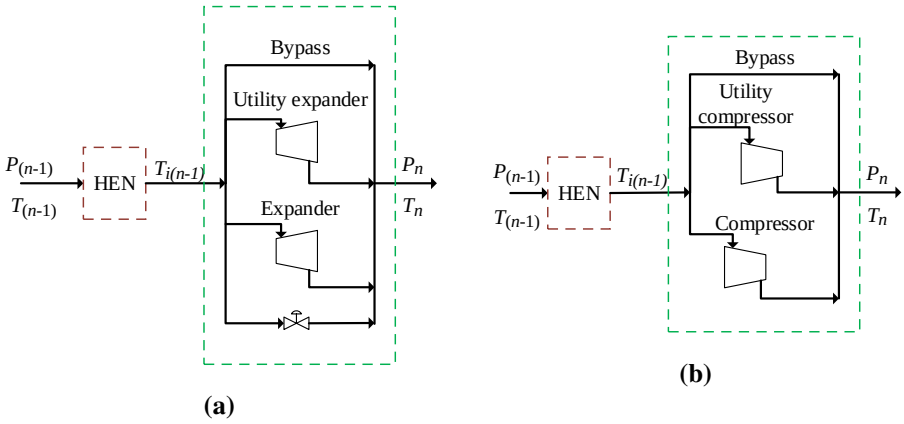

Figure 7.3 The WEN network at pressure stage n in the model by Huang and Karimi: (**a**) for high-pressure streams, (**b**) for low-pressure streams.

The model by Huang and Karimi does not rely on either heuristics from the Ex-

PAnD methodology or the theorems for appropriate placement of compressors and expanders in HENs. Instead, the model increases the net power production through expansion at high temperatures and compression at low temperatures. HP and LP streams are thus treated respectively as cold and hot streams in the HEN. The TAC analysis performed by Onishi *et al.* [127] applied the same WEN superstructure, originally proposed by Razib et al. [115]. As a result, the superstructure shows a resemblance to the one by Huang and Karimi, particularly in the WEN stage, though with some significant differences. First, the specific compression and expansion route highlighted by Wechsung *et al.* was employed, and with it the heuristic method of pinch compression and expansion. Secondly, the superstructure considers only pressure-changing gas streams, with a heater placed at the end of each HP stream and cooler at the end of each LP stream. This was a necessary requirement to guarantee that the stream is either heated or cooled to the respective target temperature. Later, Onishi et al. [130] used the same superstructure in a multi-objective optimization model with the simultaneous minimization of TAC and the environmental impact.

Nair *et al.* [131] further generalized the stage-wise superstructure by relaxing some of the model requirements. Firstly, the model no longer preclassifies streams as either HP or LP. Instead, all process streams are allowed to change pressure, those with a net pressure change of zero included. Moreover, the WEN superstructure is simplified in that the utility compressors and expanders are excluded from the model, instead treating them as a special case of SSTC without work recovery. Distinct WEN superstructures for variable pressure streams as shown in Figure 7.3 are therefore no longer necessary. As shown in Figure 7.4, the WEN module instead comprises of three distinct branches; thus including a compressor, turbine and valve in the same module, and a stream can pass through exactly one pressure changing unit at each stage. Hence, no parallel compressor and expander arrangements are allowed in the model. Preclassification into hot and cold streams is no longer necessary in the HEN module. Instead, binary variables are added to correctly identify whether the process stream is either hot or cold. Such a relaxation is important, especially for the synthesis of WHENs, as compressor and expander temperatures may vary considerably from the individual pressure stage in order to benefit from enhanced heat recovery. Lastly, the superstructure allow for thermodynamic models and individual phase changes. The result is a rich superstructure for TAC minimization of WHENs. The model was applied to optimize a propane splitter, as well as the offshore LNG process initially studied by Wechsung *et al.* as part of the liquefied energy chain [58].

A new flowsheet representation of WHENs based on the concept of abstract building blocks for process design, integration and intensification [132–134] was presen-

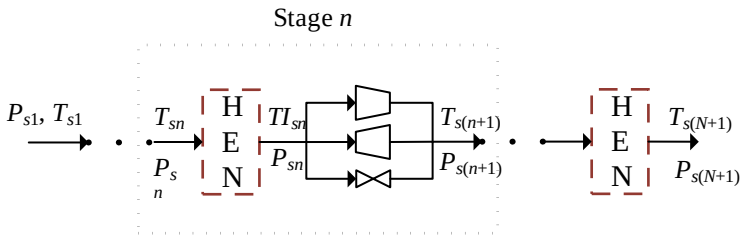

Figure 7.4 The multi-stage superstructure by Nair *et al.*

ted by Li *et al.* [135]. The methodology represents the process flowsheet using a 2D box grid, where a single box represents a certain operation, and is connected to other boxes either through an unrestricted, semi-restricted or restricted boundary. Unrestricted boundaries represent no change in stream properties such as pressures and compositions, although temperature and phase are still allowed to change. Pressure changes are represented using a semi-restricted boundary along with specific type of pressure changing equipment. Heat transfer is, on the other hand, represented using the fully restricted boundary type, and boxes with more than one fully restricted boundary are used to indicate MHEXs [135]. The alternative flowsheet depiction was used to develop an exhaustive model for WHEN synthesis under the objective of TAC minimization. Unlike the other superstructures that employ a state-space or multistage superstructure representation, where work and heat integration are handled individually in different operators, this new methodology study each box individually using material and energy balances. The stream path and grid boundaries are determined through the use of binary variables. The same also holds true for decisions regarding individual process equipment such as compressors, expanders, mixers, etc. As a result, the authors translate the various flowsheet decisions into an exhaustive MINLP formulation, which was used to solve the offshore natural gas liquefaction process from Wechsung *et al.* [58] and Nair *et al.* [131].

A superstructure developed from the theorems of appropriate integration of compressors and expanders [120–123] has been suggested by Uv [136]. Figure 7.5 presents a schematic of the WHEN superstructure, which splits each pressure-changing stream into N branches, each corresponding to a different inlet temperature to the pressure-changing unit. Following the theorems, the inlet temperatures must be either at the pinch temperature, hot or cold utility temperature, or the ambient temperature to guarantee a solution for which exergy consumption is minimal. Moreover, two additional stream segments are used for each stream branch; one before and one after the pressure-changing unit. The first segment will have

a supply temperature equal to the supply temperature of the original stream and a target temperature corresponding to the inlet temperature of the pressure-changing unit. Similarly, supply and target temperatures of the second segment are equal to the outlet temperature of the pressure-changing unit and the target temperature of the original stream, respectively. The resulting model is very similar to the manual design procedure suggested by Fu and Gundersen, where stream branches are integrated successively using the heat cascade to locate process pinch point(s).

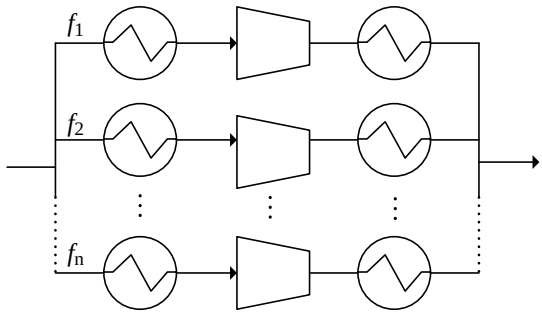

Figure 7.5 The superstructure by Uv.

7.4 Limitations of the superstructures

Recent interest in the interaction of work and heat, and more importantly how they can be enhanced in WHENs, have resulted in various superstructures. However, it is essential to consider the overall objective as well as the underlying thermodynamics to avoid cutoffs of the optimal solution. In the development of the concept of pinch analysis, as well as the use of mathematical programming, more specifically, through the development of pinch location algorithms, the focus was on obtaining a network of maximized energy recovery (MER) network. Then, once such a network has been obtained, trade-offs between energy recovery and cost could be explored to obtain a network that is both energetically and economically favorable. All the superstructures presented in the literature thus far, apart from the superstructures by Wechsung *et al.* [58] and Uv [136] have considered TAC only. In doing so, little attention has been given to the concept of appropriate integration of pressure-changing equipment on these types of networks. The superstructure by Wechsung *et al.* [58] utilized the ExPAnD methodology in the superstructure where compression and expansion are integrated at the pinch. However, as was later discovered by the previously mentioned theorems, pinch compression/expansion is not always optimal. Instead, stream splitting is sometimes required with inlet temperature to the pressure-changing unit being pinch temperatures, hot or

cold utility temperatures or ambient temperature. Therefore, not accounting for stream splitting in the superstructure may lead to suboptimal results.

Recent approaches have included stream splitting in their superstructures. A model by Huang and Karimi [129] splits streams to account for utility compressors or expanders, single shaft compressor-expander arrangements, a bypass, plus an additional branch for valves in the case of HP streams. The optimal integration of the WEN determines the stream split ratios in the network. Nevertheless, the HEN part of the model is included upstream of the stream split, such that the inlet temperatures to the various pressure-changing units remain equal between the different stream branches and thus the superstructure does not follow the result of the theorems. Instead, the model maximizes power production in expanders by increasing the inlet temperature before expansion, and minimizes the power consumption in compressors by reducing the temperature before compression. Consequently, the superstructure considers the WEN and HEN parts separately, which may lead to suboptimal solutions at least in terms of total exergy consumption. Another difficulty with this formulation is the coupling of compressors and expanders. Additional binary variables are required to accommodate this additional feature, and thus the MINLP can become difficult to solve for large problems. Binary variables are also included for generators, helper motors, utility compressors/expanders, valves, and bypasses on each stage, thus adding further complexity to the model. Although these extra features are required when minimizing Total Annual Cost, they add unnecessary complexity to exergy targeting models. Nair *et al.* [131] further expanded the superstructure to also include unclassified streams, no explicit compression and expansion scheme, and phase changes. Although it makes the model more exhaustive, it still lacks the capability of obtaining the WHEN for which thermodynamic losses are minimized. Instead, both these superstructures split the WHEN into individual WEN and HEN evaluations, with some coupling between the two at each stage.

An entirely different strategy was explored by Li *et al.* [135] where the WHEN model is developed by mass and energy balances for individual process streams through an abstract box formulation. This superstructure can be made very rich, depending on whether jump streams (streams that are not adjacent in the 2D grid are allowed to interact) are included in the balance. However, including these streams makes the resulting model very big and difficult to solve. Even without the jump streams, the model complexity was an issue, requiring about 2h to solve the test example previously examined by Wechsung *et al.* [58] and Nair *et al.* [131].

In the superstructure by Uv [136], each stream branch corresponds to a possible inlet temperature to the pressure-changing unit, i.e. a Pinch temperature, hot or

cold utility temperature or ambient temperature. The Pinch points are calculated from the heat cascade prior to optimization. Thus, the resulting algorithm is sequential, following the same calculation procedure as the manual design procedure by Fu and Gundersen [120–123]. The result is a linear model that is easy to solve, yet this sequential solution strategy suffers from several disadvantages. Integrating more than one compressor/expander sequentially can potentially lead to suboptimal results as the integration sequence might influence the set of pinch points in the network. Therefore, each possible sequence of integration should be studied in order to ensure global optimality, which can be tedious. Another problem occurs whenever the heat from compression or the cooling from expansion exceeds the heat deficit or surplus at the given temperature in the process. In this case, a new pinch point occurs, and more stream branches are required. Several additional pinch points may occur with pressure integration, in which case the heat cascade must be solved multiple times before reaching an appropriate number of stream splits in the model. Alternatively, a simultaneous optimization approach can be employed. The penalty is that a nonconvex NLP model (in case of nonsmooth pinch location algorithms) or an MINLP model will replace the much simpler LP model. In addition, the proposed superstructure with stream branches for every pinch point in the model will remain problematic in the simultaneous approach, as pinch points may be created or changed due to the integration of pressure-manipulated streams in the model. Hence, the number of branches, and thus stream segments, will remain dynamic, subjected to change during optimization. Stream identities for the individual stream branches will also be subject to change when a simultaneous approach is implemented. Temperatures of compression or expansion vary greatly depending on whether utility temperature, ambient temperature or a pinch candidate is used. Necessarily, a simultaneous approach must solve for the stream identities as part of the overall optimization problem, which considerably inflates the model scaling depending on which pinch location algorithm is used. This further complicates the problem, as the final number of variable hot or cold streams (segments) is unknown.

7.5 Conclusions

This chapter studies alternative optimization models for work and heat exchange networks. Different superstructures from the literature have been presented in view of minimizing the internal irreversebilities for the network. In particular, the placement of pressure changing equipment in relation to the heat integration network is paramount to achieve synergistic effects, as compressors and expanders provide either heating or cooling, which if integrated wrongly, may have a detrimental effect on heat recovery. Nevertheless, most of the current superstructures are focusing on a total annualized cost analysis without taking these effects into account.

Another challenge with the combined work and heat exchange networks is capturing the value of the different modes of heat transfer. Specifically, the quality of heat is secondary in above ambient networks, and thus cannot be compared with mechanical work on a 1:1 basis. Instead, the concept of exergy is a better performance indicator, which quantifies the reversible work that can be obtained from a unit heat at a given temperature.

A superstructure by Wechsung et al. [58] approach the simultaneous work and heat integration problem by decomposing the model into a pressure operator and heat integration operator, respectively. Although any pinch location algorithm can be used for modeling the heat integration operator, they employ a disjunctive model by Grossmann *et al.* [18]. Several pinch location algorithms have since then been proposed, some of which obtain a better scaling and thus are more suitable for large sized problems. The superstructure also tries to capture the relative value of heat in comparison to the mechanical work output by minimimizing the total exergy consumption in the network. Compressors and expanders are integrated in accordance with the ExPAnD methodology [117], which is a series of heuristics stating that both compression and expansion should be carried out at pinch temperature. However, it was later discovered in a series of theorems by Fu and Gundersen [120–123] that these heuristics only hold true for a small subset of the problems. In other instances, stream splitting followed by the compression and expansion at other candidate temperatures such as utility and ambient temperature, will be required to minimize the irreversibilities in the network.

Other superstructures that employ stream splitting for the variable pressure streams have been presented by Huang and Karimi [129] and Nair *et al.* [131]. However, heat integration is here included upstream of the stream splits, such that compression and expansion is done at the same temperatures in all the stream branches in violation of the theorems. Another exhaustive superstructure was developed by Li *et al.* [135] based on an alternative flowsheeting strategy using a grid representation. Although the model can be made to include all integration possibilities including those stated by the theorems, simplifications need to be made to make the superstructure suitable for solving medium to large sized problems.

Uv [136] included the theorems in a superstructure, which splits the variable pressure streams in N branches that interact individually with the heat integration model to maximize the heat recovery. Although the resulting model is an LP, which is easy to solve, its sequential approach suffers from several drawbacks. In particular, pressure manipulations may create additional pinch points, requiring several iterations of the pre-processing procedure. Furthermore, the sequence of integration may also influence the set of pinch locations and thus the solution of the model. On the other hand, a simultaneous approach is also challenging with

this superstructure, primarily due to the fact that the number of stream branches and stream segments changes in the model, and that the stream identities must be solved as part of the optimization model. Further research is therefore required to make this superstructure (1) build on the theorems for Correct Integration, (2) work well with a simultaneous approach, and (3) scale well with the number of streams and pressure-changing equipment such that the model can be applied to larger and more commercially interesting process designs.

Chapter 8

A Nonsmooth Formulation for Handling Unclassified Process Streams in the Optimization of Work and Heat Exchange Networks

Abstract

Targeting and synthesis of work and heat exchange networks by means of mathematical programming requires a rigorous optimization apporach that does not place artificial bounds on the problem. Pinch location algorithms have been widely studied in the literature, offering different modeling strategies such as disjunctive programming, or smooth approximations to address the issue of unknown supply and target temperatures. The efficiency and computational complexity depend on the method used, with some offering a better scalability by resorting to nonsmooth formulations that have traditionally been difficult to handle. A limitation with most existing pinch location algorithms, however, is that they rely on process streams being sorted into hot and cold streams a priori. Consequently, they are limited, in that the target temperature is bounded either from above or below depending on the stream classification used. Extensions have been suggested, using binary variables to assign the correct classification as part of the optimization problem. In this chapter, a nonsmooth formulation is proposed, which obtains a better scaling compared to methods in the literature. Examples related to work and heat exchange network targeting and synthesis are solved using the same modeling strategy and sensitivity calculation procedure explored in the previous chapters.

This chapter is based on the publication:

- M. Vikse, H. A. J. Watson, P. I. Barton, and T. Gundersen. Nonsmooth formulation for handling unclassified process streams in the optimization of work and heat exchange networks. *Industrial & Engineering Chemistry Research*, 58(22): 9526-9539, 2019.

Superstructures for targeting and synthesis of work and heat exchange networks were covered in the previous chapter. Different approaches were analyzed that considered either the minimization of total annualized cost or total exergy consumption in the network. Among these, a model that incorporates the theorems for the integration of pressure-changing equipment in heat exchanger models was presented [136]. The superstructure employs stream splitting, followed by compression or expansion at a set of predefined temperatures. Similar to the manual design procedure, the optimization strategy is sequential in nature, where the process pinch points are first located prior to optimization, and then included in the superstructure as individual target temperatures for the stream segments upstream of the compressors/expanders. The individual stream branches interact with the heat exchanger network both upstream and downstream of the pressure changing unit to enhance the heat recovery of the process. Temperatures are calculated by using a linear program formulation of the heat cascade to ascertain which of the theorems in Table 7.1 holds in a specific instance, and use this information to obtain a network of minimum irreversibilites for the process. The problem therefore becomes that of exergy targeting with known supply and target temperatures. However, using the said sequential approach suffers from several disadvantages such as inability to address (i) the optimal sequence of integration for compressors and expanders, and (ii) variable pressure specifications. Most importantly, the procedure is iterative in nature, and for complex integration problems, the process pinch points may change dynamically as additional pressure-changing streams are integrated. Furthermore, as pressure-changing equipment are added to the background process, the graphical representation, i.e. the grand composite curve changes, and so does the integration strategy. Hence, the sequence of integration becomes a degree of freedom subject to optimization. These limitations are eliminated with the use of a simultaneous optimization and integration strategy, however, which was the method of choice for the other superstructures. However, transitioning from a sequential to a simultaneous optimization approach, requires certain considerations to be taken into account.

8.1 Introduction

In WHEN synthesis, compression and expansion temperatures are varying considerably, making it difficult to classify the variable pressure streams into hot and

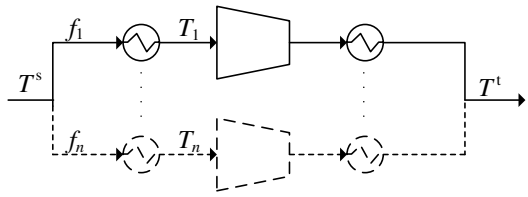

Figure 8.1 The WHEN superstructure for integration of compressors.

cold streams for heat integration. According to the theorems in Table 7.1 for the integration of compressors and expanders in above ambient networks, pressure manipulation should preferably be done at the pinch temperature(s), hot or cold utility temperatures or ambient temperature depending on the problem. Also subject to change are the required number of active stream branches, which depend on the number of candidate temperatures in the problem (see Figure 8.1). A simultaneous optimization and integration approach requires the model to treat the individual compression and expansion temperatures as variables (variables T_1 through T_n in Figure 8.1), rather than calculating these via a pre-processing procedure. Moreover, as the relative position of the individual temperature variables with respect to supply (T^s) and target (T^t) temperatures of the variable pressure streams are subject to change during optimization and such cannot be determined a priori, the identity of the individual stream branches must be treated as unknowns to be solved as part of the overall problem.

Different simultaneous optimization and heat integration algorithms were presented in Table 7.2. Primarily, these algorithms address the problem of variable supply and target temperatures with the assumption that the integration streams can be classified as either hot or cold prior to optimization. Different extensions for also handling cases where stream identities are unknown have been proposed. Kong *et al.* [137] proposed a MINLP formulation for the simultaneous optimization and heat integration problem with unclassified streams. The method assigned binary variables for the (de)activation of unclassified streams and the subsequent assignment into hot or cold process streams. Big-M constraints were employed for the assignment, with only active stream segments contributing to the overall heat integration. The methodology also featured possible extensions for modeling phase-changes, isothermal streams and multiple utilities. Simultaneous work and heat integration was not considered in their model, instead focusing on heat integration only in their illustrative examples. Yu *et al.* [138] tested different extensions to the simultaneous optimization and heat integration algorithm by Duran and Grossmann[16]. The authors presented three different modeling strategies, and applied them to the superstructure by Uv [136] for exergy targeting and synthesis

of WHENs. The first strategy used smooth approximations for the nonsmooth operators, and binary variables for the stream identities. The other two approaches replaced the nonsmooth operators with the disjunctive formulations by Grossmann *et al.* [18] and Quirante *et al.* [19], respectively. The authors concluded that the approach using smooth approximations performed better overall than the two disjunctive representations, primarily due to scaling, especially with respect to the number of binary variables in the model. Quirante *et al.* [126] presented an extension to the disjunctive pinch location algorithm [19] that handles unclassified streams, where disjunctions are included to assign the stream identity. The same formulation was later used by Onishi *et al.* [139] in an optimization model for WHEN synthesis with unclassified process streams. Nair et al. [131] allowed for unclassified process streams in the superstructure using a big-M formulation and solving an MINLP.

Computational complexity and problem scalability is vital in deciding which pinch location algorithm to be incorporated into a WHEN superstructure. Variable pressure streams complicate the heat integration problem, even when single stage compression and expansion and fixed target pressures are considered, and applying stream splits to account for pressure manipulations at different candidate temperatures can result in large optimization problems that prove difficult to solve. Although different formulations for handling unclassified process streams have been adressed in the literature, all of the above formulations rely on an MINLP formulation, all of which have a polynomial scaling according to Table 7.2. Consequently, they rely on solving large and complex optimization problems, that can be prohibitive even for relatively small problems. The present chapter presents a nonsmooth extension to the Duran and Grossmann model for handling unclassified process streams. Using the methodology described in Chapter 2, the nonsmooth operators max and min are used for assigning target temperatures for the variable temperature streams, thus removing the contribution from streams with wrong identity. The main contribution of this work is that no binary variables or disjunctive formulations are required, resulting in a more compact formulation of the WHEN targeting and synthesis problem than the different formulations discussed by Yu *et al.* [138] The extension can be applied to both the original Duran and Grossmann model and the generalized nonsmooth process integration operator provided by Nielsen and Barton, both described in detail in Section 2.1.3. The new nonsmooth extension is used for modeling different WHEN case studies presented in the papers by Fu and Gundersen [120, 121] using the superstructure in Figure 8.1. Isothermal mixing is assumed in the model, such that the individual target temperature for each of the stream branches should equal the target temperature of the parent stream. Furthermore, the supply temperature is equal for all the stream branches [136]. Therefore, each stream branch contributes to the heating or cooling of the process at differ-

ent temperature levels. Allowing non-isothermal mixing would make the problem definition richer and the feasible solution space larger, however, at the expense of computational complexity. One option could be to run an NLP optimization for the network configuration found by the current model where the isothermal mixing assumption is relaxed. This is similar to what is done with the stage-wise superstructure by Yee and Grossmann [55–57] for HEN synthesis. The allocation of pressure changing equipment between single shaft turbine compressor (SSTC) units and utility compressor/expanders are not considered in the superstructure. Instead, this could be done during post-processing, or through an economic analysis. As in Chapter 6, optimization is done using the primal-dual interior point algorithm IPOPT [85], with sensitivities obtained analytically using the automatic differentiation framework for calculating LD-derivatives.

It should be mentioned that our approach to WHENs in this chapter is not truly a simultaneous optimization procedure for work and heat exchange networks, since WEN synthesis is not included. Our focus is on utilizing the heating from compression and cooling from expansion in the heat recovery problem in order to reduce the consumption of thermal utilities by paying a small penalty in power. Integration of work between expanders (turbines) and compressors can be done directly (shaft work) or indirectly (power). As a result, work integration does not adhere to the same limitations seen in heat recovery, where a temperature gradient is observed during heat exchange, preventing a low temperature stream from providing heat to a high temperature stream. Instead, work recovery can occur independently of differences in pressure level without an accompanying "pressure pinch" similar to the temperature pinch. Synthesis of WENs therefore prove a comparably simpler task that can be handled subsequently during post-processing.

8.2 Nonsmooth extension for unclassified process streams

In the examples provided in this chapter, simultaneous optimization and heat integration is achieved using the algorithm by Duran and Grossmann [16]. The algorithm was described in detail in Section 2.1.3 and reproduced here for clarity:

$$\begin{aligned} \min_{\mathbf{x}} \quad & c_{\text{CU}} Q_{\text{CU}} + c_{\text{HU}} Q_{\text{HU}} \\ \text{s.t.} \quad & \sum_{i \in H} F_i (T_i^{\text{s}} - T_i^{\text{t}}) - \sum_{j \in C} f_j (t_j^{\text{t}} - t_j^{\text{s}}) + Q_{\text{HU}} - Q_{\text{CU}} = 0, \\ & z^p - Q_{\text{HU}} \leq 0, \quad \forall p \in H \cup C, \\ & Q_{\text{HU}} \geq 0, Q_{\text{CU}} \geq 0, \end{aligned} \tag{8.1}$$

where z^p is defined by the following expression:

$$
\begin{aligned}
z^p := & \sum_{j \in C} f_j[\max\{0, t_j^{\mathrm{t}} - (T^p - \Delta T_{\min})\} - \max\{0, t_j^{\mathrm{s}} - (T^p - \Delta T_{\min})\}] \\
& - \sum_{i \in H} F_i[\max\{0, T_i^{\mathrm{s}} - T^p\} - \max\{0, T_i^{\mathrm{t}} - T^p\}],
\end{aligned} \tag{8.2}
$$

and the pinch candidate temperatures T^p are provided by Equations (8.3) and (8.4) for hot and cold streams, respectively.

$$T^p = T_i^s, \quad \forall p = i \in H, \tag{8.3}$$

$$T^p = t_j^s + \Delta T_{\min}, \quad \forall p = j \in C. \tag{8.4}$$

The choice of pinch operator for this study was supported by its advantageous polynomial scaling (see Table 7.2) and continuous, yet nonsmooth model formulation. Moreover, the formulation satisfy the requirements for L-smoothness, and thus its LD-derivatives can readily be obtained.

In the sequential optimization procedure proposed by Uv [136], the large span in possible compression/expansion temperatures does not present a modeling issue, as each candidate inlet temperature (i.e. pinch candidates, utility temperatures and the ambient temperature) are enumerated during pre-processing. Consequently, the stream classification can be fully determined for each compression/expansion temperature prior to optimization. However, in the simultaneous approach, each compression/expansion temperature is treated as a variable by the optimization model. The temperatures can therefore vary greatly, not only between different design problems, but also for each iteration step of the optimizer. Consequently, the classification of streams cannot be determined a priori in the superstructure.

Although the formulation in Equations 8.1-8.4 can handle variable supply and target temperatures, it assumes the stream classifications to be known. However, here we show that the algorithm can be extended to the problem of unclassified process streams by the inclusion of the nonsmooth Equations (8.5) and (8.6):

$$
\begin{aligned}
& T_i^{\mathrm{s}} = S_i^{\mathrm{s}}, \quad \forall i \in U, \\
& T_i^{\mathrm{t}} = \min(S_i^{\mathrm{s}}, S_i^{\mathrm{t}}), \quad \forall i \in U,
\end{aligned} \tag{8.5}
$$

$$
\begin{aligned}
& t_j^{\mathrm{s}} = S_j^{\mathrm{s}}, \quad \forall j \in U, \\
& t_j^{\mathrm{t}} = \max(S_j^{\mathrm{s}}, S_j^{\mathrm{t}}), \quad \forall j \in U,
\end{aligned} \tag{8.6}
$$

where U is the set of unclassified process streams, S_i^{s} and S_i^{t} are the supply and target temperatures of the actual stream, T_i^{s} and T_i^{t} are the supply and target temperatures of the hot substream, and t_i^{s} and t_i^{t} are the supply and target temperatures of the cold substream. Rather than using binary variables, the nonsmooth extension divides each unclassified process stream into a hot and cold component, respectively. The supply temperature for each component stream is set equal to the parent stream, whereas the target temperature is determined by Equations (8.5) and (8.6). Depending on the target temperature only one of the two component substreams remain active in the integration problem. For the case where the target temperature is less than the supply temperature, the unclassified process stream is in fact a hot stream, and the min operator in Equation (8.5) assigns the correct target temperature. The corresponding cold component, on the other hand, is deactivated by setting the target temperature equal to its supply temperature in Equation (8.6). Consequently, it contributes neither to the overall energy balance nor to the individual energy balance above each pinch candidate (Equation (8.2)). The reverse becomes true if the unclassified stream behaves as a cold stream, when the target temperature is greater than the supply temperature. Figure 8.2 shows the target temperatures of the two component substreams as a function of the target temperature of the parent stream. As can be seen from the figure, the component substreams contribute in distinct regions of the domain, with cold substreams activated at target temperatures $\geq S^{\mathrm{s}}$ and hot substreams activated for target temperatures $< S^{\mathrm{s}}$. In the flat regions of the curves, therefore, the substreams remain passive as supply and target temperatures are the same.

8.3 Examples

Different examples are used to demonstrate the nonsmooth extension for heat integration with unclassified process streams. Examples are taken from the papers by Fu and Gundersen on the integration of compressors and expanders in above ambient networks [120, 121]. Previously, these examples were solved using a manual design procedure for WHEN synthesis with the objective of minimizing exergy losses. The procedure is iterative in nature, thus preventing the issue of unclassified process streams. In this chapter, on the other hand, the examples are solved using the WHEN superstructure from Uv [136] with the extended Duran and Grossmann formulation. The models are written in Julia v0.6.0 and run on a Dell Latitude E5470 laptop in the Ubuntu v16.10 environment with an Intel Core i7-6820HQ CPU at 2.7 GHz and 8.2 GB RAM. Optimization is done using IPOPT v3.12.6 [85] with sensitivities provided by the generalized derivative elements. Similar IPOPT settings used in Table 6.3 were used for solving the WHEN optimization problems. However, the maximum number of iterations was increased from 500 to 2000, and the tolerance (here the dual feasibility tolerance) was increased

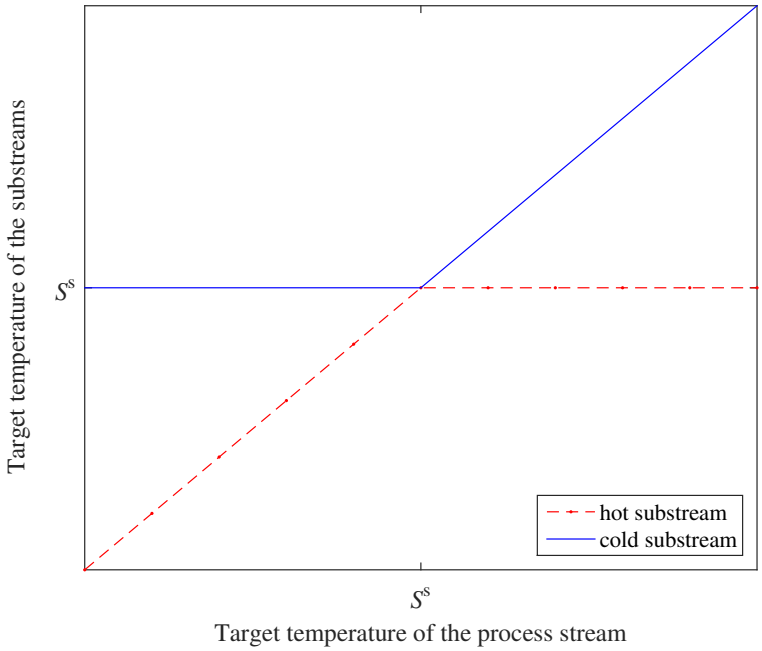

Figure 8.2 Target temperatures of the hot and cold substreams as a function of the target temperature of the parent stream.

to 1.0 due to empirical improvements to convergence for some instances.

8.3.1 Assumptions and problem formulation

Different assumptions were made when deriving the theorems for appropriate placement of pressure-changing equipment [121]. Firstly, the supply and target temperatures must be known a priori, and remain fixed during optimization. In addition, the authors assume a single hot and cold utility at constant temperature. The variable pressure streams behave as ideal gases with a constant heat capacity ratio $\kappa \equiv c_p/c_v$, and the compressor/expander efficiencies are constant. As the theorems provide the foundation for the superstructure, the same assumptions are made for the examples in this chapter.

The maximum number of stream splits for the variable pressure streams is limited to three in the model to curb the problem size, and to prevent capital intensive solutions with large number of splits and low branch flowrates. This assumption remain valid for all the case studies in this chapter, which require at most two stream branches, but can be relaxed upon obtaining an optimal solution involving

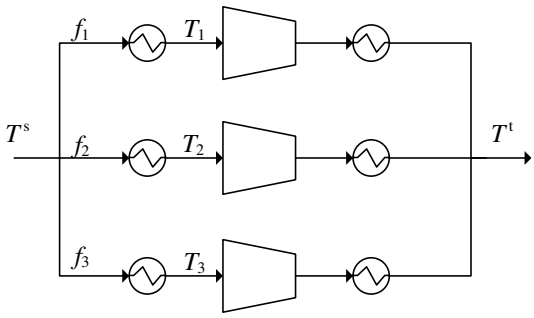

Figure 8.3 Superstructure for placement of compressors in HENs. The superstructure is analogous for expanders.

a stream split into three branches. Figure 8.3 shows the compression scheme for a variable pressure stream with three stream branches. The variables in the model are the individual branch heat capacity flowrates and temperatures, as well as the net work and hot/cold utility consumption.

As pressure changing equipment are included in the model, the objective from Equation (8.1) of minimizing hot/cold utility consumption is changed to that of minimizing the total exergy consumption:

$$Ex(\mathbf{x}) = Q_{\text{HU}}(\mathbf{x}) \left(1 - \frac{T_0}{T_{\text{HU}}}\right) - W_{\text{net}}(\mathbf{x}), \tag{8.7}$$

where T_{HU} is the hot utility temperature and T_0 is the ambient temperature, both in units of Kelvin, and $W_{\text{net}}(\mathbf{x})$ is the net power produced given a vector $\mathbf{x}$ consisting of the compression/expansion temperatures and heat capacity flowrates. The exergy of the cold utility is not included in the objective function as the cold utility temperature is equal to the ambient temperature, i.e., the reference temperature for exergy calculations, and thus the Carnot factor becomes zero. Furthermore, the superstructure assumes isothermal mixing at the outlet temperature T^{t}, which is purely a numerical consideration to avoid additional bilinear terms and nonconvexity. The temperatures after compression/expansion are calculated using the following relation:

$$T_{\text{out}} = T_{\text{in}} \left(\frac{P^{\text{t}}}{P^{\text{s}}}\right)^{(\kappa - 1.0)/\kappa}. \tag{8.8}$$

As derivatives can readily be obtained for this function using the AD framework mentioned previously in Section 2.2, Equation (8.8) is included as a subroutine rather than an equality constraint resulting in fewer variables in the model. Consequently, outlet temperatures from compression/expansion are not independent

Table 8.1 Variable bounds for the examples.

Variable	x_{L}	x_{U}	**Variable**	x_{L}	x_{U}
Q_{CU} [kW]	0.0	`inf`	Q_{HU} [kW]	0.0	`inf`
T_1	T_0	T_{HU}	T_2	T_0	T_{HU}
T_3	T_0	T_{HU}	f_1	0.0	F
f_2	0.0	F	f_3	0.0	F

Table 8.2 Stream data for Example 1.

Stream	T^{s} [°C]	T^{t} [°C]	F [kW/°C]	P^{s} [kPa]	P^{t} [kPa]
H1	400	60	3	-	-
H2	400	280	2	2500	100
C1	200	380	8	-	-
Hot utility	400	400	-	-	-
Cold utility	15	15	-	-	-

variables in the optimization model, but are instead calculated in the subroutine as functions of the stream target temperatures upstream of the pressure changing unit. A heat capacity ratio of $\kappa = 1.4$, ambient temperature $T_0 = 15$°C, and a $\Delta T_{\mathrm{min}} = 20$ K are used in all the examples. Bounds on the optimization variables are provided in Table 8.1. The hot and cold utility duties are bounded from below to only take non-negative values. Hence, no steam generation is included in this problem formulation, and utility temperatures are fixed to incorporate only a single hot and cold utility source. For the variable pressure streams, expansion and compression temperatures are bounded by the ambient and hot utility temperatures. In addition, the individual branch heat capacity flowrates are bounded between zero flow and the total heat capacity flowrate F of the variable pressure stream in question. Optimization is done from a starting point with compression/expansion temperatures of 400°C, 150°C and 100°C, and with branch heat capacity flowrates distributed equally.

Example 1: The first example is a heat integration problem taken from Fu and Gundersen [121], where a hot stream undergoes expansion from 2500 kPa to 100 kPa. Supply and target temperatures are fixed for all the streams, including the stream undergoing pressure change. Furthermore, utilities are assumed available at constant temperatures, specifically at 400°C and 15°C for hot and cold utilities, respectively. Stream data are provided in Table 8.2.

As supply and target temperatures are fixed for the constant pressure streams, only

Table 8.3 Path of the variable pressure stream at the solution of Example 1.

Stream	T^{s} [°C]	T^{t} [°C]	F [kW/°C]	P [kPa]	Classification
S1	400.00	400.00	2	2500	-
S2	-4.80	280.00	2	100	C

hot stream H2 constitutes an unclassified process stream in this example. It is denoted as a hot stream in Table 8.2, merely for convenience since it has a target temperature lower than its supply temperature. Furthermore, since a stream split with three branches is used in the superstructure and each branch is represented by substreams both upstream and downstream of the expanders, there is a total of six unclassified streams in this example. Expansion temperatures and the individual branch heat capacity flowrates are selected as decision variables in the problem. Together with hot and cold utility duties, this corresponds to 8 decision variables in total. IPOPT obtained a solution to the WHENs problem after 28 iterations and a total CPU time of 3.2 s. Expansion should be done solely from hot utility temperature, yielding a net exergy generation of 203.34 kW. The same solution was also obtained by Fu and Gundersen using the manual approach [121]. Table 8.3 shows the path of the two substreams S1 and S2 before and after expansion. As the expansion temperature is equal to the supply temperature of the variable pressure stream, no integration in the HEN is required upstream of the expander. Instead, the substream is expanded immediately to a temperature $T_{\mathrm{ex}} = -4.80$°C. As the temperature from expansion (T_{ex}) is less than the target temperature, substream S2 must be heated and hence becomes a cold stream.

The hot and cold utility consumption, net work and total exergy consumption for the WHEN solution are presented in Table 8.4. The solution of the heat integration problem with no pressure manipulation is given for comparison. Expansion at the hot utility temperature increases the hot utility consumption from 660.00 kW to 1059.91 kW as the heat contribution from the variable pressure stream is dissipated through expansion. Simultaneously, the necessary cold utility is reduced from 480.00 kW to 70.36 kW due to the additional cooling this stream provided. The net work from expansion is -809.55 kW, hence work is produced by the system. The pinch temperature remains the same for the HEN and WHEN. Furthermore, as the outlet temperature from expansion at hot utility temperature is lower than the ambient temperature, no pinch expansion is needed. Instead, IPOPT finds a solution where the variable pressure stream is expanded at the hot utility temperature directly. The Grand Composite Curves (GCCs) for the solution of (a) heat integration and (b) simultaneous work and heat integration problems are provided

Table 8.4 WHEN results and HEN targets without pressure manipulation for Example 1.

Property	No pressure manipulation	WHEN solution
Q_{HU} [kW]	660.00	1059.91
Q_{CU} [kW]	480.00	70.36
T_{PI}/t_{PI} [°C]	(220.00/200.00)	(220.00/200.00)
W_{net} [kW]	-	-809.55
Ex^* [kW]	-	-203.34

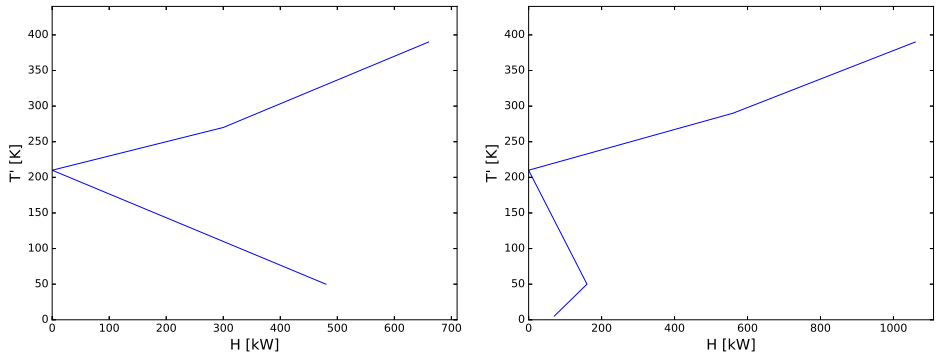

(a) **(b)**

Figure 8.4 (**a**) Grand Composite Curve for Example 1 without pressure manipulation. (**b**) Grand Composite Curve for the simultaneous work and heat integration problem.

in Figure 8.4.

Example 2: This is an example taken from Fu and Gundersen [120] where a stream undergoes a pressure change from 100 kPa to 300 kPa. Stream data and utility temperatures are presented in Table 8.5. As in the previous example, the problem has 8 continuous decision variables: the hot/cold utility consumption, compression temperatures and branch flowrates.

A solution was obtained by IPOPT after 43 iterations and 3.8 s of CPU time, corresponding to a total exergy consumption of 309.18 kW. Again, IPOPT converged to the solution predicted by the manual design procedure. Only one stream branch remains active, with heaters placed both upstream and downstream of the compressor. First, the stream is heated to the cold pinch temperature of 200.00°C (not known a priori), where it is compressed before being cooled to its target temperature. Consequently, the two substreams are classified by the optimizer as cold (S1) and hot (S2) streams in this case. Table 8.6 shows the complete path of the variable

Table 8.5 Stream data for Example 2.

Stream	T^{s} [°C]	T^{t} [°C]	F [kW/°C]	P^{s} [kPa]	P^{t} [kPa]
H1	400	60	2	-	-
C1	15	250	1	100	300
C2	200	380	4	-	-
Hot utility	400	400	-	-	-
Cold utility	15	15	-	-	-

Table 8.6 Path of the variable pressure stream at the solution of Example 2.

Stream	T^{s} [°C]	T^{t} [°C]	F [kW/°C]	P [kPa]	Classification
S1	15.00	200.00	1.00	100	C
S2	374.49	250.00	1.00	300	H

pressure stream.

The total exergy consumption, hot and cold utility consumption, and net work for the solution are presented in Table 8.7. The solution for the heat integration problem without pressure manipulation is presented in the same table for comparison. The example shows the trade-off between work and heat. Rather than cooling the stream prior to compression, the stream is heated (using surplus heat below pinch) to the pinch temperature, where it is compressed. Pinch compression provides additional heating above pinch, thus reducing the total required hot utility consumption. Consequently, through sacrificing some additional compression power due to a higher compression temperature, the total hot utility consumption in the network can be reduced. The GCCs for the two solutions are presented in Figure 8.5. The GCC for the WHEN is noticeably steeper above the pinch point due to compression. No additional pinch points are created in the WHEN solution, however, as the total heat from compression is less than the required heating at 374.49°C.

Example 3: This is an example taken from Fu and Gundersen [120] integrating four streams; two hot and two cold, where one of the cold streams are compressed from 100 kPa to 300 kPa. The same example was used for demonstrating simultaneous optimization of work and heat integration with unclassified process streams in a paper by Yu *et al.* [138]. In that article, an MINLP formulation was used to solve the problem with different pinch location algorithms embedded, using a disjunctive extension to account for unclassified streams. The resulting formulation required

Table 8.7 WHEN results and HEN targets without pressure manipulation for Example 2.

Property	No pressure manipulation	WHEN solution
Q_{HU} [kW]	410.00	235.52
Q_{CU} [kW]	135.00	135.00
T_{PI}/t_{PI} [°C]	(220.00/200.00)	(220.00/200.00)
W_{net} [kW]	-	174.48
Ex^* [kW]	-	309.18

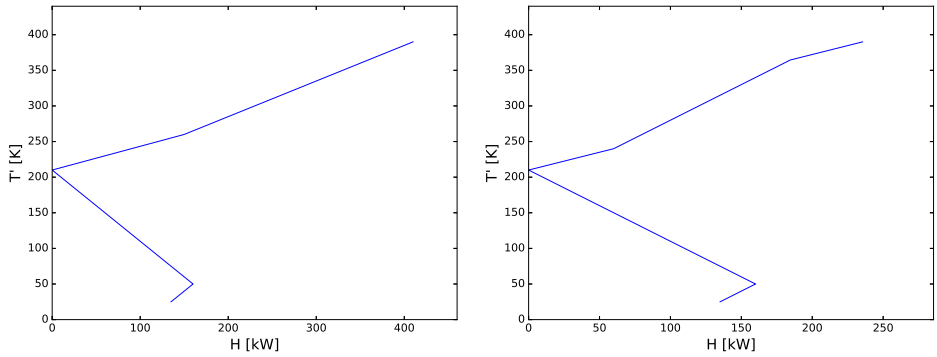

(a) **(b)**

Figure 8.5 (**a**) Grand Composite Curve for Example 2 without pressure manipulation. (**b**) Grand Composite Curve for the simultaneous work and heat integration problem.

Table 8.8 Stream data for Example 3.

Stream	T^{s} [°C]	T^{t} [°C]	F [kW/°C]	P^{s} [kPa]	P^{t} [kPa]
H1	300	50	4	-	-
H2	120	40	4	-	-
C1	70	380	3	100	300
C2	30	180	3	-	-
Hot utility	400	400	-	-	-
Cold utility	15	15	-	-	-

Table 8.9 Path of the variable pressure stream at the solution of Example 3.

Stream	T^{s} [°C]	T^{t} [°C]	F [kW/°C]	P [kPa]	Classification
Branch A:					
A1	70.00	35.00	1.53	100	H
A2	139.06	380.00	1.53	300	C
Branch B:					
B1	70.00	280.00	1.47	100	C
B2	483.63	380.00	1.47	300	H

a total of 168 continuous variables and 4 binary variables using the most compact form of the formulations considered. In comparison, using the nonsmooth extension represented by Equations (8.5)-(8.6), only the 8 decision variables observed in the previous two examples are needed in the model. Stream data is provided in Table 8.8.

A solution with a total exergy consumption of 473.79 kW was obtained by IPOPT after 52 iterations and 3.9 s of CPU time. The path of the variable pressure stream for the two branches is highlighted in Table 8.9. Unlike the previous two examples which featured a single compressor or expander, stream splitting is required here, with one stream branch (A) cooled to 35.00°C, followed by compression and heating to target. Stream branch (B), on the other hand, is first heated to the cold pinch temperature, where it is compressed and subsequently cooled to target. Consequently, the identity of both stream branches are different before and after compression. For comparison, the manual design procedure predicted identical exergy destruction and compression temperatures.

The optimization results are presented in Table 8.10, along with the results from heat integration only. If only heat integration is considered (no pressure manipula-

Table 8.10 WHEN results and HEN targets without pressure manipulation for Example 3.

Property	No pressure manipulation	WHEN solution
Q_{HU} [kW]	360.00	0.00
Q_{CU} [kW]	300.00	413.79
$T_{\text{PI}}/t_{\text{PI}}$ [°C]	(120.00/100.00)	(484.12/464.12), (300.11/280.11)
W_{net} [kW]	-	473.79
Ex^* [kW]	-	473.79

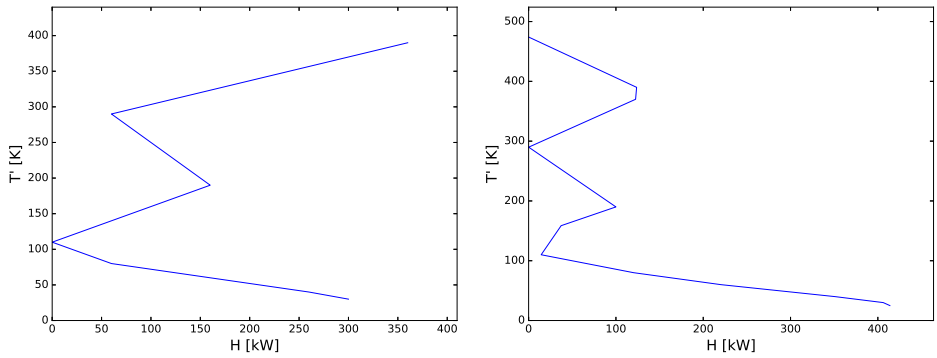

(a) **(b)**

Figure 8.6 (**a**) Grand Composite Curve for Example 3 without pressure manipulation. (**b**) Grand Composite Curve for the simultaneous work and heat integration problem.

tions in the network), the minimum hot and cold utility requirements are 360 kW and 300 kW, respectively. Provided a cold stream needs to be compressed from 100 kPa to 300 kPa, the heat of compression is sufficient to satisfy the heating demand from the process, hence resulting in a threshold problem with no external hot utility consumption. Furthermore, the cold utility demand increases slightly from 300.00 to 413.79 kW from cooling stream branch A down to 35.0°C. Pressure manipulation results in two new pinch points at ($T_{\text{H}}/T_{\text{C}} = 484.12/464.12$°C) and ($T_{\text{H}}/T_{\text{C}} = 300.11/280.11$°C). The GCCs for the WHEN solution and for the heat integration problem are presented in Figure 8.6.

Example 4: The example is taken from from Fu and Gundersen [121], and is a work and heat integration problem with four process streams; two hot and two cold, of which a hot stream needs to be expanded from 300 to 100 kPa. Detailed stream data for the problem are provided in Table 8.11.

Table 8.11 Stream data for Example 4.

Stream	T^{s} [°C]	T^{t} [°C]	F [kW/°C]	P^{s} [kPa]	P^{t} [kPa]
H1	400	60	3	300	100
H2	330	80	9	-	-
C1	15	220	6	-	-
C2	140	380	8	-	-
Hot utility	400	400	-	-	-
Cold utility	15	15	-	-	-

Table 8.12 Path of the variable pressure stream at the solution of Example 4.

Stream	T^{s} [°C]	T^{t} [°C]	F [kW/°C]	P [kPa]	Classification
Branch A:					
A1	400.00	330.02	1.19	300	H
A2	167.52	60.00	1.19	100	H
Branch B:					
B1	400.00	163.68	1.81	300	H
B2	46.00	60.00	1.81	100	C

IPOPT obtained a solution with a total exergy consumption of -206.18 kW after 53 iterations and 3.9 CPU seconds. At the solution, stream branches A and B remain active. As seen in Table 8.12, stream branch A is first cooled to the original hot pinch temperature at 330.02°C, where it is expanded and proceeds to be cooled to target. Stream branch B is cooled to 163.68°C, which is close to the new hot process pinch temperature 160°C created by the integration of the variable pressure stream, where it is expanded, before being reheated to the target temperature. Consequently, the solution features a stream classification change for branch B, where the stream goes from being a hot stream upstream of the expander to becoming a cold stream after.

Table 8.13 presents the external utility consumption, net work and total exergy consumption for the optimized WHEN network. Pinch expansion produces cooling below the original pinch point, which is accompanied by a reduction in the required cold utility from 470 kW to 63.65 kW. Furthermore, it generates another process pinch point at ($T_{\mathrm{H}}/T_{\mathrm{C}} = 160/140$°C) from pinch expansion at 330.02°C. The design corresponds to a net work generation of 406.36 kW, resulting in an overall exergy consumption of -206.18 kW. In comparison, the optimal solution with the manual procedure yields a total exergy consumption of -206.40 kW with

Table 8.13 WHEN results and HEN targets without pressure manipulation for Example 4.

Property	No pressure manipulation	WHEN solution
Q_{HU} [kW]	350.00	350.02
Q_{CU} [kW]	470.00	63.65
T_{PI}/t_{PI} [°C]	(330.00/310.00)	(160.00/140.00), (330.00/310.00)
W_{net} [kW]	-	-406.36
Ex^* [kW]	-	-206.18

expansion at the two process pinch temperatures. The difference in objective function values between the two methods are believed to be a result of expansion at a slightly higher temperature (163.68°C versus 160.00°C). IPOPT is run with a larger dual feasibility tolerance due to the limitation of dual feasibility calculations being invalid at nonsmooth points, and hence convergence to suboptimal points is possible. A significant limitation with the manual design procedure is its iterative nature, which becomes very time consuming and even prohibitive for larger problems and several active stream branches. The same example was also solved using the manual design procedure, experiencing the tediousness of the approach first hand. In particular, new heat cascades and GCCs must be calculated successively as each variable pressure stream is integrated in the network. If the heat from compression or cooling from expansion exceeds the current required heating or cooling as determined by the GCC, stream splitting and additional iterations are required for finding the optimal distribution between the stream branches. The optimization model, on the other hand, is simultaneous in nature and will allocate the branch heat capacity flowrates between the different compression and expansion temperature candidates. Although the algorithm in some cases do not obtain the exact solution due to low tolerance for the dual feasibility calculations, it locates the correct pinch candidates for the integrated network, and suggests a compression or expansion scheme close to that of the manual procedure. Therefore, the algorithm is very suitable for speeding up the manual procedure, by first giving the designer a clear indication on which temperatures to compress and expand from. Then, the designer can use the information of process pinch points and integration strategy in the manual procedure, to successfully allocate the branch heat capacity flowrates thus removing some of its iterative nature. Nevertheless, a global optimization strategy should be pursued in the future to avoid the convergence to local optima. The GCCs for the optimized WHEN and HEN are presented in Figure 8.7. The additional pinch point due to pressure manipulation can be seen in the figure. Additional cooling from expansion also makes the GCC noticeably steeper in the region below the high temperature pinch point.

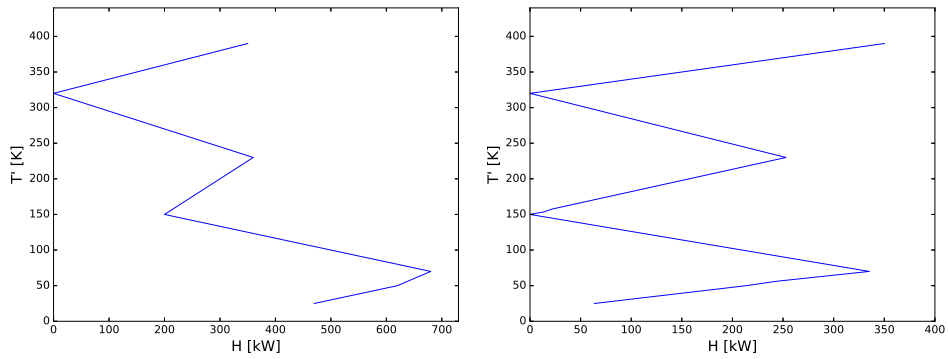

(a) **(b)**

Figure 8.7 (**a**) Grand Composite Curve for Example 4 without pressure manipulation. (**b**) Grand Composite Curve for the simultaneous work and heat integration problem.

Table 8.14 Stream data for Example 5.

Stream	T^{s} [°C]	T^{t} [°C]	F [kW/°C]	P^{s} [kPa]	P^{t} [kPa]
H1	400	35	2	200	100
H2	320	160	4	-	-
H3	110	35	3	-	-
C1	15	380	3	100	200
C2	190	250	10	-	-
Hot utility	400	400	-	-	-
Cold utility	15	15	-	-	-

Example 5: The last example looks into the simultaneous compression and expansion of a hot and cold stream in a HEN. The example is taken from Fu and Gundersen [140] and looks at the integration of five streams; three hot streams and two cold streams. A hot stream undergoes a pressure reduction from 200 kPa to 100 kPa. Simultaneously, a cold stream needs to be compressed from 100 kPa to 200 kPa. With the simultaneous integration of two variable pressure streams, the total number of variables in the problem is 14. Stream data for the WHEN problem is provided in Table 8.14.

IPOPT obtained a solution after 135 iterations and 4.07 CPU seconds with a total exergy destruction of 175.89 kW. The paths of the two variable pressure streams are presented in Table 8.15. Both streams are split into two branches. Stream branch A of H1 is first cooled to a temperature 119.79°C where it is expanded and

Table 8.15 Path of the variable pressure stream at the solution of Example 5.

Stream	T^{s} [°C]	T^{t} [°C]	F [kW/°C]	P [kPa]	Classification
H1:					
Branch A:					
A1	400.00	119.79	0.95	200	H
A2	49.19	35.00	0.95	100	H
Branch B:					
B1	400.00	209.83	1.05	200	H
B2	123.05	35.00	1.05	100	H
C1:					
Branch A:					
A1	15.00	189.98	2.66	100	C
A2	291.42	380.00	2.66	200	C
Branch B:					
B1	15.00	301.53	0.34	100	C
B2	427.40	380.00	0.34	200	H

proceeds to be further cooled to target. Branch B is expanded at a hot pinch temperature of 209.83°C, followed by additional cooling to target temperature. Similarly, stream branch A for cold stream C1 is heated to and compressed at a pinch temperature of 189.98°C, followed by additional heating to target. Stream branch B, on the other hand, is compressed at the second pinch temperature 301.53°C and then proceeds to be cooled to target. The corresponding compression and expansion temperatures determined by the manual design procedure are 110.00, 210.00, 190.00 and 300.00 for the respective stream branches, resulting in a total exergy destruction of 175.6 kW.

The optimization results are summarized in Table 8.16. Heat from compression and cooling from expansion substitute external cooling and heating requirements, hence resulting in a reduced utility consumption. Also, additional pinch points are created at ($T_{\mathrm{H}}/T_{\mathrm{C}} = 110/90$°C) and ($T_{\mathrm{H}}/T_{\mathrm{C}} = 320/300$°C) following a notable shift in the grand composite curve below the original pinch point caused by the expanding streams. The required net work for the process is 154.44 kW. The GCCs for the HEN and WHEN are given in Figure 8.8.

Table 8.16 WHEN results and HEN targets without pressure manipulation for Example 5.

Property	No pressure manipulation	WHEN solution
Q_{HU} [kW]	350.00	37.51
Q_{CU} [kW]	250.00	91.95
$T_{\text{PI}}/t_{\text{PI}}$ [°C]	(210.00/190.00)	(110.00/90.00), (210.00/190.00), (320.00/300.00)
W_{net} [kW]	-	154.44
Ex^* [kW]	-	175.89

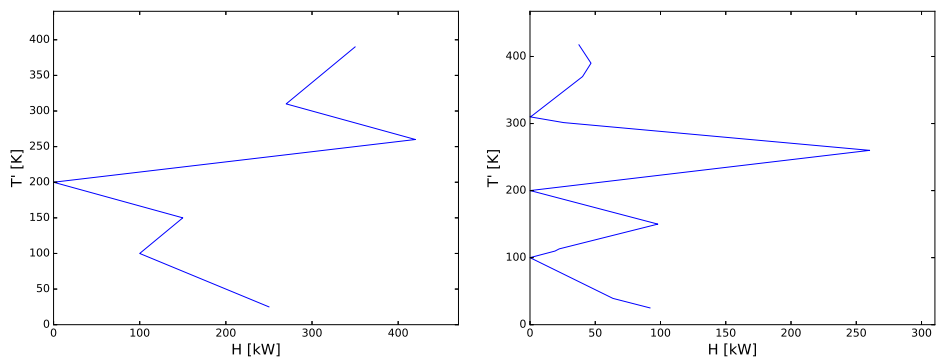

(a) **(b)**

Figure 8.8 (**a**) Grand Composite Curve for Example 5 without pressure manipulation. (**b**) Grand Composite Curve for the simultaneous work and heat integration problem.

8.3.2 Convergence characteristics

Local optimization using IPOPT was used when performing the analysis. However, IPOPT assumes twice continuously differentiable objective function and constraints for the dual feasibility calculations. In particular, this creates an issue in defining the termination criterion for nonsmooth functions, as the dual feasibility calculations are invalid at nonsmooth points [65]. This can cause the algorithm to not converge, and instead iterate in a negligibly small search space. Here, this issue was resolved by increasing the dual feasibility tolerance to 1.0. However, in order to avoid this issue completely, a new optimization solver tailored for handling L-derivatives must be developed. Nevertheless, solutions very close to the results from the manual design procedure were obtained in the examples. To investigate the performance of the local solver, multistart analysis were done for the five examples. The solutions were compiled into four main categories:

- A: Within 0.5% of the best known value.
- B: 0.5-2% of the best known value.
- C: 2-5% of the best known value.
- D: More than 5% of the best known value.

Multistart was performed by doing 500 runs and varying the initial guesses for the compression and expansion temperatures, which were varied in the ranges 15-100°C, 100-300°C and 300-400°C, respectively for the three stream branches. The results are given in Figure 8.9. The results show that IPOPT, although only a local algorithm, obtains the best known value or close to the best known value in most of the examples. Compressors and expanders add nonconvexity to the problem making it harder to achieve global convergence. However, even with the integration of two compressors and two expanders in Example 5, IPOPT still converges to solutions within 5% of the best known solution in 85% of the cases.

The model needs to be tested for larger problems with more process streams, including streams that are subject to pressure change. The results from the five examples discussed in this chapter are, however, quite promising when it comes to model performance. The required CPU times to solve these problems are really low, and only increases from 3.2 to 4.1 seconds when the number of streams increases from three to five. The number of pressure-changing streams increase from one to two.

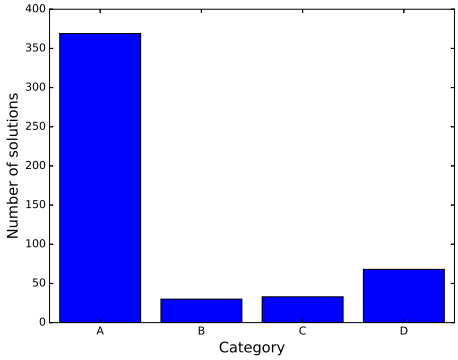

(a) Example 1.

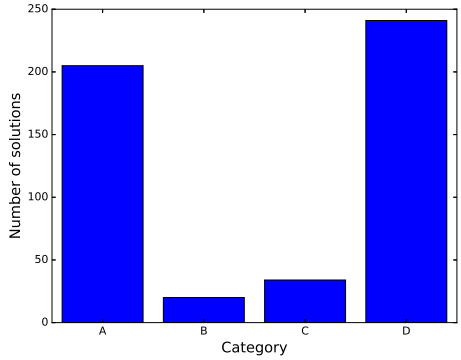

(b) Example 2.

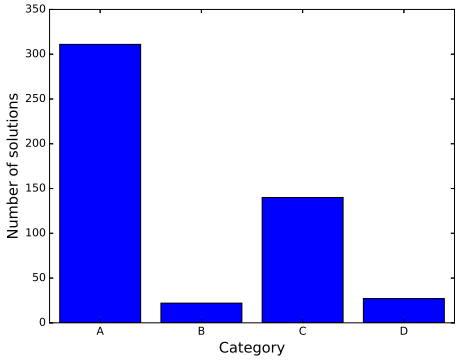

(c) Example 3.

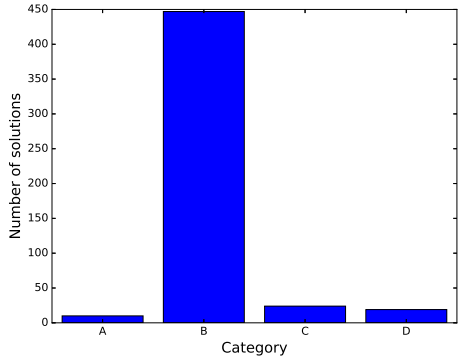

(d) Example 4.

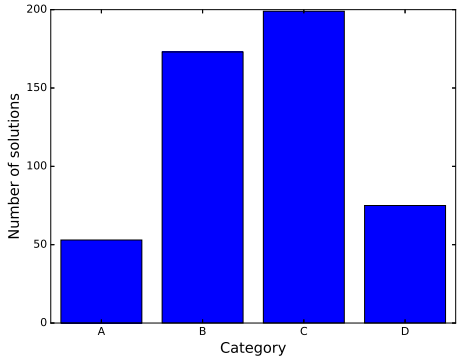

(e) Example 5.

Figure 8.9 Multistart results for the five examples.

8.4 Conclusions

A nonsmooth extension of the pinch location algorithm by Duran and Grossmann has been suggested for handling unclassified process streams. The extension uses the nonsmooth operators max and min for assigning target temperatures for streams of unknown classification. Streams that are inactive are given a target temperature equal to the supply temperature, and thus do not contribute to the overall energy balance, nor the individual pinch balances in the model. Moreover, no binary variables are needed in the formulation, thus considerably reducing the computational efforts and improving the overall scalability of the optimization model. The extension can be used both for the Duran and Grossmann formulation and the generalized nonsmooth process integration operator presented in Section 2.1.3. However, examples are here done with the Duran and Grossmann formulation, as it was shown to provide better overall convergence characteristics. The extension was tested for five different work and heat integration problems of varying complexity using the local optimization algorithm IPOPT and a superstructure by Uv [136] for exergy targeting of WHENs. Sensitivities for the nonsmooth operators are calculated analytically using recent advances in nonsmooth analysis presented in Chapter 2 and experience in modeling, simulation and optimization of nonsmooth flowsheet models for natural gas liquefaction. Although only local optimization was considered in this chapter, solutions were obtained very close to the best known solution as determined by the manual and iterative design procedure for WHEN targeting. Furthermore, in several examples the solutions featured stream identity changes upon compression and expansion. Nonconvexity increases with additional streams in the problem, making it challenging to find global optima using only local solvers. Nevertheless, multistart analysis shows that IPOPT is still capable of finding good quality solutions even for more complex examples.

Chapter 9

Conclusions and future work

9.1 Conclusions

Flowsheet models of single mixed and dual mixed refrigerant liquefaction processes for natural gas were constructed as part of the work in this thesis. At the center of these models is a nonsmooth multistream heat exchanger model that enforces feasible heat transfer throughout, using a specialized form of the generalized nonsmooth operator for process integration where utility duties are set to zero. Moreover, to reduce the number of variables in the model, flash calculations required for modeling two-phase behavior, as well as auxiliary equipment such as valves and compressors, were nested in modular subroutines where derivatives are passed on using a nonsmooth analog of the implicit function theorem. Although the nonsmooth framework has already proved successful in simulating the PRICO process, this particular process with a single refrigerant cycle, features a simple design that has been widely explored by existing multistream heat exchanger models. Therefore, to truly demonstrate the capabilities of the new framework, more complex refrigerant cycles had to be studied.

In light of this, simulation models for single mixed and dual mixed refrigerant processes were constructed and results were compared with those obtained from commercial simulation tools. At first glance, the results show a close correlation between the different tools, however, the nonsmooth approach offers several advantageous features otherwise missing from current process simulators. For instance, multistream heat exchangers in a simulation environment are traditionally handled by solving an overall energy balance for an unknown outlet stream temperature. No explicit constraints or correlations are used for preventing temperature crossovers, and as such, the model cannot enforce a feasible heat transfer at the

solution. With the nonsmooth models, however, three equations rather than one is used to describe the individual heat exchangers, which in turn can be used to solve for three unknown variables. Moreover, the user is no longer restricted to solving for an unknown stream temperature only, but can instead choose from a library of other operating variables such as pressure levels, component molar flowrates, heat exchanger conductance and the minimum approach temperatures. As a result, the models offer added versatility in design, making it possible to find solutions where commercial simulation tools cannot. The cases studied in this thesis were all selected to manifest this feature, by choosing initial starting points for which the commercial process simulators could not obtain any feasible solutions.

Despite the added features, the models maintain a manageable size even when scaled up to accommodate larger and more complex configurations. In fact, the model for the AP-DMR process only requires about double the number of operating variables needed to describe the smallest single-mixed refrigerant process (Example 1), although it includes two additional multistream heat exchangers, an additional refrigeration cycle, plus an NGL separator. As a result, the total convergence time is also workable with less than two minutes required for simulating the dual mixed refrigerant processes. It should be mentioned, however, that the code is unoptimized in its present form, and improvements are to be expected given its due attention. Currently, operator overloading is used for providing the LD-derivatives, requiring memory allocation for storing the individual sensitivities upon initialization of the individual variables. Furthermore, bubble-sort, which is an exponential algorithm, is used for sorting the individual enthalpy intervals needed to construct the composite curves. The number of variables in the models can be reduced by using a different partitioning of the individual substreams. Throughout this thesis, five substreams were used for representing the single-phase vapor and liquid regions in the individual heat exchangers, while the two-phase region was divided among 20 segments. That particular partitioning was found to be the minimum required for the PRICO process without sacrificing accuracy. However, as additional multistream heat exchangers are included in the model, each will contribute to a smaller portion of the total duty, distributed over a shorter temperature span. Consequently, the nonlinearity in enthalpy will be less pronounced than in its PRICO counterpart, and thus fewer segments will be required in practice.

Unoptimized code aside, the models remain suitable for flowsheet optimization. Using the primal-dual feasible optimization algorithm IPOPT, improvements of up to 21% in total compressor duties could be achieved compared to the initial feasible design. Optimization using sensitivity information provided by the LD-derivatives in a deterministic solver also proved better than what is currently considered state-of-the-art methods for these types of configurations for natural gas liquefaction

processes, where a stochastic solver is used together with a commercial simulation tool. Attempts have previously been made in the literature to optimize dual mixed refrigerant processes using sequential quadratic programming, however, excessive tuning of these solvers makes such an approach impractical. Instead, a hybrid approach was suggested, where the bulk of the optimization was performed using stochastic solvers, and the deterministic solver was used only for fine-tuning. On the other hand, IPOPT does not require prior tuning to tailor each specific problem, but can instead be used directly for all instances along with the changes made to the default settings. As for convergence, solutions were obtained in 25-80 times less computing time than what was needed when using particle swarm optimization and Aspen HYSYS. A higher success rate was also achieved than what was reported for the PRICO process using the same formulation and an SQP solver. In addition, results from multistart optimization showed that process simulation complemented to this success rate with better quality solutions obtained overall when starting from an initial feasible point.

Advantages provided by a nonsmooth modeling approach could also be transferred to the more general concept of work and heat integration. A superstructure for targeting networks of minimum exergy consumption, which applied theorems for appropriate integration of pressure changing equipment in heat exchanger networks, had already been developed. However, a sequential integration strategy was attempted for solving the model, which imposed several restrictions on the model such as the integration sequence, and soft specifications on supply and target pressures. Furthermore, the heat cascade and ensuing integration problem had to be recomputed whenever additional stream segments or variable pressure streams are introduced, adding to the computational complexity for larger integration problems. As a result, a simultaneous strategy is preferred, although it comes with some modeling challenges. The most important of these is the issue of handling unclassified process streams. In a sequential approach, all potential temperatures for compression and expansion are determined a priori, and thus the identity is known prior to optimization. With the simultaneous integration and optimization approach, however, these candidate temperatures are determined as part of the optimization problem. Different formulations for handling unclassified process streams had already been addressed in the literature, yet they all involve auxiliary binary variables, and an underlying mixed integer nonlinear program that can be computationally demanding for larger problems. Instead, this thesis propose an alternative formulation that applies two nonsmooth equations for the assignment of stream identities. The formulation features fewer variables compared to a disjunctive formulation already presented in the literature, and can be used to solve the superstructure in a simultaneous fashion. Different case studies were presented, and although a local optimization procedure was used throughout, multistart

results indicate that good quality results were obtained even from largely different initial conditions. In its current state, the simultaneous optimization procedure is suitable to be used in conjunction with a manual design procedure, e.g. by locating pinch points and stream identities efficiently using a local solver and provide this information to the manual procedure for fine tuning without the required iterative steps.

9.2 Future work

Although a nonsmooth modeling framework proved successful in modeling natural gas liquefaction processes and work and heat exchange networks, it still is in its infancy and will benefit from further advances. In particular, a current limitation imposed on the definition of LD-derivatives is that the functions must be locally Lipschitz continuous, and as a result, cannot feature integer variables. Integer variables are important in for instance a cost analysis, which typically differentiate between variable and fixed costs in the analysis. Moreover, selection of different equipment in a superstructure would require discrete decisions that can easily be modeled using an integer representation. In order to bring the framework further and opening it up for new applications, a suggestion would therefore be to expand the definition to also account for mixed integer models.

The dual mixed refrigerant process is the only configuration for large-scale production of LNG adressed thus far by the nonsmooth framework. However, other large-scale liquefaction processes exists, most notably the propane precooled mixed refrigerant (C3MR) and refrigerant cascade processes, where the former remains the undisputed market leader accounting for around 60% of the total liquefaction capacity. Even though the processes have already worked up a considerable market maturity, it would be interesting to incorporate them in the nonsmooth framework. For the C3MR process, this would involve changes primarily to the precooling section, where a pure propane cascade is used in place of the warm mixed refrigerant. Pressure levels and number of propane stages would be natural choices for decision variables here.

Shortcomings with using IPOPT as a solver for the nonsmooth models have already been discussed in Chapters 6 and 8. Although inherently developed for twice continuously differentiable functions, IPOPT obtained overall better results than customized nonsmooth constrained optimization solvers, i.e. the proximal bundle solver, for programs with LD-derivative information provided. However, the termination criterion for the algorithm assumes twice continuous differentiability, and in its current implementation, therefore, IPOPT is unable to successfully converge to nonsmooth points. Attempts at circumvent this obstacle was made by increasing the dual feasibility tolerance accordingly, which improved convergence though

made it difficult to prove optimality. The primary issue here is that there currently exists no practical way of testing the nonsmooth KKT conditions necessary for optimality. An important next step to expand the nonsmooth framework would hence be to develop a nonsmooth optimization solver tailored for LD-derivatives. A branch and bound option should also be studied for the global optimization of nonsmooth programs. Work has currently been done on this using smooth McCormick relaxations for nonsmooth functions. However, the work was done using IPOPT as local solvers, and with nonoptimal bilinear relaxations, which made the relaxations too weak to be included for solving the WHENs problem sets to global optimality. Alternative relaxations should therefore be applied instead, such as the one proposed by Khan *et al.* [141], for tighter upper and lower bounding problems to speed up the branch and bound algorithm.

Bibliography

[1] S. Balakrishna and L. T. Biegler. Targeting strategies for the synthesis and energy integration of nonisothermal reactor networks. *Industrial & Engineering Chemistry Research*, 31(9):2152–2164, 1992.

[2] H. H. Rachford and J. D. Rice. Procedure for use of electronic digital computers in calculating flash vaporization hydrocarbon equilibrium. *Journal of Petroleum Technology*, 4(10):327–328, 1952.

[3] M. M. F. Hasan, I. A. Karimi, H. Alfadala, and H. Grootjans. Modeling and simulation of main cryogenic heat exchanger in a base-load liquefied natural gas plant. *Computer Aided Chemical Engineering*, 24:219–224, 2007.

[4] M. M. F. Hasan, I. A. Karimi, H. Alfadala, and H. Grootjans. Operational modeling of multistream heat exchangers with phase changes. *AIChE Journal*, 55(1):150–171, 2009.

[5] R. S. Kamath, L. T. Biegler, and I. E. Grossmann. Modeling multistream heat exchangers with and without phase changes for simultaneous optimization and heat integration. *AIChE Journal*, 58(1):190–204, 2012.

[6] H. A. J. Watson and P. I. Barton. Modeling phase changes in multistream heat exchangers. *International Journal of Heat and Mass Transfer*, 105:207–219, 2017.

[7] A. M. Sahlodin, H. A. J. Watson, and P. I. Barton. Nonsmooth model for dynamic simulation of phase changes. *AIChE Journal*, 62(9):3334–3351, 2016.

[8] J. F. Boston and H. I. Britt. A radically different formulation and solution

of the single-stage flash problem. *Computers & Chemical Engineering*, 2(2):109–122, 1978.

[9] *Aspen Technology Inc., Aspen Plus v9*. Aspen Technology Inc., Bedford, MA, 2016.

[10] *Aspen Technology Inc., Aspen HYSYS v9*. Aspen Technology Inc., Bedford, MA, 2016.

[11] V. S. Parekh and P. M. Mathias. Efficient flash calculations for chemical process design – extension of the Boston–Britt 'Inside–out' flash algorithm to extreme conditions and new flash types. *Computers & Chemical Engineering*, 22(10):1371–1380, 2005.

[12] H. A. J. Watson, M. Vikse, T. Gundersen, and P. I. Barton. Reliable flash calculations: Part 1. Nonsmooth inside-out algorithms. *Industrial & Engineering Chemistry Research*, 56(4):960–973, 2017.

[13] D. G. Anderson. Iterative procedures for nonlinear integral equations. *Journal of the ACM (JACM)*, 12(4):547–560, 1965.

[14] H. F. Walker and P. Ni. Anderson acceleration for fixed-point iterations. *SIAM Journal on Numerical Analysis*, 49(4):1715–1735, 2011.

[15] H. A. J. Watson and P. I. Barton. Reliable flash calculations: Part 3. A nonsmooth approach to density extrapolation and pseudoproperty evaluation. *Industrial & Engineering Chemistry Research*, 56(50):14832–14847, 2017.

[16] M. A. Duran and I. E. Grossmann. Simultaneous optimization and heat integration of chemical processes. *AIChE Journal*, 32(1):123–138, 1986.

[17] C. J. Nielsen and P. I. Barton. 110th anniversary: A generalized nonsmooth operator for process integration. *Submitted*, 2019.

[18] I. E. Grossmann, H. Yeomans, and Z. Kravanja. A rigorous disjunctive optimization model for simultaneous flowsheet optimization and heat integration. *Computers & Chemical Engineering*, 22:157–164, 1998.

[19] N. Quirante, J. Caballero, and I. E. Grossmann. A novel disjunctive model for the simultaneous optimization and heat integration. *Computers & Chemical Engineering*, 96:149–168, 2017.

[20] D. P. Bertsekas. *Nondifferentiable Optimization*, chapter Nondifferentiable optimization via approximation. Springer Berlin Heidelberg, Berlin, Heidelberg, 1975.

[21] J. Kreimer and R. Y. Rubinstein. Nondifferentiable optimization via smooth approximation: General analytical approach. *Annals of Operations Research*, 39(1):97–119, 1992.

[22] I. Zang. A smoothing-out technique for min–max optimization. *Mathematical Programming*, 19(1):61–77, 1980.

[23] I. E. Grossmann and F. Trespalacios. Systematic modeling of discrete-continuous optimization models through generalized disjunctive programming. *AIChE Journal*, 59(9):3276–3295, 2013.

[24] N. V. Sahinidis. *BARON 2019.7.13: Global Optimization of Mixed-Integer Nonlinear Programs,* User's Manual, 2019.

[25] R. Misener and C. A.. Floudas. ANTIGONE: Algorithms for coNTinuous / Integer Global Optimization of Nonlinear Equations. *Journal of Global Optimization*, 59(2):503–526, 2014.

[26] A. Griewank and A. Walther. *Evaluating derivatives: principles and techniques of algorithmic differentiation*, volume 105. SIAM, 2008.

[27] S. Scholtes. *Introduction to piecewise differentiable equations*. SpringerBriefs in Optimization, New York, 1 edition, 2012.

[28] Frank H. Clarke. *Optimization and Nonsmooth Analysis*. SIAM, Philadelphia, PA, 1990.

[29] Y. Nesterov. Lexicographic differentiation of nonsmooth functions. *Mathematical Programming*, 104(2):669–700, 2005.

[30] K. A. Khan and P. I. Barton. A vector forward mode of automatic differentiation for generalized derivative evaluation. *Optimization Methods and Software*, 30(6):1185–1212, 2015.

[31] K. A. Khan and P. I. Barton. Generalized derivatives for solutions of parametric ordinary differential equations with non-differentiable right-hand sides. *Journal of Optimization Theory and Applications*, 163(2):355–386, 2014.

[32] T. H. Sweetser. A minimal set-valued strong derivative for vector-valued lipschitz functions. *Journal of Optimization Theory and Applications*, 23(4):549–562, 1977.

[33] P. I. Barton, K. A. Khan, P. Stechlinski, and H. A. J. Watson. Computationally relevant generalized derivatives: theory, evaluation and applications. *Optimization Methods & Software*, 33(4-6):1030–1072, 2018.

[34] F. Facchinei and J-S. Pang. *Finite-Dimensional Variational Inequalities and Complementarity Problems*. Springer-Verlag New York, Inc., New York, NY, vol. 2 edition, 2003.

[35] L. Qi and J. Sun. A nonsmooth version of newton's method. *Mathematical Programming*, 58(1):353–367, 1993.

[36] F. Facchinei, A. Fischer, and M. Herrich. An LP-newton method: nonsmooth equations, KKT systems, and nonisolated solutions. *Mathematical Programming*, 146(1):1–36, 2014.

[37] A. Fischer, M. Herrich, A. F. Izmailov, and M. V. Solodov. A globally convergent LP-newton method. *SIAM Journal on Optimization*, 26(4):2012–2033, 2016.

[38] *BP Energy Outlook*. British Petroleum, London, England, 2017.

[39] S. Thomas and R. A. Dawe. Review of ways to transport natural gas energy from countries which do not need the gas for domestic use. *Energy*, 28(14):1461–1477, 2003.

[40] *World LNG report*. International Gas Union, Barcelona, Spain, 2019.

[41] J-H. Hwang, N-K. Ku, M-I. Roh, and K-Y. Lee. Optimal design of liquefaction cycles of liquefied natural gas floating, production, storage, and offloading unit considering optimal synthesis. *Industrial & Engineering Chemistry Research*, 52(15):5341–5356, 2013.

[42] W. Lim, K. Choi, and I. Moon. Current status and perspectives of liquefied natural gas (LNG) plant design. *Industrial & Engineering Chemistry Research*, 52(9):3065–3088, 2013.

[43] S. Cornot-Gandolphe. LNG cost reductions and flexibility in lng trade add to security of gas supply. *IEA: Energy Prices and Taxes, Quarterly Statistics*, First Quarter, 2005.

[44] P. Bosma and R. K. Nagelvoort. *Proceedings of the 1st Annual Gas Processing Symposium*, chapter Liquefaction Technology; Developments through History. Elsevier, Amsterdam, 2009.

[45] W. Lim, K. Choi, and I. Moon. Current status and perspectives of liquefied natural gas (LNG) plant design. *Industrial & Engineering Chemistry Research*, 52(9):3065–3088, 2013.

[46] J. B. Maher and J. W. Sudduth. *Method and apparatus for liquefying gases*. U.S. Patent No. 3,914,949, 1975.

[47] F. A. Michelsen, I. J. Halvorsen, B. F. Lund, and P. E. Wahl. Modeling and simulation for control of the TEALARC liquified natural gas process. *Industrial & Engineering Chemistry Research*, 49(7389-7397):16, 2010.

[48] M. M. H. Shirazi and D. Mowla. Energy optimization for liquefaction process of natural gas in peak shaving plant. *Energy*, 35(7):2878–2885, 2010.

[49] C. W. Remeljej A. F. A. Hoadley. An exergy analysis of small-scale liquefied natural gas (LNG) liquefaction processes. *Energy*, 31(12):2005–2019, 2006.

[50] L. Gaumer and C. Newton. *Combined cascade and multicomponent refrigeration system and method*. U.S. Patent No. 3,763,658, 1973.

[51] I. Lee and I. Moon. Strategies for process and size selection of natural gas liquefaction processes: Specific profit portfolio approach by economic based optimization. *Industrial & Engineering Chemistry Research*, 57(17):5845–5857, 2018.

[52] M. J. Roberts and R. Agrawal. *Dual Mixed Refrigerant Cycle for Gas Liquefaction*. U.S. Patent No. 6,269,655 B1, 2001.

[53] B. Austbø, S. W. Løvseth, and T. Gundersen. Annotated bibliography – use of optimization in lng process design and operation. *Computers & Chemical Engineering*, 71:391–414, 2014.

[54] T. He, I. A. Karimi, and Y. Ju. Review on the design and optimization of natural gas liquefaction processes for onshore and offshore applications. *Chemical Engineering Research and Design*, 132:89–114, 2018.

[55] T. F. Yee, I. E. Grossmann, and Z. Kravanja. Simultaneous optimization models for heat integration – I. Area and energy targeting and modeling of multi-stream exchangers. *Computers & Chemical Engineering*, 14(10):1151–1164, 1990.

[56] T. F. Yee, I. E. Grossmann, and Z. Kravanja. Simultaneous optimization models for heat integration – III. Process and heat exchanger network optimization. *Computers & Chemical Engineering*, 14(11):1185–1200, 1990.

[57] T. F. Yee and I. E. Grossmann. Simultaneous optimization models for heat integration – II. Heat exchanger network synthesis. *Computers & Chemical Engineering*, 14(10):1165–1184, 1990.

[58] A. Wechsung, A. Aspelund, T. Gundersen, and P. I. Barton. Synthesis of heat exchanger networks at subambient conditions with compression and expansion of process streams. *AIChE Journal*, 57(8):2090–2108, 2011.

[59] A. Aspelund and T. Gundersen. A liquefied energy chain for transport and utilization of natural gas for power production with co2 capture and storage – Part 1. *Applied Energy*, 86(6):781–792, 2009.

[60] M. J. Bagajewicz, R. Pham, and V. Manousiouthakis. On the state space approach to mass/heat exchanger network design. *Chemical Engineering Science*, 53(14):2595–2621, 1998.

[61] H. N. Rao and I. A. Karimi. A superstructure-based model for multistream heat exchanger design within flow sheet optimization. *AIChE Journal*, 63(9):3764–3777, 2017.

[62] R. C. Pattison and M. Baldea. Multistream heat exchangers: Equation-oriented modeling and flowsheet optimization. *AIChE Journal*, 61(6):1856–1866, 2015.

[63] C. Tsay, R. C. Pattison, and M. Baldea. Equation-oriented simulation and optimization of process flowsheets incorporating detailed spiral-wound multistream heat exchanger models. *AIChE Journal*, 63(9):3778–3789, 2017.

[64] K. Tak, H. Kwon, J. Park, J. H. Cho, and I. Moon. A multistream heat exchanger model with enthalpy feasibility. *Computers & Chemical Engineering*, 115:81–88, 2018.

[65] H. A. J. Watson, M. Vikse, T. Gundersen, and P. I. Barton. Optimization of single mixed-refrigerant natural gas liquefaction processes described by nondifferentiable models. *Energy*, 150:860–876, 2018.

[66] H. A. J. Watson, K. A. Khan, and P. I. Barton. Multistream heat exchanger modeling and design. *AIChE Journal*, 61(10):3390–3403, 2015.

[67] R. Anantharaman, E. L. Johnsen, and T. Gundersen. Revisiting the simultaneous process optimization with heat integration problem. *Computer Aided Chemical Engineering*, 34:243–248, 2014.

[68] M. A. Navarro-Amorós, J. A. Caballero, R. Ruiz-Femenia, and I. E. Grossmann. An alternative disjunctive optimization model for heat integration with variable temperatures. *Computers & Chemical Engineering*, 56:12–26, 2013.

[69] H. A. J. Watson, M. Vikse, T. Gundersen, and P. I. Barton. Reliable flash calculations: Part 2. Process flowsheeting with nonsmooth models and generalized derivatives. *Industrial & Engineering Chemistry Research*, 56(50):14848–14864, 2017.

[70] M. Vikse. *Design and Implementation of Modular Subroutines for Simulation of LNG Plantss*. Master thesis, Norwegian University of Science and Technology, Deptartment of Energy and Process Engineering, Trondheim, Norway, 2016.

[71] K. Tak, I. Lee, H. Kwon, J. Kim, D. Ko, and I. Moon. Comparison of multistage compression configurations for single mixed refrigerant processes. *Industrial & Engineering Chemistry Research*, 54(41):9992–10000, 2015.

[72] P. E. Wahl, S. W. Løvseth, and M. J. Mølnvik. Optimization of a simple lng process using sequential quadratic programming. *Computers & Chemical Engineering*, 56:27–36, 2013.

[73] A. Aspelund, T. Gundersen, J. Myklebust, M. P. Nowak, and A. Tomasgard. An optimization-simulation model for a simple lng process. *Computers & Chemical Engineering*, 34(10):1606–1617, 2010.

[74] W. Lee, J. An, J. M. Lee, and Y. Lim. Design of single mixed refrigerant natural gas liquefaction process considering load variation. *Chemical Engineering Research and Design*, 139:89–103, 2018.

[75] F. D. Nogal, J-K. Kim, S. Perry, and R. Smith. Optimal design of mixed refrigerant cycles. *Industrial & Engineering Chemistry Research*, 47(22):8724–8740, 2008.

[76] M. S. Khan and M. Lee. Design optimization of single mixed refrigerant natural gas liquefaction process using the particle swarm paradigm with nonlinear constraints. *Energy*, 49:146–155, 2013.

[77] M. Wang, R. Khalilpour, and A. Abbas. Thermodynamic and economic optimization of LNG mixed refrigerant processes. *Energy Conversion and Management*, 88:947–961, 2014.

[78] M. S. Khan, I. A. Karimi, and M. Lee. Evolution and optimization of the dual mixed refrigerant process of natural gas liquefaction. *Applied Thermal Engineering*, 96:320–329, 2016.

[79] J.-H. Hwang, M.-I. Roh, and K.-Y. Lee. Determination of the optimal operating conditions of the dual mixed refrigerant cycle for the LNG FPSO topside liquefaction process. *Computers & Chemical Engineering*, 49:25–36, 2013.

[80] A. Morin, P. E. Wahl, and M. Mølnvik. Using evolutionary search to optimise the energy consumption for natural gas liquefaction. *Chemical Engineering Research and Design*, 89(11):2428–2441, 2011.

[81] K. Y. Lee, S. H. Cho, and M. I. Roh. An efficient global-local hybrid optimization method using design sensitivity analysis. *International Journal of Vehicle Design*, 28(4):300–317, 2002.

[82] M. J. Roberts and R. Agrawal. *Dual Mixed Refrigerant Cycle for Gas Liquefaction*. U.S. Patent No. 6,119,479, 2000.

[83] F. A. Aly and L. L. Lee. Self-consistent equations for calculating the ideal gas heat capacity, enthalpy, and entropy. *Fluid Phase Equilibria*, 6(3):169–179, 1981.

[84] D. Kim and T. Gundersen. Constraint formulations for optimisation of dual mixed refrigerant lng processes. *Chemical Engineering Transactions*, 61:643–648, 2017.

[85] A. Wächter and L. T. Biegler. On the implementation of an interior-point filter line-search algorithm for large-scale nonlinear programming. *Mathematical Programming*, 106(1):25–57, 2006.

[86] Federico Marini and Beata Walczak. Particle swarm optimization (pso). a tutorial. *Chemometrics and Intelligent Laboratory Systems*, 149:153–165, 2015.

[87] Luis Miguel Rios and Nikolaos Sahinidis. Derivative-free optimization: a review of algorithms and comparison of software implementations. *Journal of Global Optimization*, 56(3):1247–1293, 2013.

[88] M. Vikse, H. A. J. Watson, T. Gundersen, and P. I. Barton. Versatile simulation method for complex single mixed refrigerant natural gas liquefaction processes. *Industrial & Engineering Chemistry Research*, 57(17):5881–5894, 2018.

[89] Bjørn Austbø and Truls Gundersen. Optimal distribution of temperature driving forces in low-temperature heat transfer. *AIChE Journal*, 61(8):2447–2455, 2015.

[90] Bjørn Austbø and Truls Gundersen. Impact of problem formulation on lng process optimization. *AIChE Journal*, 62(10):3598–3610, 2016.

[91] J. B. Jensen and S. Skogestad. Problems with specifying $\Delta T_{\min}$ in the design of processes with heat exchangers. *Industrial & Engineering Chemistry Research*, 47(9):3071–3075, 2008.

[92] N. Karmitsa, A. Bagirov, and M. M. Mäkelä. Comparing different nonsmooth minimization methods and software. *Optimization Methods and Software*, 27(1):131–153, 2012.

[93] Napsu Karmitsa, Adil Bagirov, and M. M. Mäkelä. Empirical and theoretical comparisons of several nonsmooth minimization methods and software. *TUCS Technical Report 959, Turku Centre for Computer Science*, 28, 2009.

[94] M. M. Mäkelä. Multiobjective proximal bundle method for nonconvex nonsmooth optimization: Fortran subroutine mpbngc 2.0. *Reports of the Department of Mathematical Information Technology, Series B, Scientific Computing*, 2003.

[95] L. Lukšan and J. Vlček. A bundle-newton method for nonsmooth unconstrained minimization. *Mathematical Programming, Series B*, 83(3):373–391, 1998.

[96] N. Karmitsa and M. M. Mäkelä. Limited memory bundle method for large bound constrained nonsmooth optimization: convergence analysis. *Optimization Methods and Software*, 25(6):895–916, 2010.

[97] N. Karmitsa and M. M. Mäkelä. Adaptive limited memory bundle method for bound constrained large-scale nonsmooth optimization. *Optimization*, 59(6):945–962, 2010.

[98] M. Vikse, C. Fu, P. I. Barton, and T. Gundersen. Towards the use of mathematical optimization for work and heat exchange networks. *Chemical Engineering Transactions*, 61:1351–1356, 2017.

[99] E. C. Hohman. *Optimum Networks for Heat Exchange*. PhD thesis, University of Southern California, 1971.

[100] D. F. Rudd. The synthesis of system designs: I. Elementary decomposition theory. *AIChE Journal*, 14(2):343–349, 1968.

[101] A. H. Masso and D. F. Rudd. The synthesis of system designs. II. Heuristic structuring. *AIChE Journal*, 15(1):10–17, 1969.

[102] K.-F. Lee, A. H. Masso, and D. F. Rudd. Branch and bound synthesis of integrated process designs. *Industrial & Engineering Chemistry Fundamentals*, 9(1):48–58, 1970.

[103] B. Linnhoff and J. R. Flower. Synthesis of heat exchanger networks: I. Systematic generation of energy optimal networks. *AIChE Journal*, 24(4):633–642, 1978.

[104] B. Linnhoff and J. R. Flower. Synthesis of heat exchanger networks: II. Evolutionary generation of networks with various criteria of optimality. *AIChE Journal*, 24(4):642–654, 1978.

[105] B. Linnhoff, D. R. Mason, and I. Wardle. Understanding heat exchanger networks. *Computers & Chemical Engineering*, 3(1):295–302, 1979.

[106] B. Linnhoff and E. Hindmarsh. The pinch design method for heat exchanger networks. *Chemical Engineering Science*, 38(5):745–763, 1983.

[107] M. M. El-Halwagi V. Manousiouthakis. Synthesis of mass exchange networks. *AIChE Journal*, 35(8):1233–1244, 1989.

[108] Y. P. Wang and R. Smith. Wastewater minimisation. *Chemical Engineering Science*, 49(7):981–1006, 1994.

[109] T. Gundersen and L. Naess. The synthesis of cost optimal heat exchanger networks. an industrial review of the state of the art. *Computers & Chemical Engineering*, 12(6):503–530, 1988.

[110] K. C. Furman and N. V. Sahinidis. A critical review and annotated bibliography for heat exchanger network synthesis in the 20th century. *Industrial & Engineering Chemistry Research*, 41(10):2335–2370, 2002.

[111] J. J. Klemeš and Z. Kravanja. Forty years of heat integration: Pinch analysis (PA) and mathematical programming (MP). *Current Opinion in Chemical Engineering*, 2(4):461–474, 2013.

[112] D. W. Townsend and B. Linnhoff. Heat and power networks in process design. part i: Criteria for placement of heat engines and heat pumps in process networks. *AIChE Journal*, 29(5):742–748, 1983.

[113] R. Smith. *Chemical process design and integration*. John Wiley & Sons, Chichester, UK, 2 edition, 2016.

[114] Y. L. Huang and L. T. Fan. Analysis of a work exchanger network. *Industrial & Engineering Chemistry Research*, 35(10):3528–3538, 1996.

[115] M. S. Razib, M. M. F. Hasan, and I. A. Karimi. Preliminary synthesis of work exchange networks. *Computers & Chemical Engineering*, 37(Supplement C):262–277, 2012.

[116] H. Yu, C. Fu, M. Vikse, C. He, and T. Gundersen. Identifying optimal thermodynamic paths in work and heat exchange network synthesis. *AIChE Journal*, 65(2):549–561, 2019.

[117] A. Aspelund, D. O. Berstad, and T. Gundersen. An extended pinch analysis and design procedure utilizing pressure based exergy for subambient cooling. *Applied Thermal Engineering*, 27(16):2633–2649, 2007.

[118] T. Gundersen, D. O. Berstad, and A. Aspelund. Extending pinch analysis and process integration into pressure and fluid phase considerations. *Chemical Engineering Transactions*, 18:33–38, 2009.

[119] T. J. Kotas. *The Exergy Method of Thermal Plant Analysis*. Exergon Publishing Company with Paragon Publishing, London, UK, 3rd edition, 2012.

[120] C. Fu and T. Gundersen. Integrating compressors into heat exchanger networks above ambient temperature. *AIChE Journal*, 61(11):3770–3785, 2015.

[121] C. Fu and T. Gundersen. Integrating expanders into heat exchanger networks above ambient temperature. *AIChE Journal*, 61(10):3404–3422, 2015.

[122] C. Fu and T. Gundersen. Sub-ambient heat exchanger network design including compressors. *Chemical Engineering Science*, 137:631–645, 2015.

[123] C. Fu and T. Gundersen. Sub-ambient heat exchanger network design including expanders. *Chemical Engineering Science*, 138:712–729, 2015.

[124] C. Fu and T. Gundersen. Heat and work integration: Fundamental insights and applications to carbon dioxide capture processes. *Energy Conversion and Management*, 121:36–48, 2016.

[125] S. A. Papoulias and I. E. Grossmann. A structural optimization approach in process synthesis–II: Heat recovery networks. *Computers & Chemical Engineering*, 7(6):707–721, 1983.

[126] N. Quirante, I. E. Grossmann, and J. Caballero. Disjunctive model for the simultaneous optimization and heat integration with unclassified streams and area estimation. *Computers & Chemical Engineering*, 108:217–231, 2018.

[127] V. C. Onishi, M. A. S. S. Ravagnani, and J. A. Caballero. Simultaneous synthesis of heat exchanger networks with pressure recovery: Optimal integration between heat and work. *AIChE Journal*, 60(3):893–908, 2014.

[128] V. C. Onishi, M. A. S. S. Ravagnani, and J. A. Caballero. Retrofit of heat exchanger networks with pressure recovery of process streams at sub-ambient conditions. *Energy Conversion and Management*, 94(Supplement C):377–393, 2015.

[129] K. Huang and I. A. Karimi. Work-heat exchanger network synthesis (WHENS). *Energy*, 113(Supplement C):1006–1017, 2016.

[130] V. C. Onishi, M. A. S. S. Ravagnani, L. Jiménez, and J. A. Caballero. Multiobjective synthesis of work and heat exchange networks: Optimal balance between economic and environmental performance. *Energy Conversion and Management*, 140(Supplement C):192–202, 2017.

[131] S. K. Nair, H. N. Rao, and I. A. Karimi. Framework for work-heat exchange network synthesis (WHENs). *AIChE Journal*, 64(7):2472–2485, 2018.

[132] S. E. Demirel, J. Li, and M. M. F. Hasan. Systematic process intensification using building blocks. *Computers & Chemical Engineering*, 105:2–38, 2017.

[133] J. Li, S. E. Demirel, and M. M. F. Hasan. Process synthesis using block superstructure with automated flowsheet generation and optimization. *AIChE Journal*, 64(8):3082–3100, 2018.

[134] J. Li, S. E. Demirel, and M. M. F. Hasan. Process integration using block superstructure. *Industrial & Engineering Chemistry Research*, 57(12):4377–4398, 2018.

[135] J. Li, S. E. Demirel, and M. M. F. Hasan. Building block-based synthesis and intensification of work-heat exchanger networks (WHENS). *Processes*, 7(1), 2019.

[136] P. M. Uv. *Optimal design of heat exchanger networks with pressure changes*. Master thesis, Norwegian University of Science and Technology, Trondheim, Norway, 2016.

[137] L. Kong, V. Avadiappan, K. Huang, and C. T. Maravelias. Simultaneous chemical process synthesis and heat integration with unclassified hot/cold process streams. *Computers & Chemical Engineering*, 101:210–225, 2017.

[138] H. Yu, M. Vikse, R. Anantharaman, and T. Gundersen. Model reformulations for work and heat exchange network (WHEN) synthesis problems. *Computers & Chemical Engineering*, 125:89–97, 2019.

[139] V. C. Onishi, N. Quirante, M. A. S. S. Ravagnani, and J. A. Caballero. Optimal synthesis of work and heat exchangers networks considering unclassified process streams at sub and above-ambient conditions. *Applied Energy*, 224:567–581, 2018.

[140] C. Fu and T. Gundersen. Correct integration of compressors and expanders in above ambient heat exchanger networks. *Energy*, 116:1282–1293, 2016.

[141] H. A. J. Watson K. A. Khan and P. I. Barton. Differentiable mccormick relaxations. *Journal of Global Optimization*, 67(4):687–729, 2017.